Final Scientific/Technical Report
January 1, 2014 – April 30, 2017

Bench-Scale Process for Low-Cost Carbon Dioxide (CO_2) Capture Using a Phase-Changing Absorbent

Award Number:	DE-FE0013687
DUNS Number:	086188401
Project Period:	January 1, 2014 – April 30, 2017
Submission Date:	May 2017
Principal Investigator:	Tiffany Westendorf Chemical Engineer 518-387-7347 westendo@research.ge.com
Contributors:	Stanlee Buddle, Joel Caraher, Wei Chen, Mark Doherty, Rachel Farnum, Mark Giammattei, Dan Hancu, Barbara Miebach, Robert Perry, Gosia Rubinsztajn, Irina Spiry, Paul Wilson, Benjamin Wood
Recipient Organization:	GE Global Research 1 Research Circle Niskayuna, NY 12309-1027
Submitted To:	U.S. Department of Energy National Energy Technology Laboratory 626 Cochrans Mill Road P.O. Box 10940 Pittsburgh, PA 15236-0940
Signature of Submitting Official	 Tiffany Westendorf

Acknowledgement and Disclaimer

This material is based upon work supported by the Department of Energy under Award Number DE-FE0013687.

Abstract

The objective of this project is to design and build a bench-scale process for a novel phase-changing aminosilicone-based CO_2-capture solvent. The project will establish scalability and technical and economic feasibility of using a phase-changing CO_2-capture absorbent for post-combustion capture of CO_2 from coal-fired power plants. The U.S. Department of Energy's goal for Transformational Carbon Capture Technologies is the development of technologies available for demonstration by 2025 that can capture 90% of emitted CO_2 with at least 95% CO_2 purity for less than $40/tonne of CO_2 captured. In the first budget period of the project, the bench-scale phase-changing CO_2 capture process was designed using data and operating experience generated under a previous project (ARPA-e project DE-AR0000084). Sizing and specification of all major unit operations was completed, including detailed process and instrumentation diagrams. The system was designed to operate over a wide range of operating conditions to allow for exploration of the effect of process variables on CO_2 capture performance. In the second budget period of the project, individual bench-scale unit operations were tested to determine the performance of each of each unit. Solids production was demonstrated in dry simulated flue gas across a wide range of absorber operating conditions, with single stage CO_2 conversion rates up to 75mol%. Desorber operation was demonstrated in batch mode, resulting in desorption performance consistent with the equilibrium isotherms for GAP-0/CO_2 reaction. Important risks associated with gas humidity impact on solids consistency and desorber temperature impact on thermal degradation were explored, and adjustments to the bench-scale process were made to address those effects. Corrosion experiments were conducted to support selection of suitable materials of construction for the major unit operations in the process. The bench scale unit operations were assembled into a continuous system to support steady state system testing. In the third budget period of the project, continuous system testing was conducted, including closed-loop operation of the absorber and desober systems. Slurries of GAP-0/GAP-0 carbamate/water mixtures produced in the absorber were pumped successfully to the desorber unit, and regenerated solvent was returned to the absorber. A techno-economic analysis, EH&S risk assessment, and solvent manufacturability study were completed.

Table of Contents

List of Figures

List of Tables

Executive Summary

The goal of this project is to design and optimize a bench-scale system utilizing a phase-changing aminosilicone CO_2 capture solvent, and to establish scalability and potential for commercialization of post-combustion capture of CO_2 from coal-fired power plants. The system should be capable of 90% CO_2 capture efficiency and enable capture cost of less than $40/tonne of CO_2 captured. The project consists of three phases: design and construction of the bench scale system, unit operations testing, and continuous system integration and operation.

The bench-scale CO_2 capture system was initially envisioned to consist of a spray absorber, an extruder, and a two-stage desorber. This process configuration was designed to handle a solid carbamate rich phase generated in the absorber and produce a pressurized CO_2 product via high-pressure desorption. During unit operations testing, certain experimental results led to reconfiguration of the bench scale system to handle a carbamate slurry rich phase and produce only a low pressure CO_2 product via atmospheric pressure desorption. The adjusted process consists of a spray absorber, a slurry pump, and a single stage atmospheric pressure desorber. This document will discuss unit operations testing completed for the unit operations described in the original (dry solids) and current (slurry) process concepts.

Spray absorber experiments focused on defining the operating conditions that would produce dry, flowable GAP-0 carbamate solids. Spray absorber experiments were conducted under dry simulated flue gas conditions at CO_2 feed concentrations in the range of 2-100%. A designed experiment was conducted to explore the effects of feed CO_2 concentration, feed GAP-0 : CO2 mole ratio, and feed gas flow rate on carbamate quality for dry simulated flue gas. The data from this series of experiments yielded a transfer function quantifying the effects of these parameters on solids quality (GAP-0 conversion). Dry, flowable solids were produced at all of these conditions, with single stage CO_2 conversion rates up to 75mol%. This experiment series was followed by a series conducted at fixed gas flow rate, CO_2 concentration, and GAP-0 : CO2 mole ratio, and simulated flue gas humidity up to 6.5mol% (approximately 38°C dewpoint). In these humid absorption experiments, the consistency of the GAP-0 carbamate phase gradually transitioned from dry, powdery solids to a wet slurry of water and carbamate solids. Because of this result, the process was reconfigured for rich slurry handling via a slurry pump.

The viscosity of GAP-0 carbamate/water slurries was characterized as a function of water loading and temperature to inform selection of a suitable bench scale slurry pump and for incorporation into the Aspen process model. A progressive cavity pump was successfully used to pump GAP-0/GAP-0 carbamate/water slurries produced in the spray absorber, up to 83wt% solids.

Desorber experiments focused on defining the operating conditions that maximized CO_2 desorption at temperatures that minimize thermal degradation. A designed experiment to investigate the effect of temperature, carbamate loading, and water

content on urea formation from GAP-0 carbamate was performed. This experiment demonstrated that urea formation is favored by high temperature and absence of water, which led to refocusing of the desorber development effort from a two-stage, high pressure and temperature desorption process to a single stage desorber operating at low pressure and temperature in the presence of water. The atmospheric pressure desorber was tested in batch mode, and performance was consistent with the equilibrium isotherms for GAP-0/CO_2 reaction.

Materials of construction experiments were completed for conditions simulating the wet and dry process conditions in various unit operations of the process. Coupons of C1010 carbon steel and 304L stainless steel were exposed to GAP-0 carbamate and water at varying temperatures. Samples were exposed continuously for 6 weeks, and sample mass loss was monitored. Coupon mass loss was used to calculate the estimated corrosion rate in terms of mm/year erosion of equipment wall thickness. Carbon steel was found to be more susceptible to corrosion than stainless steel at the conditions tested. The absorber and extruder conditions were the mildest (5-200microns/yr carbon steel erosion rates), and desorber conditions were the most aggressive (0.2-0.9mm/yr carbon steel erosion rates). Efficacy of selected corrosion inhibitors was screened.

A techno-economic assessment was prepared using bench scale experimental data, an Aspen process model, and Thermoflow power plant models. Performance of the phase-changing CO_2 capture process was compared to that of a conventional monoethanolamine (MEA) process. The analysis demonstrated that the aminosilicone process has significant advantages relative to an MEA-based system. The first-year CO_2 removal cost for the phase-changing CO_2 capture process is $52.1/tonne, compared to $66.4/tonne for the aqueous amine process. The phase-changing CO_2 capture process is less costly than MEA because of advantageous solvent properties that include higher working capacity, lower corrosivity, lower vapor pressure, and lower heat capacity. The phase-changing aminosilicone process has approximately 32% lower equipment capital cost compared to that of the aqueous amine process. However, this solvent is susceptible to thermal degradation at CSTR desorber operating temperatures, which could add as much as $88/tonne to the CO_2 capture cost associated with solvent makeup. Future work should focus on mitigating this critical risk by developing an advanced low-temperature desorber that can deliver comparable desorption performance and significantly reduced thermal degradation rate.

Introduction

Global concern over rising levels of atmospheric CO_2 and its implication in climate change has spawned numerous efforts aimed at mitigation greenhouse gas emissions. The U.S. Department of Energy (DOE)'s goal for Transformational Carbon Capture Technologies is the development of technologies available for demonstration by 2025 that can capture 90% of emitted CO_2 with at least 95% CO_2 purity for less than $40/tonne of CO_2 captured.

Organic materials known as alkanolamines have been the most heavily studied materials for post-combustion capture from flue gas. Of these materials, aqueous monoethanolamine (MEA) is the most widely used solvent, having been used for over half a century for natural gas purification and production of food-grade CO_2, and more recently as a candidate for CO_2 capture from flue gas. However, MEA-based systems have several negative attributes that have hindered their commercial adoption, including the huge parasitic energy demand required to heat and condense large quantities of water. This has resulted in an estimated increase in the cost of electricity (COE) of about 80% and a decrease in power plant efficiency of 30%[1], corresponding to $60-70/tonne CO_2 captured. In addition, MEA is relatively volatile, corrosive, and has poor thermo-oxidative stability.

Our research has focused on the use of aminosilicones for post-combustion CO_2 capture. Aminosilicones have lower volatility, lower corrosivity, greater thermal stability, lower heat capacity, and higher CO_2 capacity compared to aqueous amines, all of which can contribute to lower cost of capture. Many aminosilicones solidify upon reaction with CO_2, which requires use of a co-solvent for use in traditional gas absorption process equipment like packed columns. Elimination of the co-solvent can enable further reduction in CO_2 capture cost, and requires development of new process unit operations like spray absorbers.

The phase-changing CO_2 capture process developed in this project consists of three main process steps: capturing CO_2 in aminosilicone carbamate form, transporting it, and heating it to desorb CO_2 and regenerate the solvent. During the project, the effect of water on carbamate consistency was more clearly understood, which led to an evolution of the specific unit operations utilized in the process.

The phase-changing CO_2 capture process was initially envisioned to be optimized for a dry carbamate solid product and to consist of the unit operations shown in Figure 1. A dry solid carbamate salt was formed in a spray absorber. Solids were separated from the scrubbed flue gas and transported to the desorber using an extruder, which could operate at high discharge pressure. In the desorber, the solids were heated to release the captured CO_2 and regenerate the phase-changing solvent for recycle in the process. Desorption was conducted in a two-stage unit such that the first stage was operated at elevated pressure and the second stage was operated at near-atmospheric pressure.

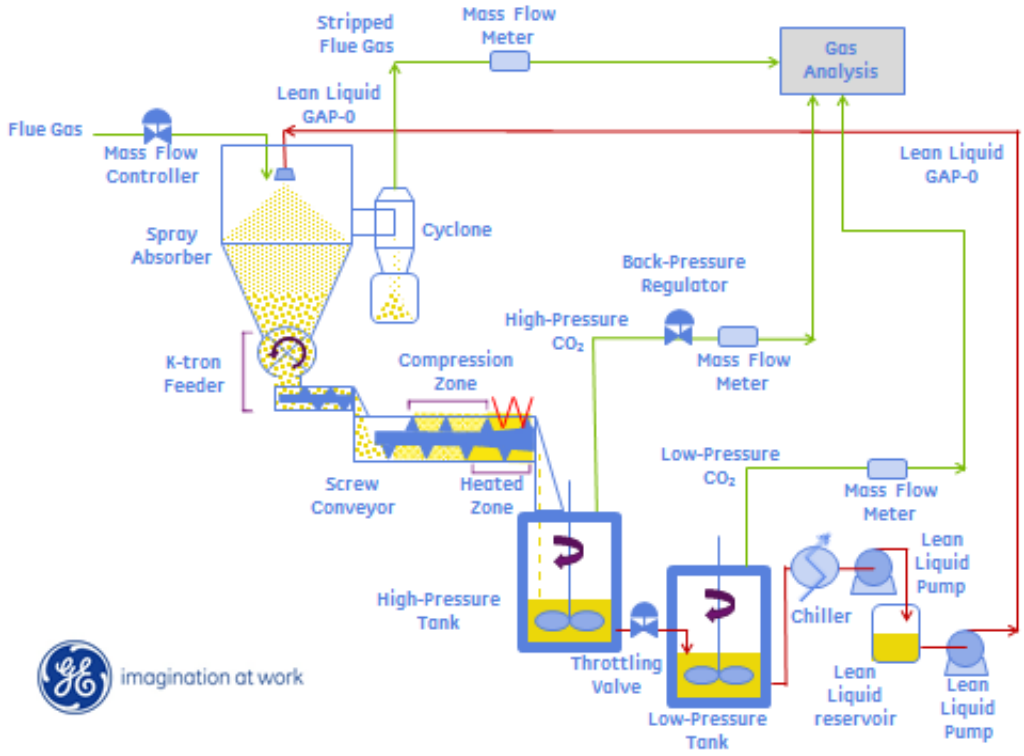

Figure 1. Original concept of phase-changing CO_2 capture process, designed for dry rich phase.

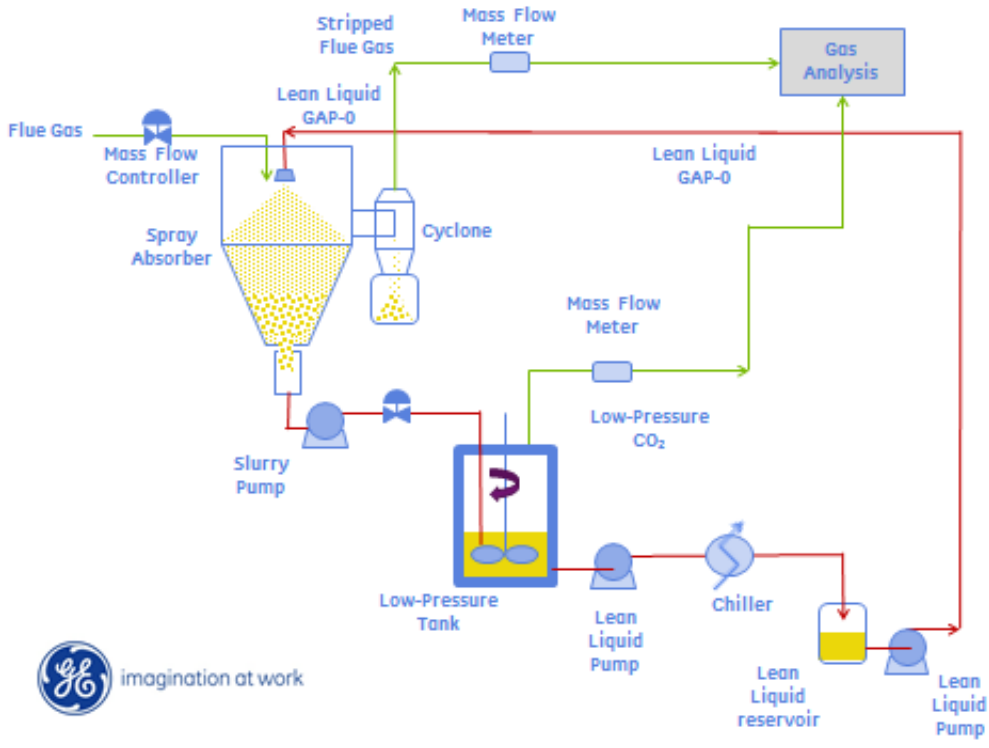

Figure 2. Phase-changing CO_2 capture process designed for slurry rich phase.

Through the execution of this project, the phase-changing CO_2 capture process concept evolved to reflect advancements in understanding of the effect of water on the carbamate and thermal stability of the carbamate, as shown in Figure 2. In the modified process, a slurry of water and carbamate solids was produced in the spray absorber. A slurry pump transported the slurry to the desorber inlet. The slurry was heated in a single stage desorber operating at near-atmospheric pressure.

In this report, the accomplishments achieved within each task will be discussed. The work contained within Tasks 2, 5, and 7 represents the evolving technoeconomic analysis of the process, the results of which will be discussed in Task 7. Accomplishments associated with the scope extension that were achieved before the close of the project will be discussed as appropriate in Task 8.

Task 1.0 – Project management and planning

The project delivered 12 quarterly technical progress reports, 2 annual continuation applications, 5 special reports, and 4 topical reports. Project updates were presented at the annual DOE CO_2 Capture Technology Meetings held in 2014, 2015, and 2016. Finally, 2 patent applications were filed based on this process. The status of project milestones is shown in Table 1.

Table 1. Milestone status summary.

Budget Period	Task	Milestone Title/Description	Planned Completion Date	Actual Completion Date	Verification Method	Comments
1	1	Updated Project Management Plan	1/31/2014	1/31/2014	Project Management Plan file	
1	1	Kickoff Meeting	12/31/2013	11/20/2013	Presentation file	
1	2.1-2.2	Preliminary process and cost modeling complete	3/31/2015	3/31/2015	Preliminary Process and Cost Modeling Report	
1	3.1	Absorber Built and Operational	12/31/2014	12/31/2014	Research Performance Progress Report file	
1	3.2	Extruder Built and Operational	3/31/2015	3/31/2015	Research Performance Progress Report file	
1	3.3	Desorber Built and Operational	12/31/2014	12/31/2014	Research Performance Progress Report file	
1	3.4	Integrated system design complete	3/31/2015	3/31/2015	Bench-Scale System Design Topical report	
2	4.2	Absorber Parameters Established	3/31/2016	3/31/2016	Unit Operations Testing Topical report	
2	4.2	Extruder Parameters Established	3/31/2016	N/A	Unit Operations Testing Topical report	stopped this effort
2	4.2	Desorber Parameters Established	12/31/2015	3/31/2016	Unit Operations Testing Topical report	
2	4.5	Continuous System Assembled	3/31/2016	3/31/2016	Research Performance Progress Report file	
2	5.1	Technology EH&S Risk Assessment	3/31/2016	4/15/2016	EH&S Risk Assessment Topical report	extension to 4/30/2016
2	5.2	Preliminary cost study completed	3/31/2016	3/31/2016	Preliminary Cost Study report	
3	6	State Point Data Table updated	9/30/2017	5/1/2017	Updated State Point table	Included in Final Report file
3	6	Continuous steady state operation demonstrated	12/31/2016	9/28/2016	Research Performance Progress Report file	
3	6	Material and energy balance for continuous bench-scale system completed	9/30/2017	5/1/2017	Final Report file	
3	7.1	Scale-up strategy completed	9/30/2017	5/1/2017	Final Report file	
3	7.2	Techno-economic assessment completed	12/31/2016	1/27/2017	Techno-Economic Analysis Topical Report file	extension to 1/31/2017
3	8.1	Continuous steady state operation of advanced desorber demonstrated	9/30/2017		Research Performance Progress Report file	stopped due to end of project
3	8.4	Techno-economic assessment of advanced desorber completed	9/30/2017		Techno-Economic Analysis Topical Report file	stopped due to end of project

Task 2.0 – Generate preliminary process and cost model

Process and economic models of the CO_2 capture system were updated to reflect the best available data relating to solvent properties and system performance. Aspen™ chemical process simulation software was used to prepare the mass and energy balances for the system. Integration of the capture system with a coal-fired power plant was performed, using a power plant model developed with Thermoflow™ software. Sensitivity of CO_2 capture cost to several different parameters, including process configuration and performance, was evaluated. This analysis yielded cases that met the target of \$50/tonne CO_2 captured, which was the goal defined for the first budget period of the project. The discussion of the technoeconomic analysis results is

presented in Task 7.2 of this report.

Task 3.0 – Design and build bench-scale system

During the first budget period of the project, the conceptual design of a process utilizing phase-changing aminosilicone CO_2 capture solvent was developed into a detailed design of a bench-scale system. The major unit operations were retrofitted from components that are typically used for other applications. Each unit operation was designed to be operated individually, to allow for optimization of each unit separately before integration of the units into a complete system. The system was designed using data generated under a previous project[2], including lessons learned from operation of the continuous laboratory-scale system built in the final year of that project. The bench-scale system was fitted with as much data acquisition instrumentation as possible, including temperatures, pressures, stream compositions, and flow rates. The system was installed at GE Global Research. The Bench Scale Design Topical Report is included in DOE's OSTI database, report number DOE-GEGR-0013687.

Task 3.1 Design and build absorber

Solvent Properties, Equilibrium Loading, and Reaction Kinetics
Physical and thermodynamic properties of GAP-0 aminosilicone obtained in the previous project[2] were used to design the bench scale system. Heat of absorption, heat capacity, surface tension, vapor pressure, and viscosity are summarized in Table 2 for reference. More complete data (for example, lean solvent viscosity, heat capacity, and vapor pressure as a function of temperature) is documented elsewhere.

Table 2. Summary of GAP-0 physical and thermal properties.

Property	GAP-0
Heat of absorption, kJ/kg CO_2	2577
Heat capacity, J/g/°C	2.2
Surface tension, dyne/cm	24.93
Vapor Pressure at 161°C, bara	0.036768
Viscosity at 25°C, cP	4.4

Equilibrium CO_2 loading of GAP-0 was measured previously[2] as a function of temperature and CO_2 partial pressure, covering the range of conditions that are expected in the absorber. Under these conditions, the reaction proceeds to at least 80% of the theoretical maximum CO_2 loading for CO_2 partial pressures up to 17mol%, as shown in Figure 3. As is clear from this data, at temperatures of 75°C and less the reaction equilibrium is strongly shifted toward absorption of CO_2 in GAP-0, and little differentiation is evident between the temperatures evaluated.

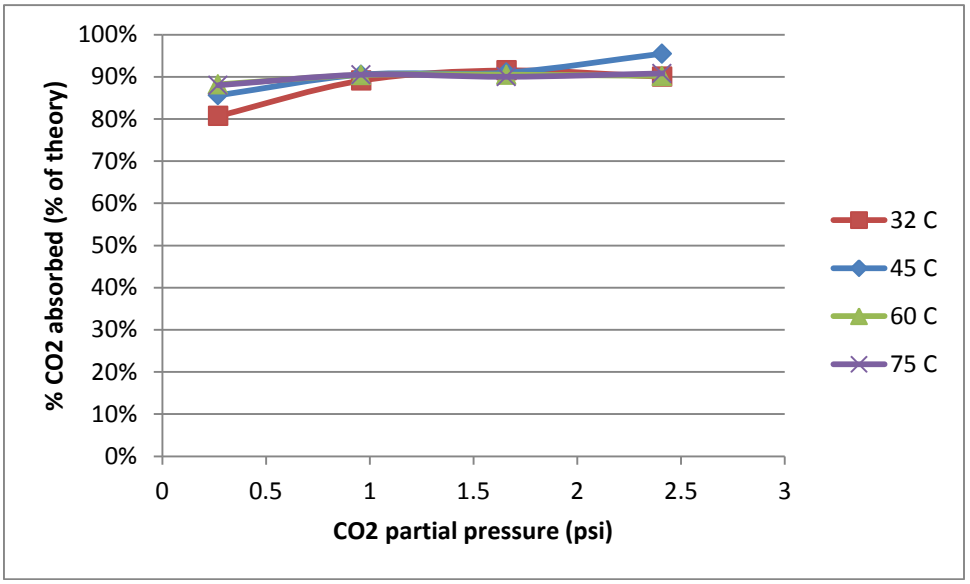

Figure 3. Equilibrium isotherms for CO_2 absorption in GAP-0.

Kinetic parameters for the absorption of CO_2 by GAP-0 were estimated previously[2] using experimental data generated for GAP-0 dissolved in triethylene glycol. This solution was used to eliminate the effect of mass transfer limitations caused by the formation of solid carbamate as the reaction proceeds.

Reactor Sizing

The bench-scale spray absorber is a co-current gas/liquid contactor in which the liquid is atomized into fine droplets for intimate contact with the gas stream. Solids must be efficiently separated from the gas stream and continuously collected from the unit for transport to the inlet of the extruder. A downward-spray arrangement is preferred for more efficient collection of the solids generated in absorption. The unit includes

sightglasses to allow for observation of the spray during operation. In the previous project[2], phase-changing spray absorption was demonstrated at the lab scale in a retrofitted spray dryer and in a custom-built spray vessel. Both of these options (custom-built and retrofit) were explored for the bench-scale absorber.

While packed column and tray tower absorber design and scale-up is achieved using a well-established set of design equations, spray absorber design and scale-up is a largely empirical procedure due to the highly complex and difficult to characterize fluid dynamics of spray absorption. For lack of a better design approach, relevant elements of the design procedure for packed column and tray tower absorbers were applied to design of the spray absorber as follows. Data obtained using the Yamato laboratory scale semi-batch spray dryer in the previous project was used to estimate the overall gas-phase mass transfer coefficient (K_Ga) for absorption of CO_2 from 16% CO_2 in N_2 using GAP-0 aminosilicone, according to Equation 1[3].

Equation 1. Calculation of overall gas-phase mass transfer coefficient.

$$K_G a = \left(\frac{G_I}{P(y_{CO2} - y^*_{CO2}}\right)\left(\frac{dY_{CO2}}{dz}\right)$$

K_Ga = overall gas-phase mass transfer coefficient
G_I = inert molar gas flux
P = total system pressure
y_{CO2} = mole fraction of CO_2 in gas phase
y^*_{CO2} = mole fraction of CO_2 in gas phase in equilibrium with liquid phase
Y_{CO2} = mole ratio of CO_2 in the gas phase
z = height of absorber

This K_Ga reflects the atomization performance of the two-fluid nozzle employed in the Yamato spray dryer and the fluid dynamics of the Yamato spray dryer. For the purpose of vessel design, this K_Ga value was assumed to be held constant for the bench scale absorber. This assumption may be valid if the bench scale absorber generates droplets of similar size to those formed in the Yamato spray dryer and if the bench scale absorber vessel can achieve similar fluid dynamics to the Yamato spray dryer. It is assumed that the latter condition can be approximated by designing the absorber vessel for the same average gas velocity as the Yamato spray dryer. The average gas residence time should also be at least as long as was typical of the Yamato spray dryer experiments. The overall height of a gas-phase transfer unit (H_{OG}) was calculated from K_Ga and the design gas feed rate and pressure[4] according to Equation 2.

Equation 2. Calculation of overall gas-phase transfer unit.

$$H_{OG} = \frac{G_M}{K_G a P}$$

H_{OG} = overall height of a gas-phase transfer unit
G_M = total molar gas flux
$K_G a$ = overall gas-phase mass transfer coefficient
P = total system pressure

As discussed in the literature[5], spray absorbers are treated as a single equilibrium stage (number of overall gas-phase transfer units N_{OG} = 1). Thus, the absorber height should be no less than the H_{OG}. The absorber height was set according to the height:diameter ratio of the Yamato spray dryer, or by the H_{OG}, whichever yielded a larger height. The absorber diameter was defined by the design gas flow rate and the desired gas velocity (assumed to be equal to that in the Yamato spray dryer). A sketch of the resulting design is shown in Figure 4.

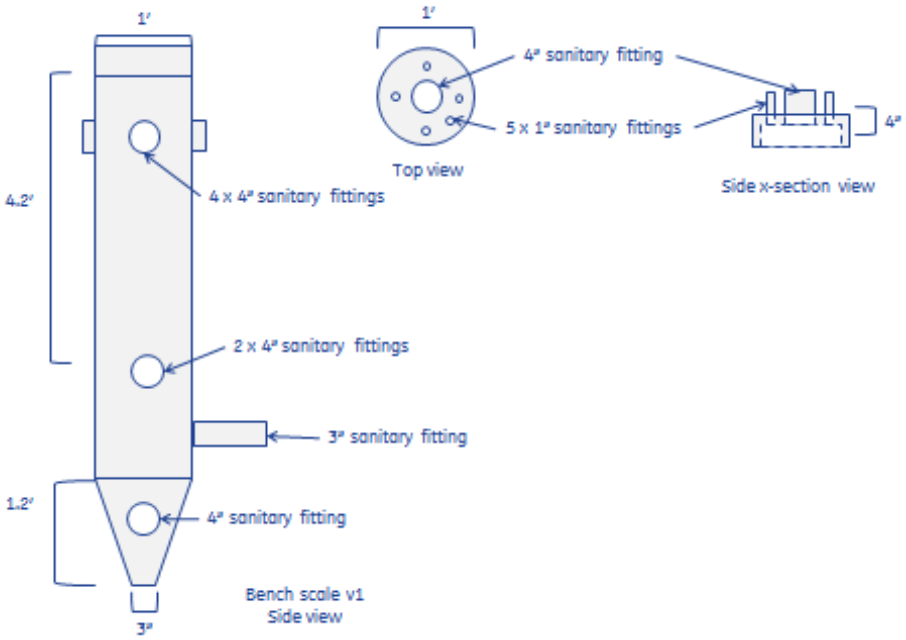

Figure 4. Sketch of preliminary spray absorber design.

The retrofit option that was evaluated was a secondhand spray dryer originally manufactured by GEA Niro. This unit, which is shown in Figure 5, offered important technical advantages over the grassroots option, as summarized in Table 3. The retrofit option has a larger reactor diameter than that specified for the grassroots option, which results in different reactor hydrodynamics as well as an increase in average gas residence time at the design basis gas flow rate. While this means that the $K_G a$ for the retrofit absorber might be meaningfully different from that of the grassroots absorber, the extended residence time may result in greater extent of conversion of the liquid during operation. The two reactors have similar heights. It is believed that either of these options would be suitable for bench-scale phase-changing spray absorption.

Figure 5. Secondhand spray dryer.

By choosing the retrofit option, the team would gain access to certain features that would be too costly to implement in a grassroots reactor design at this scale. These features include a rotary atomizer (discussed in more detail in a later section), which allows for separation of CO_2:GAP-0 stoichiometry and droplet size in experimental design, and a pneumatically-actuated lid design, which allows easy access to the reactor internals for cleaning and maintenance. Based on this technical and economic assessment, the team chose to retrofit the secondhand spray dryer for this project.

Table 3. Summary of retrofit vs. grassroots spray absorber options.

	Secondhand Spray Dryer (Retrofit)	**Spray Absorber Design (Grassroots)**
Flow mode	Co-current	Co-current
Atomizer	Rotary Atomizer Two-Fluid Nozzle	Two-Fluid Nozzle
Solids disengagement and collection	Cyclone, primary collection	Cyclone, secondary collection
Insulated	Y	Y
Lid design	Pneumatically actuated	Flanged

Atomizer Selection

Previous analysis[2] of the phase-changing aminosilicone spray absorber indicated that the absorption reaction rate is limited by liquid-side mass transfer effects. This means

that one of the critical parameters to optimize in this process is the droplet size, which directly controls the interfacial area between the gas and liquid phases in the absorber. For this reason, selection of atomizers is an important design consideration.

Research on commercially available atomizers was conducted, and suitable candidates were identified for testing in the bench scale system. Atomizers were selected based on mode of atomization, droplet size distribution, startup considerations, and liquid flow rate, as summarized in Table 4. The three atomizer types that were considered for use in this project were hydraulic nozzles, two-fluid nozzles, and rotary atomizers. The potential applicability of each of these atomizer types for the bench scale system is discussed below.

Table 4. Summary of atomizers considered for bench-scale system.

	Hydraulic Nozzle	**Two-Fluid Nozzle**	**Rotary Atomizer**
Atomization mode	Liquid pressure, internal geometry	Gas pressure	Spinning disk
Cost at bench scale	+	+	-
Droplet size	-	+	+
Droplet size during startup	-	+	+
Atomization independent of CO_2:GAP-0 feed ratio	+	-	+
Compatible with bench-scale liquid flowrate	+	+	+

Hydraulic nozzles rely on liquid pressure and the internal geometry of the nozzle to produce droplets. Benefits of hydraulic nozzles include low cost and separation of CO_2:GAP-0 reaction stoichiometry from atomization performance/droplet size. Commercially available nozzles from several manufacturers were reviewed and nozzles were identified that would achieve the desired liquid flowrate for this project. However, the droplet size distributions generated by hydraulic nozzles tend to be larger than those desired for the phase-changing spray absorber. Because the reaction rate of GAP-0 with CO_2 in the spray absorber is believed to be limited by the rate of diffusion of CO_2 through the droplet, reaction rate observed in the absorber is dominated by droplet size. Smaller droplets yield a faster reaction rate, which results in more complete conversion of GAP-0 to dry carbamate solids. Incomplete conversion of GAP-0 can result in problematic solids collection and handling. Further, droplet size tends to be larger during startup of the nozzle than during steady state operation, because the liquid pressure during startup is lower than at steady state. This startup condition was observed in the spray absorber built in a previous project[2]. For these reasons, and the availability of more suitable atomizer options, this project will not use hydraulic nozzles to atomize GAP-0.

A two-fluid, or air atomizing, nozzle utilizes a compressed gas to atomize the liquid. The mixing of the gas and the liquid may occur either internally or externally, depending on the nozzle set-up. For this system, simulated flue gas was used as the atomizing gas to avoid diluting the reactor CO_2 concentration. Because CO_2 was present in the atomizing gas, external mix nozzles were used to reduce the potential for clogging within the nozzle. Two-fluid nozzles produce very small droplets at both steady state and during startup.

In the previous project[2], a two-fluid nozzle was used at a smaller scale in the Yamato laboratory spray dryer. In those experiments, dry, flowable powder was consistently produced at a range of gas and liquid flowrates using simulated flue gas as the atomizing gas. The nozzle used in that project was an external mix nozzle manufactured by Spraying Systems. Spraying Systems recommended nozzles for scale-up based on the liquid flowrates desired for this design. As a result of those recommendations, two nozzles were purchased. The nozzles have different fluid caps, which adjust the liquid flowrate ranges. The different fluid caps could produce different droplet size distributions for the two nozzles.

Rotary atomizers rely on a rotating disk to form liquid droplets. The rotational speed of the disk is controlled by compressed air flow rate. Benefits of rotary atomizers include small droplet size both at steady state and during startup, and separation of atomization performance from reaction stoichiometry. Generally, rotary atomizers at small scale are not economic; however, the used spray dryer that was identified for this project includes a rotary atomizer. Like the spray dryer, this rotary atomizer was manufactured by GEA Niro. According to GEA Niro product literature, this atomizer is capable of forming droplets in the range of 5-25 μm at liquid flowrates of ~160mL/min, which are within the desired ranges for the bench scale system.

Task 3.2 Design and build extruder

In the bench scale system, the extruder is a pressurized transport mechanism to deliver carbamate solids from the atmospheric pressure absorber to the pressurized desorber. As in the previous project, the extruder will be a twin-screw unit that is fed by a K-Tron loss-in-weight feeder. The solids may be heated to initiate desorption within the extruder.

A K-Tron loss-in-weight feeder, shown in Figure 6, will be used in the bench-scale system to meter carbamate solids into the extruder at a uniform rate. The feeder consists of a hopper that is mounted on a load cell and feeds a rotating screw. The feeder control system varies the screw rotation speed according to the mass loss rate of the hopper. A similar unit was employed in the lab-scale system in a previous project[2].

Figure 6. K-Tron feeder for supplying carbamate solids to WP ZSK25 extruder.

The bench scale system will use a Coperion WP ZSK25 extruder having co-rotating fully intermeshing twin screws. The unit is a polymer extrusion device that will be retrofitted for the bench scale system. In the extruder, the solids are transported at a rate of 190-225g/min by rotation of the screws. The solids may be heated to initiate CO_2 desorption. The extruder screw is assembled from elements of varying geometries to allow for solids transport, heat transfer, and dynamic sealing against pressures up to 10bar. Extruder screw design involves proper selection of the screw elements and length of the shaft. The screw design used in the successful demonstration of pressurized carbamate delivery in the previous project[2] is replicated in the bench-scale extruder, and is shown in Figure 7. In Budget Period 2, screw design will be optimized for heat transfer and pressure sealing capability for the phase-changing CO_2 capture process. The screw design from the lab-scale system will be the benchmark against which future screw designs will be compared.

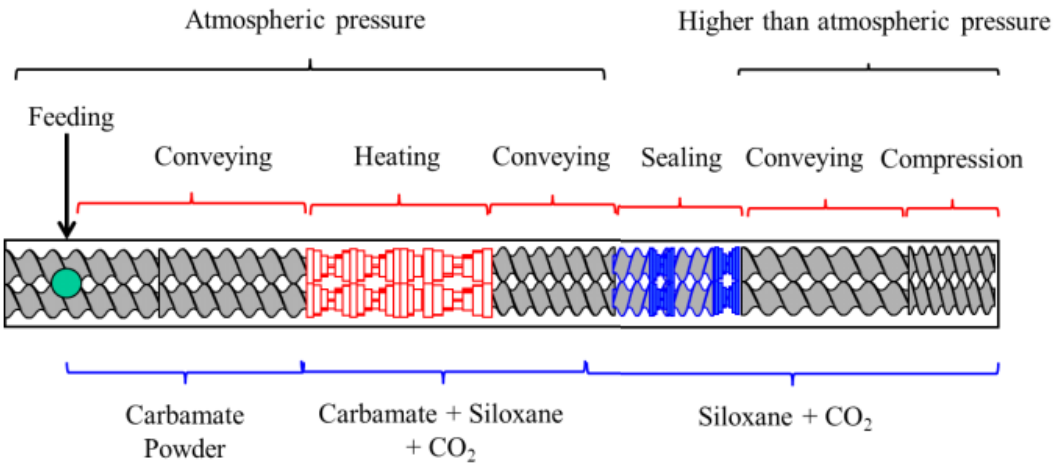

Figure 7. Conceptual extruder screw design for the lab-scale extruder used in the previous project.

It is possible to estimate the length of solids seal required in the extruder barrel to prevent back flow of CO_2 from the pressurized desorber via the Burke-Plummer equation[6], shown in Equation 3. Powder properties, including true density, bulk density, particle size, and particle sphericity, were determined previously[2] and were used in this calculation. It was estimated that length of carbamate seal required to prevent back flow of CO_2 is approximately 7 inches. This length is easily accommodated by the ZSK25 extruder specified for the bench scale system.

Equation 3. Burke-Plummer equation

$$\frac{\Delta p}{L} = \frac{1.75 \rho {V_0}^2}{g_c \Phi_s D_p} * \frac{1-\varepsilon}{\varepsilon^3}$$

Where Δp – pressure drop across the seal
L – length of seal
ρ – true density of powder
V_0- linear velocity of CO_2 back flow inside the extruder
g_c – Newton's law proportionality factor (British/SI units conversion[7])
Φ_s – particle sphericity
D_p – particle diameter
ε – powder porosity

The die plate, which is located at the outlet end of the extruder, provides a passage between the extruder barrel and die exit[5]. The die plate will include ports for extruder discharge and pressure relief, and means of attachment to the extruder barrel. Stainless steel tubing will be used to connect the die plate discharge port to the high pressure desorber. Figure 8 and Figure 9 show the die plate that was fabricated for this project.

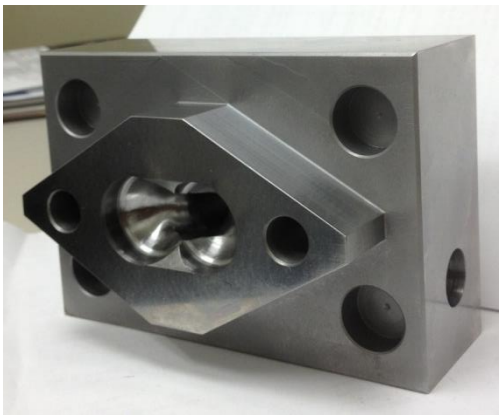

Figure 8. Die Plate for WP ZSK 25 twin screw extruder.

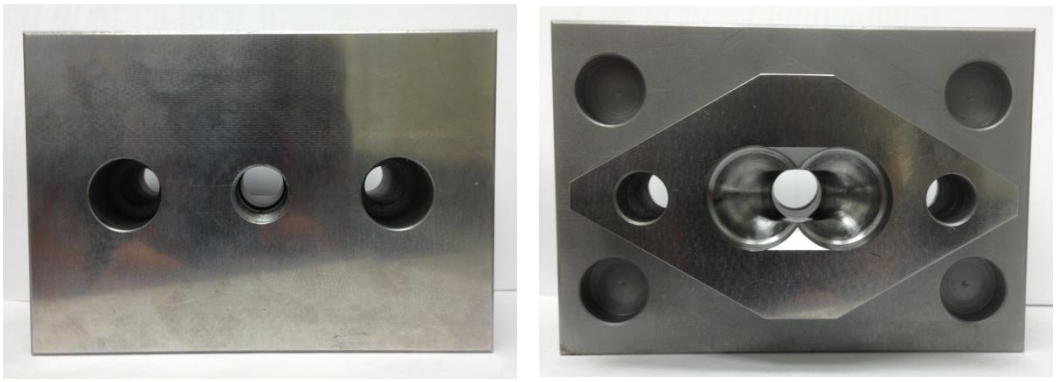

Figure 9. Die Plate for WP ZSK 25 twin screw extruder: Front and Back views.

Task 3.3 Design and build desorber

The desorber unit operation was initially designed to be a two-stage process. Extruder effluent would be fed to a pressurized desorber, in which the carbamate solids would be heated to regenerate the liquid CO_2 capture solvent and release pressurized CO_2 gas. As shown in the equilibrium isotherms in Figure 10, the hot regenerated liquid leaving the pressurized desorer would likely retain a significant CO_2 loading at elevated pressure, which must be released before the liquid can be recycled to the spray absorber. Thus the partially-regenerated solvent leaving the pressurized desorber would be heated at atmospheric pressure in a polishing desorber to finish the desorption reaction.

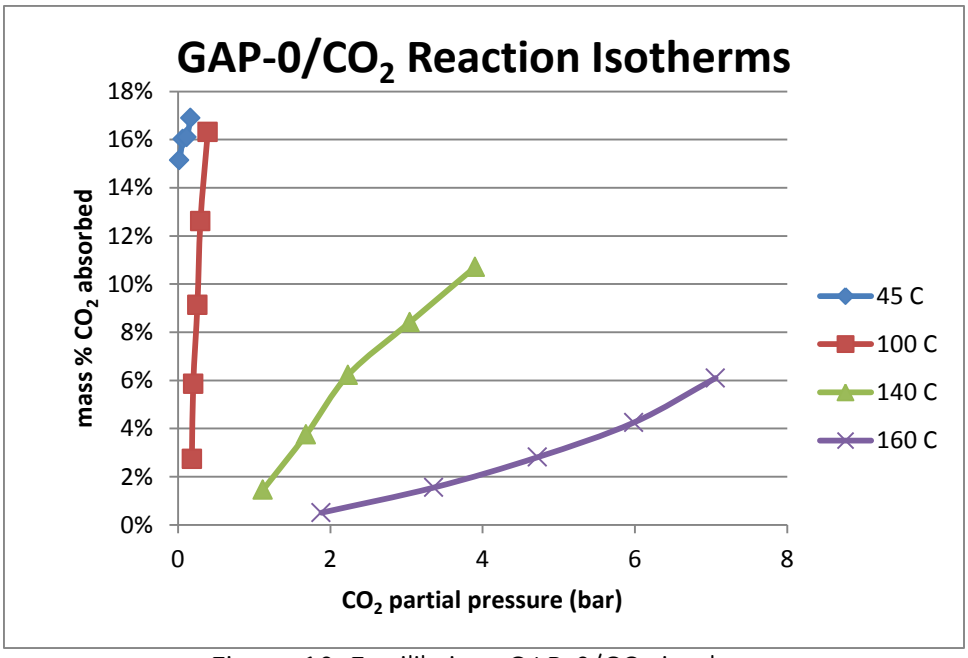

Figure 10. Equilibrium GAP-0/CO_2 isotherms.

The pressurized desorber was an electrically-heated 4L Parr pressure vessel constructed of Hastelloy C that will operate at temperatures of 140-160°C and pressures up to 10bar. The polisher will be a 5L ChemGlass 3-neck jacketed flask constructed of glass that is heated via a hot oil circulator to temperatures of 140-160°C. The system can be operated at liquid residence times in the range of 15-36 minutes. Energy balance calculations were performed around the desorption unit operations, in order to size the heaters required. It was estimated that the total energy required to heat the carbamate-rich aminosilicone leaving the extrusion process to the temperature of desorption (~140 °C) and to desorb the majority of CO_2 contained in the rich stream was ~ 2 kW. Both vessels are instrumented with liquid level controllers, temperature controllers, and pressure gauges/controllers as appropriate, and are fitted with integrated mixing capability.

As discussed in Task 4.2, the two-stage desorber concept was ultimately not impemented in bench-scale testing. Instead, a single stage atmospheric pressure desorber as described above was used.

Task 3.4 Design complete system

Simulated Flue Gas Supply System

A gas supply system was designed to generate simulated flue gas for use in bench-scale experiments. The system consisted of mass flow controllers for each of the major gas constituents (N_2, CO_2) and the toxic gas constituents (NO, SO_2), and a gas humidifier. A slipstream of simulated flue gas could be optionally used as atomizing gas for pneumatic atomizers.

The gas humidifier consisted of a heated packed bed to which water and a carrier gas (e.g., N_2) were continuously fed. As the water contacted the heated packed bed, it evaporated and was carried out of the humidifier by the carrier gas. This humidified stream was mixed with other components (e.g., CO_2) to generate the humid simulated flue gas to be fed to the absorber. The humidity of the simulated flue gas was controlled by the feed rate of water and carrier gas to the humidifier system, and was measured using a humidity sensor mounted at the absorber inlet. Optimization of the gas humidifier to deliver reproducible and robust humidified simulated flue gas is discussed in Task 4.2.

During rotary atomizer operation, all simulated flue gas was fed to the spray absorber via a circular port oriented around the atomizer. During two-fluid atomizer operation, the humidified carrier gas effluent from the gas humidifier was used as the atomizing gas. The rest of the simulated flue gas stream was fed to the spray absorber via the circular port oriented around the atomizer. In this way, the total feed rate and composition of the simulated flue gas could be controlled independently from the atomizing gas flow rate needed for two-fluid atomizer operation.

Peristaltic Pump Tubing Compatibility

In the bench-scale system, aminosilicone must be pumped into the spray absorber and from the polishing desorber to the solvent storage tank. For the bench scale system, peristaltic pumps will be used. This necessitates the use of flexible tubing that is compatible with the pump operating parameters and can withstand the chemical demands of the aminosilicone solvent. Gore style 500 peristaltic pump tubing was identified as such a material and was tested initially by filling the tube with aminosilicone and allowing the filled tube to remain in contact with the solvent for 2 weeks. No bleed through, sweating, discoloration, or embrittlement of the tubing was observed after this time. Then a continuous pumping loop was built as shown in Figure 11. The aminosilicone reservoir was a 3-neck round bottom flask with a nitrogen head space maintained to prevent unwanted carbamate formation. The aminosilicone solvent was pumped continuously for 120 hours at 100 mL/min flow rate and at ambient temperature. After this time, the tubing was again examined and no sign of any detrimental effect was observed. This tubing is the current material of choice for the peristaltic pumps for aminosilicone handling in the bench scale system.

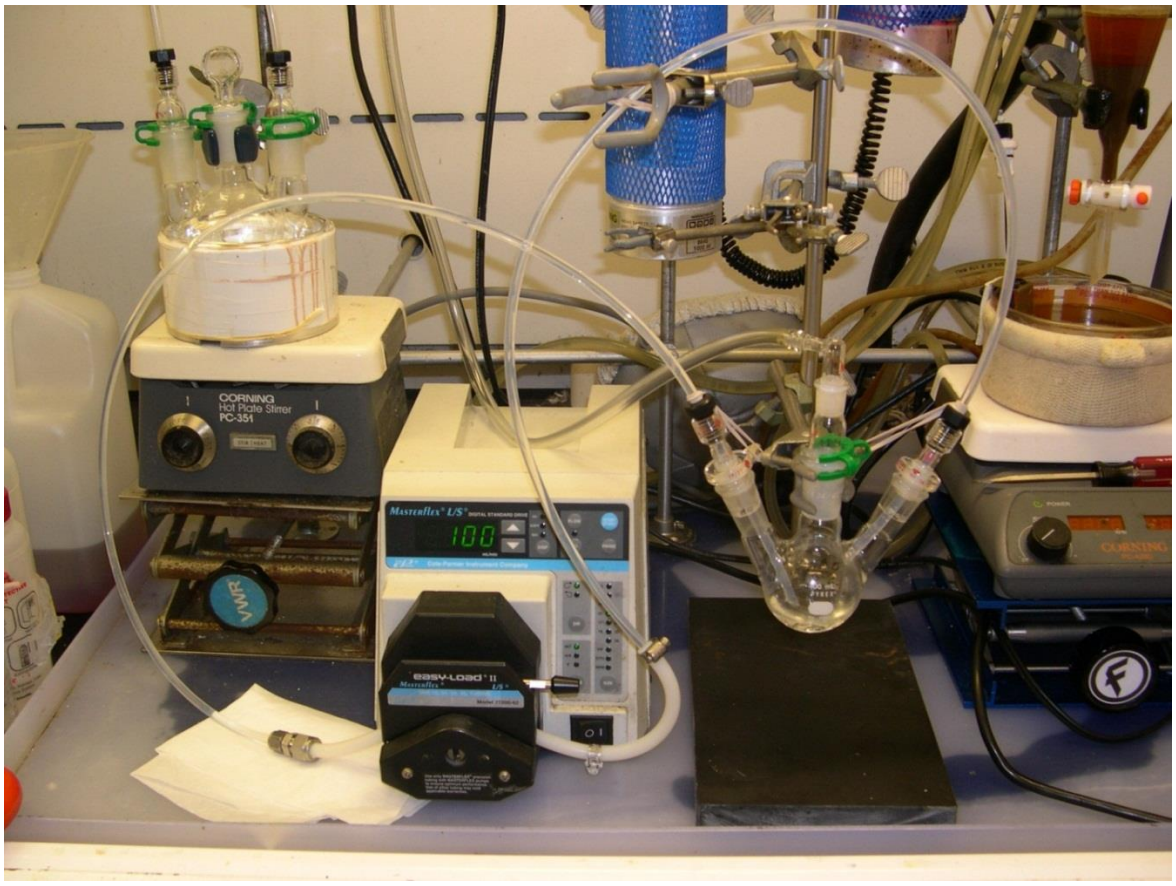

Figure 11. Peristaltic pump tubing test assembly.

Absorber/Extruder Solids Transfer

Two main modes of solids transfer from the absorber to the extruder inlet were evaluated: flexible screw conveyance and pneumatic transfer. The performance, capacity, and footprint of each of these modes were evaluated relative to the needs of the bench-scale system.

Flexible screw conveyers (for example, those manufactured by Flexicon) were of interest due to their simple mechanism of operation, but were ultimately not pursued because the smallest commercially available unit was oversized for the bench-scale system. Further, the footprint of the smallest unit was incompatible with the layout of the bench-scale system in the Process Development Facility.

A vacuum transfer system similar to that shown in Figure 12 was selected for the bench-scale phase-changing CO_2 capture system. Solids will accumulate in a vessel mounted at the outlet of the spray absorber and will be pneumatically transferred to a buffer tank mounted above the KTron inlet hopper. As the KTron inlet hopper solids inventory is depleted, the hopper will be refilled by gravity from the buffer tank. The timing of this transfer, which includes actuation of several isolation valves throughout the system, will be managed by a controls system that will be integrated with the KTron feeder loss-in-weight controller.

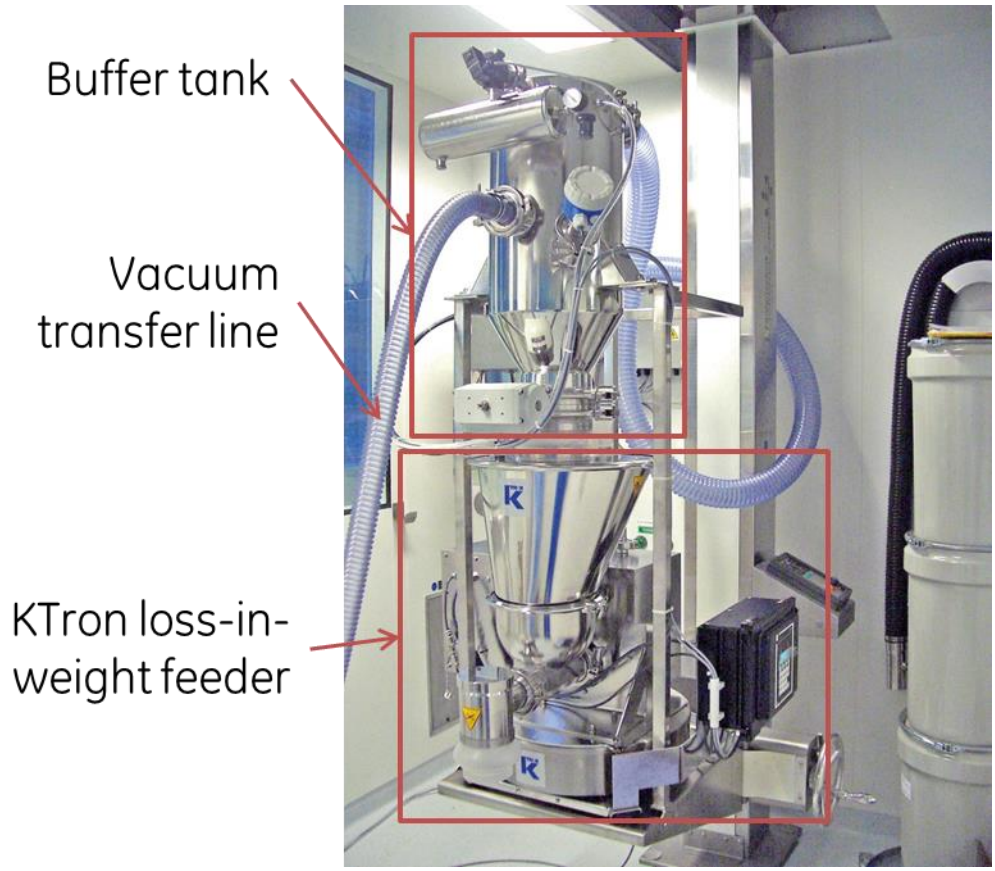

Figure 12. Example of vacuum solids transport device integrated with KTron feeder.

Extruder/Desorber Integration

A fluid connection between the extruder outlet and the desorber inlet is needed to allow for continuous operation of the desorber. A length of stainless steel tubing forms this connection, which is fitted with a three-way ball valve that allows for isolation of the extruder from the desorber during startup, shutdown, or transients. The three-way valve is pneumatically actuated. Its fail/safe position is to isolate the desorber from the extruder and provide a flow path for the extruder to discharge into a safe catch pan. The valve can be controlled by extruder stop/e-stop, elevated CO_2 concentration in the feed hopper, or manually.

Viscosity of Water-Free GAP-0/Carbamate Mixtures

For the design of the bench-scale unit and future scale-up to a pilot unit, it is crucial that the pumps that transport GAP-0/GAP-0 carbamate mixtures be of the appropriate size and power to handle the viscosity of these solutions. To address this issue, a series of GAP-0 samples with varying carbamate contents were prepared and examined via rheological measurements over several decades of shear rates and between temperatures of 30-100˚C. These data will provide guidance needed in the selection of suitable pumps and enable more accurate process modeling.

This series of experiments is differentiated from previous rheological experiments[2] with

GAP-0/GAP-0 carbamate slurries in that the current experiments were aimed at characterizing homogenous mixtures of GAP-0 liquid and GAP-0 carbamate. Previous experiments focused on slurries of solids and liquid, and were found to exhibit highly non-Newtonian rheology.

Measurements were conducted in a TA Instruments AR G2 Rheometer with a cup and bob fixture. The rheometer is fitted with pressurized and ambient pressure cells, both of which were used in these experiments. The non-pressurized cell volume was ~15 mL and the pressurized cell volume was ~9mL. Shear rates and temperatures are as shown in the plots below.

Samples for analyses were produced by heating GAP-0 carbamate powder in a round bottom flask at 120-140°C for varying periods of time. After several hours, an aliquot of the homogeneous solution was taken for solids determination via the heptane extraction method described in an earlier report[2]. In this manner homogenous samples of approximately 20, 40 and 60% carbamate were obtained. Table 5 shows the carbamate content of the samples determined by this method.

Table 5. GAP-0/GAP-0 carbamate samples for viscosity testing

Sample	% GAP-0	% GAP-0 Carbamate
A (F2131-32-1)	100	0
B (F2131-32-0)	77.4	22.6
C (F2131-32-2)	58.9	41.1
D (F2131-28-1)	42.4	57.6
E (F2131-28-2/BRWCP2)	40.2	59.8

Initially, the pressurized cell was used to measure the D and E samples. The reason for the pressure cell was to eliminate any chance of CO_2 desorption from the sample at the higher temperatures. Figure 13 and Figure 14 show that, over the temperature ranges tested and the shear rates applied, the samples exhibited Newtonian behavior; i.e. no change in viscosity vs shear rate.

The data shown in Figure 13 is corrected for the torque resistance in the rheometer. One can see that at low shear rates and high temperatures, the lines deviate from Newtonian behavior, but this may be an artifact of the very low viscosities and the inability of the instrument to make accurate measurements under these conditions.

Figure 14 (Sample E) is a repeat of the Sample D experiment. Again, Newtonian behavior was observed for samples heated between 40˚C–80˚C, but the 30˚C sample behaved oddly; perhaps because of solidification in the rheometer. At the highest temperature, the sample did not show linear behavior. After testing at 100˚C, the sample was retested at 90˚C. No change in viscosity was observed, indicating that no CO_2 desorption had occurred.

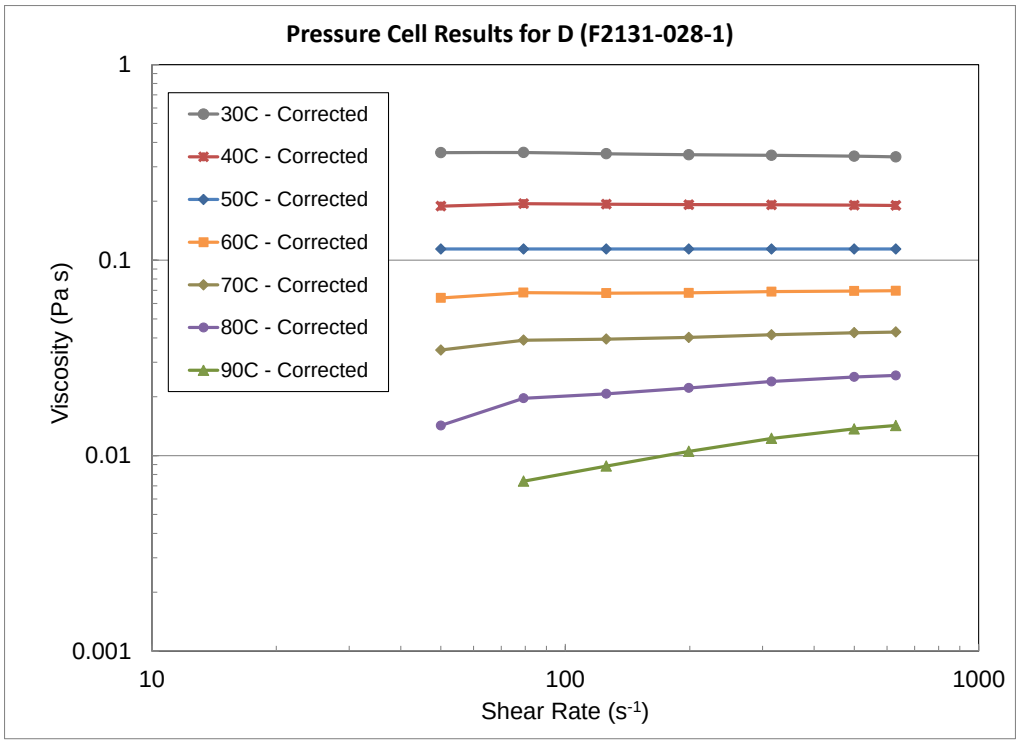

Figure 13. Results for Sample D

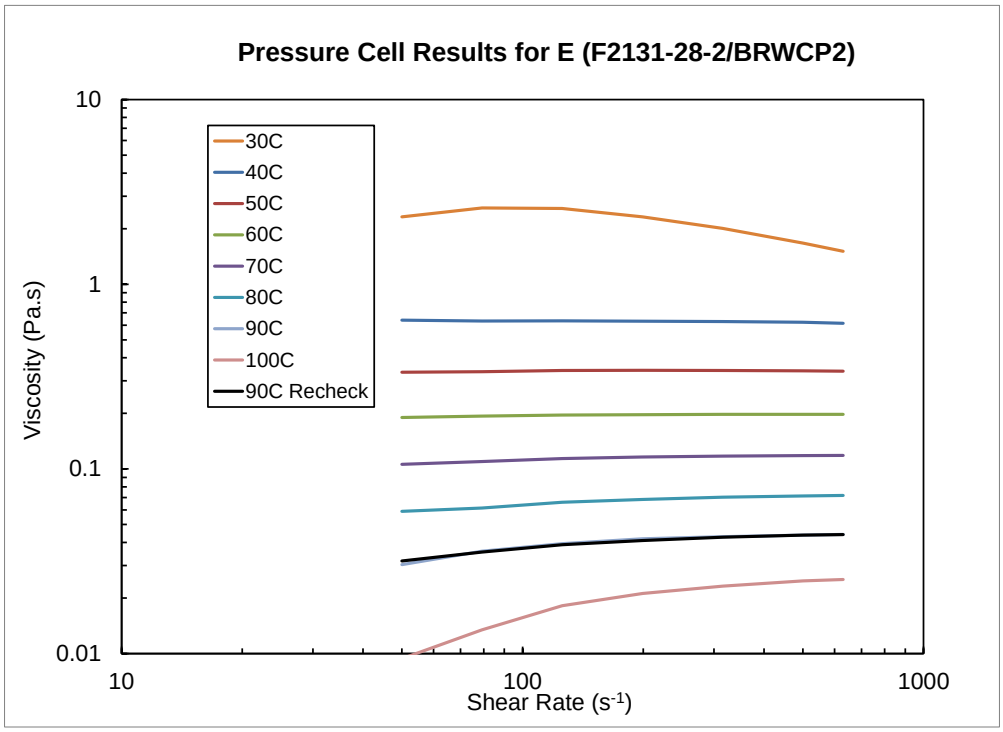

Figure 14. Results for Sample E

The one observation that was puzzling was that the viscosity data for a given temperature were not consistent between samples D and E. For instance, at 100sec^{-1}, the 50˚C results showed a viscosity of 0.35Pa-s for E and 0.13Pa-s for D. The same trend was seen for all temperatures. One possible explanation was that, with the pressure cell in operation, the sensitivity of the rheometer was diminished and the values obtained for samples D and E were within experimental error of each other. As a result, use of the pressure cell was discontinued and the remaining experiments were conducted at atmospheric pressure. Results for Samples A, B, and C are shown in Figure 15, Figure 16, and Figure 17.

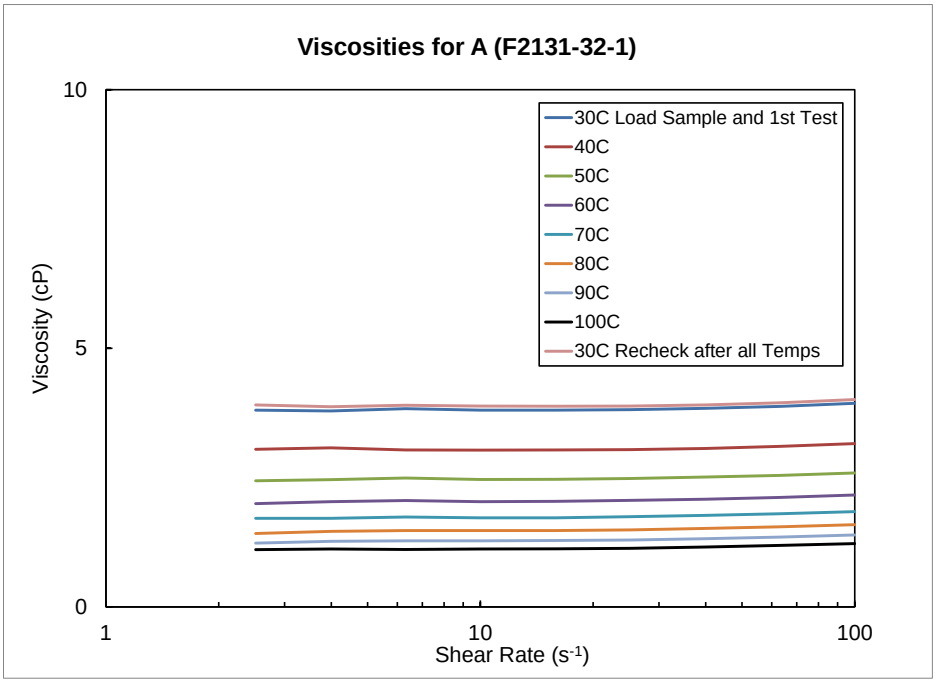

Figure 15. Viscosities for Sample A

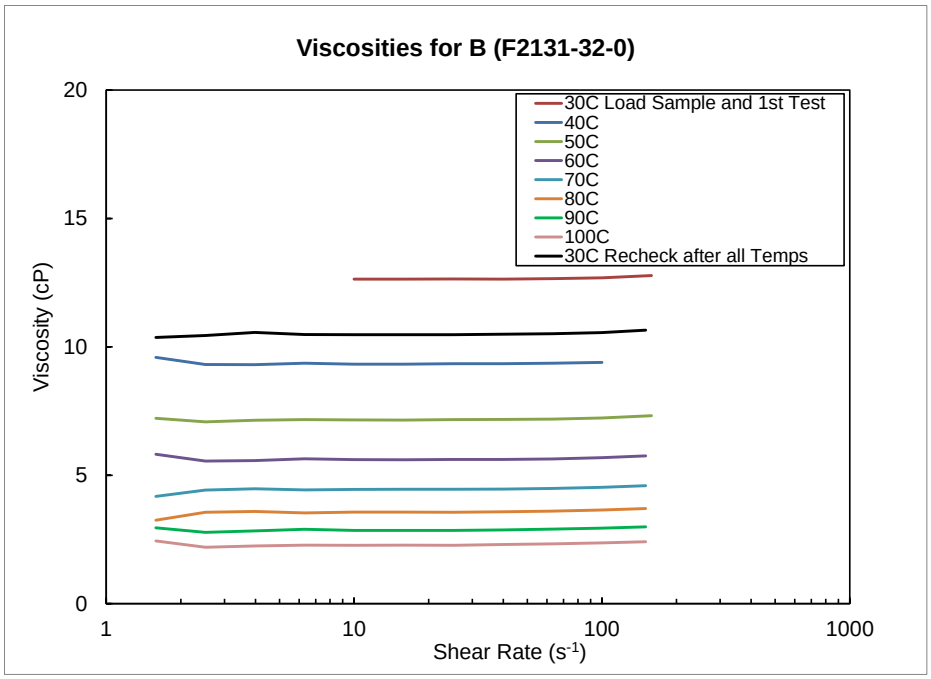

Figure 16. Viscosities for Sample B

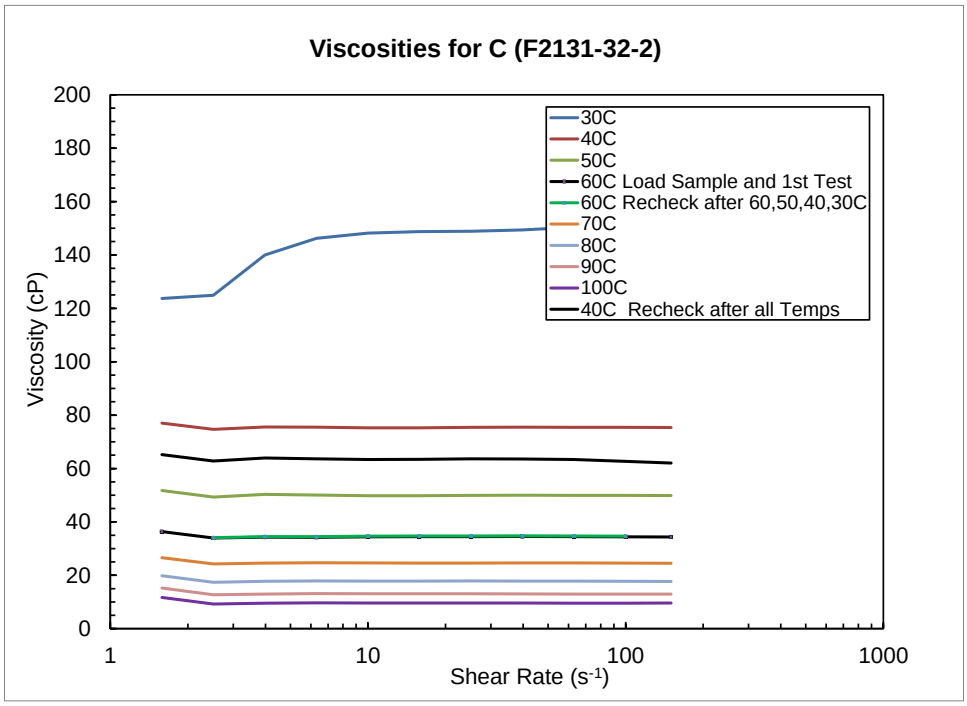

Figure 17. Viscosities for Sample C

With the exception of the 30˚C run for Sample C, all materials showed Newtonian performance. On heating, some loss of CO_2 did occur as shown by the hysteresis in the 30 and 40˚C temperature profiles for Samples B and C.

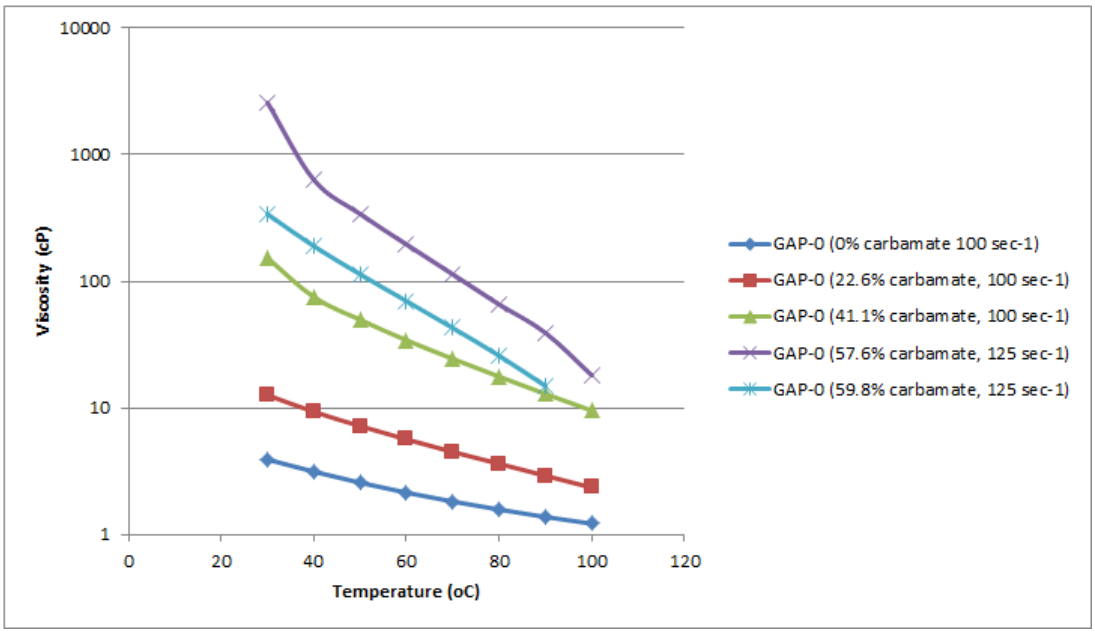

Figure 18. Compiled Viscosities for all runs

Figure 18 shows the compiled data from all the runs. Taking into account the possibility that data from samples D and E were within experimental error of one another, the average was taken and substituted in the plot in Figure 19. The data graphed are at shear rates of 100-125sec^{-1}, which were chosen for convenience. Since the fluids were Newtonian (independent of shear rate), it did not matter which shear rates were picked.

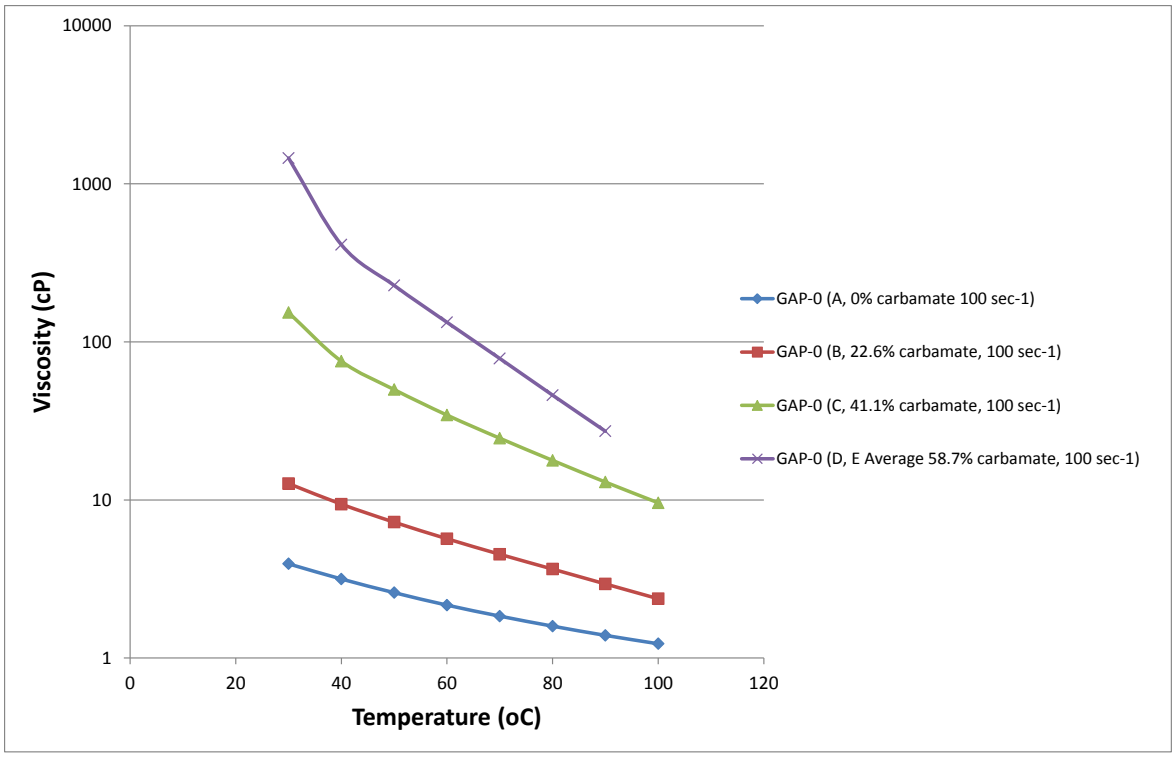

Figure 19. Revised Summary Plot

These viscosity data were used to aid in pump selection for liquid transport as the phase-changing CO_2 capture process is scaled up, and in process models of the commercial system. These results are for water-free GAP-0/carbamate mixtures; mixtures including water are reported in Task 4.5.

Slurry Transport

Per the results of experiments discussed in Task 4.2, the bench scale system was ultimately modified to support the production of a rich slurry phase, rather than rich dry solids. These modifications include replacement of the extruder and dry solids transport system with a slurry pump, and are discussed in Task 4.5.

Lean Solvent Recycle

The lean aminosilicone liquid exiting the polisher was cooled and sent to a solvent storage tank for recycle to the absorber. The heat duty required to cool the aminosilicone from 160°C to 30°C was calculated, and a suitable heat exchanger was selected. A peristaltic pump fitted with chemical-resistant tubing was used to facilitate this transfer.

Task 4.0 – Perform bench-scale testing on unit ops

During the first budget period (BP1) of the project, a bench-scale process utilizing phase-changing aminosilicone CO_2 capture solvent was designed, constructed, and installed at GE Global Research. During the second budget period (BP2) of the project,

the bench-scale unit operations of the phase-changing CO_2 capture process were tested individually to define the operating parameters for each unit that yielded the desired unit performance. Effects of scaling up from the lab-scale system were quantified. Experiments were conducted to inform selection of suitable materials of construction. The bench scale unit operations were assembled into a continuous system to support steady state system testing to be conducted in the third budget period (BP3) of the project. The Unit Operations Testing Topical Report is included in DOE's OSTI database, report number DOE-GEGR-0013687-2.

Task 4.1 Procure solvent

A 60-kg sample of the phase-changing aminosilicone CO_2 capture solvent, GAP-0, was procured in Budget Period 1 to support equipment commissioning activities and individual unit operations testing. In BP2, an additional 400kg of GAP-0 was ordered to support bench-scale continuous system experiments. The same supplier was selected for both solvent orders, and the same product quality was specified. The second shipment of GAP-0 solvent was received in November 2015 and met the product quality specifications.

Task 4.2 Determine operating parameters for unit ops

The goal of this task was to establish the operating window for each unit operation on an individual basis, and for the operators to gain experience running each unit. The effect of varying primary process parameters on unit performance was measured, and correlations between these parameters and unit performance were created as appropriate. Analytical methods (i.e., mass spectrometer, CO_2 analyzer, IR probe) that were built into the bench scale unit operations were brought online. A summary of the process parameters varied and the performance parameters that were measured is shown in

Table 6. This table also defines the performance parameters to be optimized for each unit operation.

Table 6. Summary of parameters varied, measured, and optimized in bench-scale unit operations testing.

	Absorber	Extruder	Desorber/Polisher
Vary	• Gas inlet composition • Gas flow rate • Liquid flow rate • CO_2 : GAP-0 mole ratio • Atomizer type • Atomizer operation	• Solids flow rate • Screw RPM • Screw design • Barrel T profile • Outlet pressure	• Feed rate • Temperature • Pressure • Agitation rate • Residence time
Measure	• % CO_2 capture • % GAP-0 conversion • Gas outlet T • Solids quality	• Maximum delivery pressure	• % GAP-0 conversion • CO_2 flow rate
Optimize	High % GAP-0 conversion (high quality solids)	High delivery pressure (stable solids seal)	• High CO_2 desorbed at pressure (desorber) • Complete solvent regeneration (polisher)

Absorber Experiments in Dry Simulated Flue Gas

The goal of this series of experiments was to define the operating conditions for each inlet CO_2 concentration setpoint that produced dry, flowable carbamate solids. The effect of CO_2 feed concentration, liquid flow rate, and feed gas flow rate was evaluated using a rotary atomizer. The ranges of each absorber parameter studied are shown in Table 7. Gas and liquid flow rates were selected to ensure that solids formation is possible for each CO_2 inlet composition studied (i.e., molar excess CO_2 relative to GAP-0).

Table 7. Ranges of parameters to be studied in absorber unit operation testing.

Parameter	Range
Gas Feed Composition (mol% CO_2)	1.6-100%
Gas Flow Rate (slm)	100-500
Liquid Flow Rate (mL/min)	25-200
CO_2 : GAP-0 Mole Ratio	>1.1
Atomizer Type	Rotary atomizer Pneumatic nozzle
Atomizer Operation	Rotary atomizer: RPM 0-100% Pneumatic nozzle: Atomizing gas flow rate

Absorber performance was quantified using the methods shown in Table 8. The extractables method used to evaluate the solids outlet composition is a wet-chemistry technique wherein the solids product is mixed with a solvent in which GAP-0 is soluble but GAP-0 carbamate is insoluble. The mass of unreacted GAP-0 that is extracted from the solid by the solvent is quantified. Solids composition is an important parameter, both for mass balance calculations and for evaluation of the solids handling behavior (e.g., flowability) of the carbamate.

Table 8. Measurement methods for performance parameters evaluated in absorber unit operation testing.

Parameter	Measurement Method
% CO_2 Capture (mol%)	Calculated from gas inlet/outlet and liquid inlet/solid outlet compositions
% GAP-0 Conversion (mol%)	Calculated from liquid inlet/solid outlet compositions
Gas Outlet Temperature (°C)	Thermocouple
Gas Inlet/Outlet Compositions	Mass spectrometer (online) CO_2 analyzer (online)
Liquid Inlet Composition	NMR (offline) IR (offline)
Solids Outlet Composition	Extractables measurement (offline)

The first spray experiments in the absorber were conducted at high CO_2 feed concentration and low gas and liquid flow rates. These conditions, which correspond to high mass transfer driving force, high average gas residence time, and low droplet size, represent the most favorable conditions for solids formation. In subsequent experiments the feed CO_2 concentration and gas and liquid flow rates were incrementally transitioned to more realistic conditions.

Following this transition, an experiment series was designed to explore the effects of feed CO_2 concentration, feed GAP-0 : CO_2 mole ratio, and feed gas flow rate on carbamate quality in dry simulated flue gas. The data from this series of experiments yielded a transfer function quantifying the effects of gas flow rate, feed CO_2 concentration, and feed GAP-0 : CO_2 mole ratio on solids quality. This experiment was a 2-level factorial with a center point and star points assigned to GAP-0 : CO_2 mole ratio and is summarized in Figure 20. The lower limit for feed CO_2 concentration was set to model the later stages in the commercial spray absorber concept described in the Preliminary Process and Cost Modeling Report[8]. In this absorber concept, absorption is achieved in multiple stages in which lean aminosilicone is sprayed in each stage and the flue gas CO_2 concentration at the inlet to each stage decreases with each subsequent stage.

Variable	Minimum	Maximum	Low "Star"	High "Star"
Feed CO_2 Concentration	2mol%	16mol%	-	-
GAP-0:CO_2 Mole Ratio	0.6	1	0.5	1.1
Gas Flow Rate	150slm	200slm	-	-

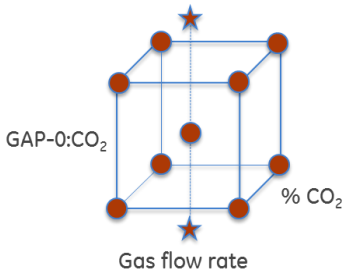

Figure 20. Summary of absorber designed experiment.

All experiments shown in Table 9 were conducted using the rotary atomizer at constant disc speed. The rotary atomizer is driven by a compressed air drive mechanism. In preliminary tests with the rotary atomizer[9], a sharp increase in atomizer disc speed was observed at 7scfm compressed air flow rate. In the first GAP-0 spray experiment in the absorber, the atomizer flow rate was initially set to 3scfm, at which condition large droplets of liquid were produced. As the atomizer flow rate was increased to 10scfm, the droplets transitioned to a fine mist. Because small droplet size is important for fast absorption kinetics, subsequent experiments were conducted at 10scfm.

Table 9. Absorber experiments conducted in dry simulated flue gas.

Run ID	Liquid flow rate - setpoint (mL/min)	Gas flow rate (slm)	Gas composition (mol% CO2 in N2)	GAP0/CO2 molar ratio	Atomizer	Est. avg. gas Residence time (min)	mol% GAP-0 conversion (per extractables)	mol% CO2 conversion (per extractables)	mol% CO2 conversion (per CO2 analyzer)
2015-04-29	50	50	100%	0.09	rotary	8.0	95.6%	8.5%	
2015-05-01	50	50	100%	0.09	rotary	8.0			
	200	50	100%	0.35	rotary	8.0			
2015-05-06	50	50	50%	0.18	rotary	8.0			
	200	50	50%	0.71	rotary	8.0			
2015-05-07	200	100	50%	0.35	rotary	4.0	93.8%	33.3%	19.7%
2015-05-13	50	100	20%	0.22	rotary	4.0			
	200	100	20%	0.89	rotary	4.0			
2015-05-14	50	200	25%	0.09	rotary	2.0			
	200	220	25%	0.32	rotary	1.8			
2015-05-27	200	200	16%	0.55	rotary	2.0	89.5%	49.6%	50.7%
2015-05-29	200	150	16%	0.74	rotary	2.7	88.3%	65.2%	53.5%
2015-06-02	100	200	16%	0.28	rotary	2.0	93.2%	25.8%	34.5%
2015-06-04	170	150	16%	0.63	rotary	2.7	89.7%	56.3%	55.3%
2015-06-05	200	200	8%	1.11	rotary	2.0	61.2%	67.8%	71.8%
2015-06-11	270	150	16%	1.00	rotary	2.7	76.5%	76.3%	64.1%
2015-06-12	360	200	16%	1.00	rotary	2.0	66.9%	66.8%	60.1%
2015-06-25	160	150	16%	0.59	rotary	2.7	86.2%	50.9%	57.0%
2015-07-01	30	200	2%	0.66	rotary	2.0	78.5%	52.2%	57.7%
2015-07-02	140	175	9%	0.79	rotary	2.3	77.5%	61.1%	64.5%
2015-07-09	30	150	2%	0.89	rotary	2.7	70.6%	62.6%	74.2%
2015-07-10	220	200	16%	0.61	rotary	2.0	83.0%	50.6%	54.1%
2015-07-16	80	175	9%	0.45	rotary	2.3	91.6%	41.3%	49.1%
2015-07-22	20	150	2%	0.59	rotary	2.7	83.2%	49.2%	51.0%
2015-07-23	200	175	9%	1.13	rotary	2.3	67.9%	76.4%	74.5%
2015-09-10	140	175	9%	0.79	rotary	2.3	79.4%	62.5%	61.8%
2015-09-14	40	200	2%	0.89	rotary	2.0	71.2%	63.1%	73.9%

Carbamate solids were formed at all conditions tested under dry conditions, across a range of GAP-0 conversion of 61-96mol% as measured by the extractables technique. CO_2 conversion inferred from the extractables technique was in reasonable agreement with that inferred from online measurement of the absorber effluent gas CO_2 concentration. To satisfy the success criterion of 90% GAP-0 conversion in a single stage, the GAP-0 : CO2 molar feed ratio should be low (i.e., excess CO_2 conditions). It is anticipated that multiple absorption stages will be needed to achieve 90% CO_2 capture.

Gas and solid outlet temperature was monitored during spray absorption at the point of solids separation from the absorber effluent gas. Because the reaction of GAP-0 with CO_2 is exothermic, the temperature of the gas and carbamate solids increases during a spray experiment. The magnitude of the temperature rise observed was comparable to that observed in previous experiments at the lab scale. For example, as shown in Figure 21, the gas temperature increased from approximately 27°C (ambient conditions) to approximately 55°C and solids temperature reached approximately 50°C during a typical spray experiment conducted in dry conditions. This outlet temperature is within the range of temperatures at which CO_2 absorption by the phase-changing aminosilicone solvent is favored.

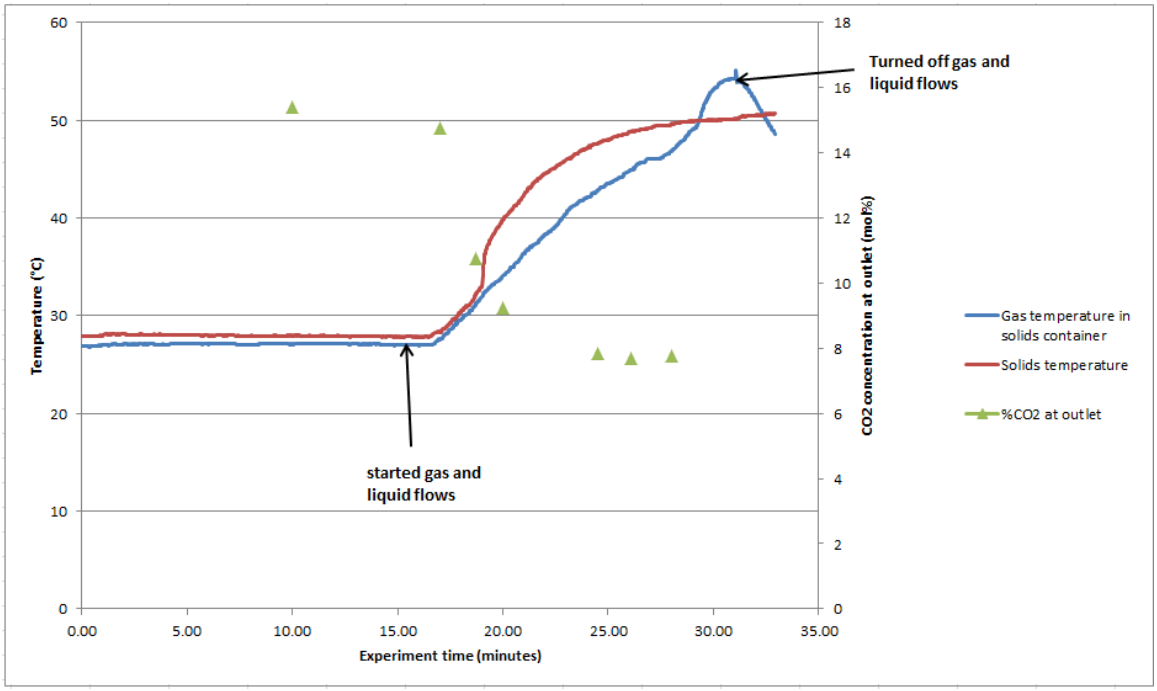

Figure 21. Temperature rise with CO_2 absorption in bench-scale absorber.

Average particle size was measured for carbamate powders produced in dry flue gas, as shown in Table 10. These results lend insight to the order of magnitude of the droplet size produced by the rotary atomizer with the phase-changing solvent. This range, 1-48 microns, is consistent with droplet size predicted by correlations found in the literature[10,11] for rotary atomizers.

Table 10. Particle size of carbamate solids generated in dry flue gas.

Run ID	Liquid flow rate setpoint (mL/min)	Gas flow rate (slm)	Gas composition (mol% CO2 in N2)	GAP0/CO2 molar ratio	Avg. Particle Size (um)
2015-05-07	200	100	50%	0.35	48.3
2015-05-27	200	200	18%	0.49	14
2015-05-29	200	150	16%	0.74	21.5
2015-06-02	100	200	16%	0.28	23.9
2015-06-04	170	150	16%	0.63	24.2
2015-06-05	200	200	8%	1.11	21.3
2015-06-11	270	150	16%	1.00	45.1
2015-06-12	360	200	16%	1.00	10.2
2015-06-25	160	150	16%	0.59	40
2015-07-01	30	200	2%	0.66	43.4
2015-07-02	140	175	9%	0.79	20.5
2015-07-09	30	150	2%	0.89	5.4
2015-07-10	220	200	16%	0.61	24.3
2015-07-16	80	175	9%	0.45	0.92
2015-07-22	20	150	2%	0.59	38.8
2015-07-23	200	175	9%	1.13	9
2015-09-10	140	175	9%	0.79	17.6
2015-09-14	40	200	2%	0.89	16.3
2015-10-15	160	150	16%	0.59	12.4

Simulated Flue Gas Humidifier Optimization

In experiments conducted in the previous project[12] involving absorption with humid simulated flue gas, solid carbamate was formed both in a stirred flask and in the lab scale spray absorber. Based on these results, absorption testing with humid simulated flue gas in this project was scheduled for BP3. However, during bench-scale testing in BP2, it was observed that GAP-0 carbamate solids often liquefied in ambient conditions having high humidity. As a result, humid absorption experiments were conducted earlier than initially planned. These experiments were designed to confirm solids formation during CO_2 absorption from a humid gas, at moisture loadings that are representative of coal-fired power plant flue gas (up to 40°C dewpoint / 7vol% water vapor).

Optimization of the gas humidifier system was needed to ensure robust and reproducible simulated flue gas humidity. Humidifier experiments were completed to determine the experimental conditions necessary to reliably produce a gas stream with a dew point in the range of 38-40°C. The dew point was measured after the gas leaving the humidifier has mixed with the gas stream entering the absorber. The initial experimental conditions for the first test are summarized in Table 11.

Table 11. Initial experimental conditions for humidifier testing on 3/2/16.

Parameter	Value
Nitrogen flowrate to humidifier	47 SLM
Nitrogen flowrate to absorber	103 SLM
Ambient temperature	21°C
Ambient relative humidity	9.7%
Initial band heater limit temperature	375°C
Initial band heater setpoint	300°C
Temperature of gas in humidifier prior to water addition	258°C
Water flowrate	8 mL/min

The results for the humidifier temperature and the dew point are provided in Figure 22. It was noted that the inlet gas temperature was approximately the same as the dew point using these experimental conditions. To maintain the inlet gas temperature above the dew point, the setpoint for the band heater temperature was increased to 340°C, and the limit temperature for the band heater was increased to 450°C. The actual temperatures on the temperature controller were in the range of 330-335°C for the band heater and 400-418°C for the limit after the setpoint changes were applied.

At the end of the experiment, the dew point and gas inlet temperature were 40°C and 47°C, respectively. The steam temperature was 166°C. It was noted during this experiment that the location of the inlet gas temperature measurement should be changed to avoid water build-up on the thermocouple over time.

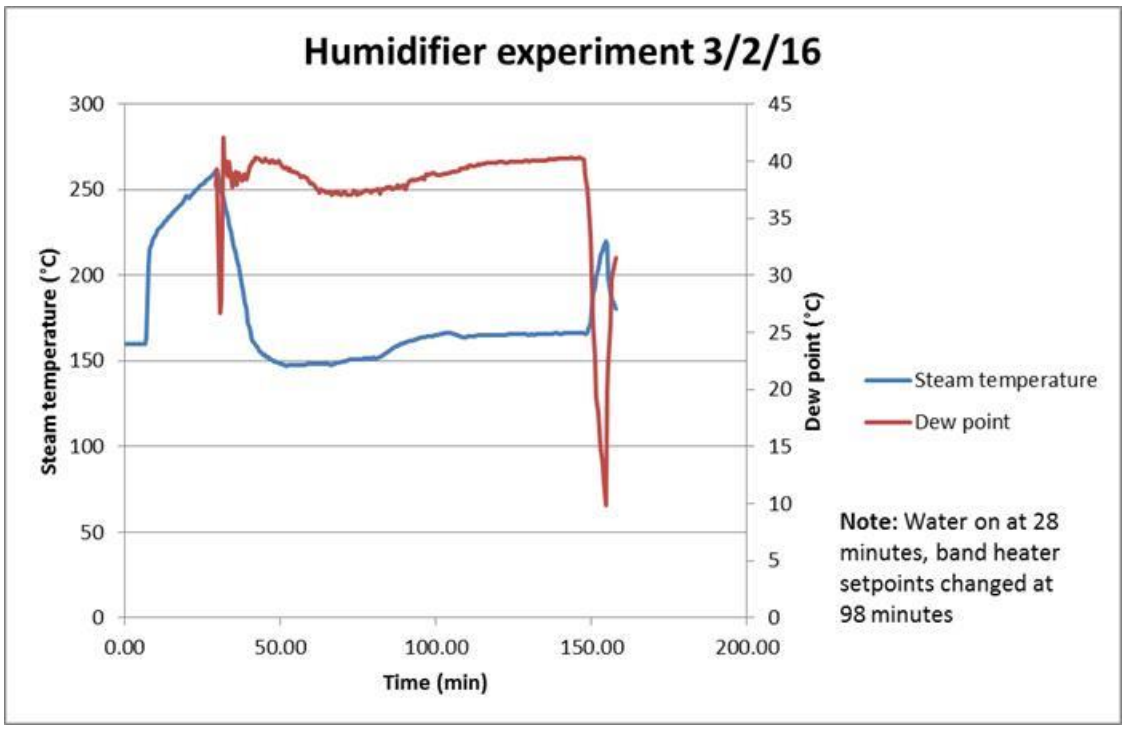

Figure 22. Results of 3/2/16 humidifier reproducibility experiment.

A second experiment was completed to confirm that the same dew point could be achieved again under similar conditions. These experimental conditions are summarized in Table 12. The results for the conditions summarized in Table 12 are provided in Figure 23. This experiment showed a very stable result for the dew point of approximately 40°C. The steam temperature was approximately 175°C.

Table 12. Initial experimental conditions for humidifier testing on 3/7/16.

Parameter	Value
Nitrogen flowrate to humidifier	47 SLM
Nitrogen flowrate to absorber	103 SLM
Ambient temperature	29.2°C
Ambient relative humidity	12.8%
Band heater limit temperature	450°C
Band heater setpoint	340°C
Temperature of gas in humidifier prior to water addition	283.6°C
Water flowrate	8 mL/min

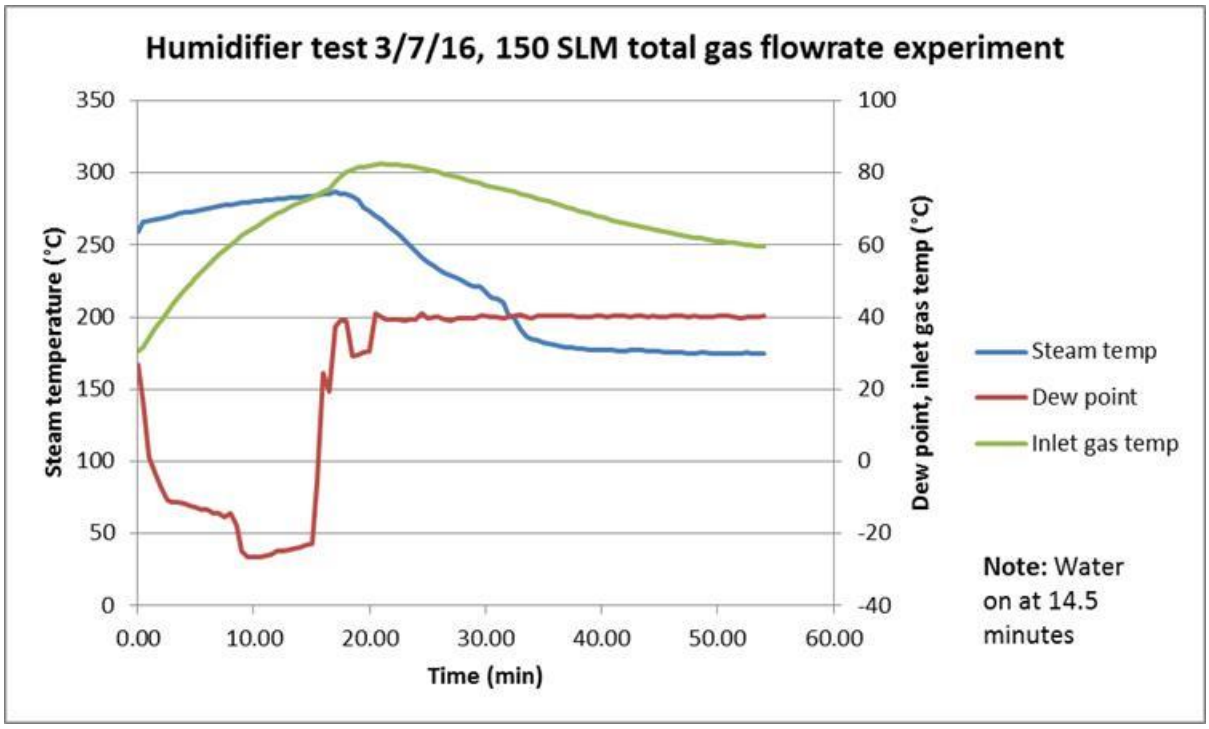

Figure 23. Results for 3/7/16 humidifier experiment at 150 SLM total gas flowrate.

To determine the effect of increased gas flowrates on the humidifier performance, the flowrate of nitrogen to the absorber was increased from 103 SLM to 153 SLM for a total of 200 SLM gas flowrate to the absorber. Water flowrates of 5, 8, 9, 10 and 11 mL/min were tested in this experiment. Table 13 lists the times when the water flowrate changes were made during this experiment. The results are provided in Figure 24.

Table 13. Water flowrate changes for 200 SLM gas flowrate experiment.

Water flowrate (mL/min)	Start time (min)
8	0
9	2
10	5
11	42
5	47

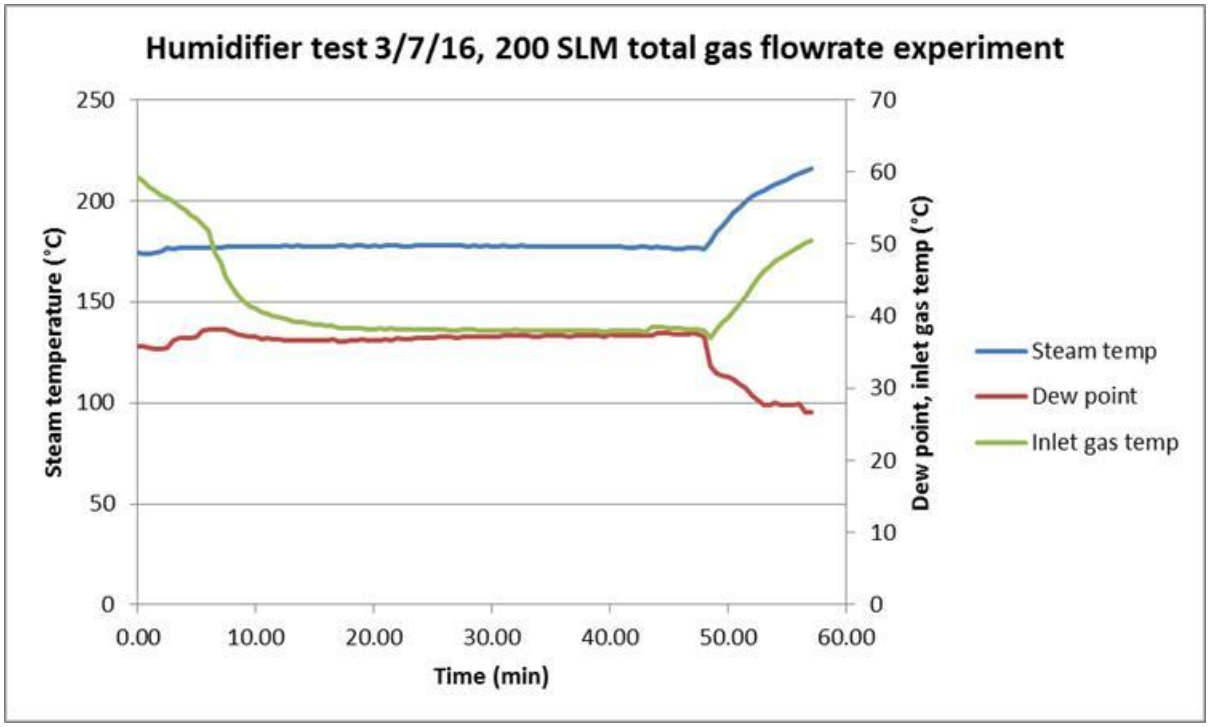

Figure 24. Results for 3/7/16 humidifier experiment at 200 SLM total gas flowrate.

The desired dew point range (38-40°C) was not reliably achieved for the 200 SLM gas flowrate experiment. Though the steam temperature was very similar to the 150 SLM gas flowrate experiments, the dew point was in the range of 35.4 to 37.6°C when the water flowrate was increased from 8 to 11 mL/min. The inlet gas temperature was only slightly higher than the dew point for these experiments. It is not known if this is an issue with the placement of the thermocouple used for that measurement, but it does raise a concern regarding the potential for condensation under these experimental conditions.

After the 200 SLM experiments were completed, a short repeat test using the conditions in Table 12 was completed to confirm that the system would return to the 40°C dew point at 150 SLM. When the gas and water flowrates were adjusted accordingly, the dew point was 40.6°C, with an inlet gas temperature of 63.8°C and a steam temperature of 177.8°C, which is consistent with the results from earlier in the

day. The results obtained in these experiments indicate that the system can more reliably produce a gas stream with the target dew point at a total gas flowrate of 150 SLM with the current experimental set-up.

Absorber Experiments in Humid Simulated Flue Gas

Spray absorption experiments were conducted at increasing levels of humidity in the simulated flue gas, up to approximately 6.5vol% water, as summarized in Table 14. At low moisture levels, the solids produced were sticky, but still friable and flowable as in dry absorption experiments. As the moisture content in the gas increased, moisture condensed on the interior walls of the absorber. Up to approximately 5vol% moisture, solid particles were observed to impact the wet walls of the absorber through the absorber windows. This suggests that at low moisture levels, solids form in the spray suspension. However, at 6.5vol% moisture, wet droplets impacted the windows during operation, suggesting that solids were not produced as they were at lower moisture levels. This transition, as observed through the absorber windows, is illustrated in Figure 25.

Table 14. Summary of humid absorption experiments conducted in BP2.

Date	mol% water in feed gas	mol% water in outlet gas	% CO2 capture	% carbamate	Carbamate quality notes
6/25/2015	0%	-	54.3%	88.0%	dry, powdery solids
10/15/2015	0%	-	49.6%	88.3%	dry, powdery solids
10/23/2015	3%	2.0%	55.6%	87.6%	white powder, somewhat stickier but still flowable
10/29/2015	5%	2.7%	43.5%	91.3%	flowable white powder in solids container - some sludge on the sides and a few blobs of liquid in the middle
10/30/2015	6.5%	2.5%	-	79.2%	wet, slushy mixture of carbamate + water
11/10/2015	4.7%	2.3%	47.5%	87.3%	white powder in solids container - some sludge on the sides and large blobs of pasty fluid in the middle

Dry – powder clings to dry windows

5vol% – solids impact wet windows

6.5vol% – wet droplets impact wet windows

Figure 25. Transition of absorption product from dry powder to wet slurry with increasing gas moisture content.

The consistency of the carbamate product was also assessed at the end of each experiment. At moisture levels up to approximately 5vol%, somewhat sticky, but flowable, solids were collected, along with some stickier clumps of wet carbamate. At 6.5vol% moisture, the carbamate product was a mixture of water and carbamate resembling a slurry. This fluid accumulated on the walls of the reactor and was observed to flow under gravity from the reactor. These dry and wet products are shown in Figure 26.

Dry – "cake flour"

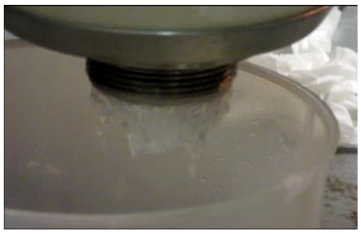

6.5vol% - "hair gel", "slurry"

Figure 26. Comparison of dry carbamate solids produced at low humidity and carbamate slurry produced at 6.5vol% moisture.

As shown in Table 14, the extent of GAP-0 conversion and CO_2 capture were modestly affected by the presence of water. In experiments with dry simulated flue gas, dry carbamate solids were produced having extractables as low as 65wt%. At 6.5vol% water in the flue gas, the slurry was 79.2wt% extractables, which suggests that the fluid phase of the slurry product shown in Figure 26 is water, rather than unconverted GAP-0 solvent. Moisture balance calculations, using the humidity measured for the feed and effluent gases, suggest that the slurry produced at 6.5vol% gas humidity was approximately 3wt% water.

Solids production was demonstrated in dry simulated flue gas across a wide range of operating conditions, with single stage CO_2 conversion rates up to 75mol%. In humid simulated flue gas, CO_2 absorption was demonstrated at levels consistent with those obtained in dry flue gas, but the consistency of the rich phase was a slurry of carbamate in water. Because of these results, the process was reconfigured for a slurry CO_2-rich phase as discussed in Task 4.5.

Extruder

The goal of these experiments was to determine the optimal extruder operating conditions at a given screw design to enable continuous, stable delivery of carbamate from the extruder into the pressurized desorber. The effects of solids flow rate, screw rotation speed, and barrel temperature on maximum delivery pressure were evaluated. The ranges of these parameters to be studied in extruder testing are shown in Table 15. All experiments were conducted using the screw design used in a previous project[12]. Efforts initially dedicated to optimizing the screw design were redirected as

the humid absorption experiment results led to a reprioritization of project objectives.

Table 15. Ranges of parameters studied in extruder unit operation testing.

Parameter	Range
Solids Flow Rate (lb/hr)	10-33
Screw Rotation Speed (% of maximum rpm)	0-100%
Barrel Temperature (°C)	20-160
Screw design	Reproduced design used in previous project

These experiments were performed initially using a valve mounted at the outlet of the extruder to simulate backpressure. This approach allowed for isolation of extruder performance from desorber performance, enabling the operators to generate more experience running the extruder with the unique behavior of the phase-changing carbamate. When melted, the phase-changing carbamate is much less viscous than molten polymers, and thus their behavior in the extruder was expected to be different.

Extruder performance was measured in terms of the maximum pressure at which solids could be delivered without backflow of pressurized CO_2 through the extruder barrel. This was assessed using a CO_2 analyzer mounted at the extruder inlet.

In extruder commissioning experiments, carbamate was fed against pressures up to 200psig at barrel temperatures up to 70°C and dieplate temperatures up to 100°C. The extruder feed rate was controlled to 10-20lb/hr, which is consistent with the GAP-0 flow rate used in the spray absorber. Under these conditions, carbamate exiting the extruder was very viscous, indicative of very little desorption of CO_2. These conditions represent the minimum temperature at which the bench scale extruder could reliably feed carbamate to the pressurized desorber.

Subsequent extruder experiments were conducted at barrel temperatures approaching desorber operating temperatures. These experiments were conducted to evaluate extruder performance at conditions that were most likely to enable robust carbamate transfer to the pressurized desorber under typical desorber operating conditions. This experiment was designed to evaluate the maximum operable screw speed at a given feed rate, temperature profile, and degree of simulated backpressure (valve opening). The extruder barrel and dieplate temperatures were controlled to 120-140°C. During these experiments, no measureable backpressure was achieved, even with the valve almost fully closed. This suggests that the viscosity of the carbamate material at these temperatures was too low to generate a seal at this feed rate, which is consistent with the observed gas flow exiting the extruder. Further, the observed torque, a measure of the viscosity of the extruder contents, was no more than 10% of the maximum torque rating. It is believed that the valve was oversized for the feed rate of interest at these operating temperatures.

In light of the results of the humid absorption experiments described above, efforts to

develop the bench scale extruder for dry solids transport were redirected to focus on development of a slurry pump for rich transfer at the bench scale.

Solvent Thermal Degradation during Desorption

It was observed in a parallel project[13] that at elevated temperatures GAP-1 aminosilicone carbamate readily formed urea byproducts as shown in Figure 27 below. The phase-changing aminosilicone, GAP-0, differs from GAP-1 in that the value of the silicone repeat unit is zero, rather than one.

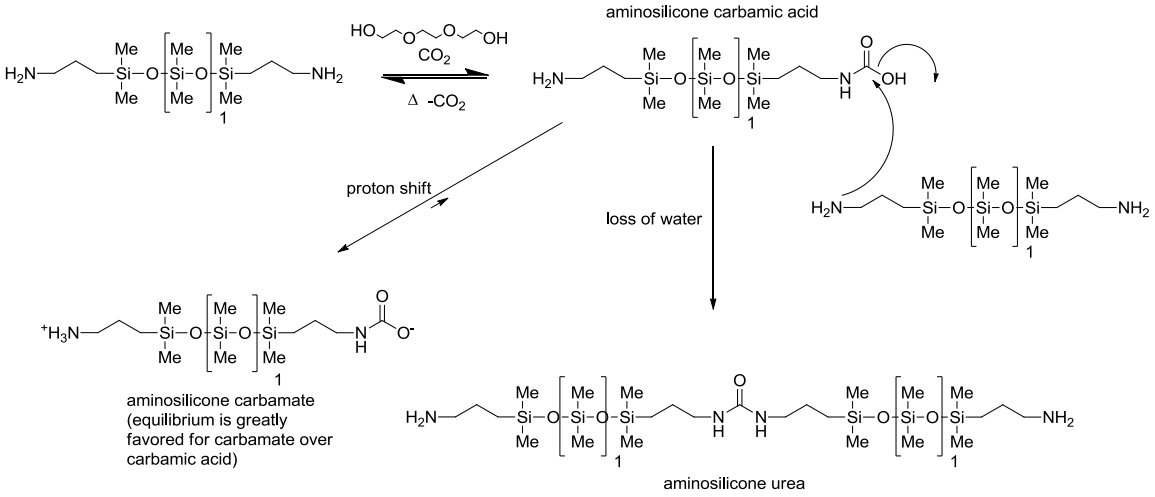

Figure 27. Formation of urea by-product in GAP-1/TEG system.

The similarities of the aminosilicone in both systems raised the question of the thermal stability of the GAP-0 material during the desorption step. To address this potential issue, a designed experiment was created to interrogate the variables that may have impact on the formation of such a by-product. The designed experiment assessed the impact of carbamate loading (10-100%), temperature (120-140°C), and water loading (0-10%) on urea formation rate.

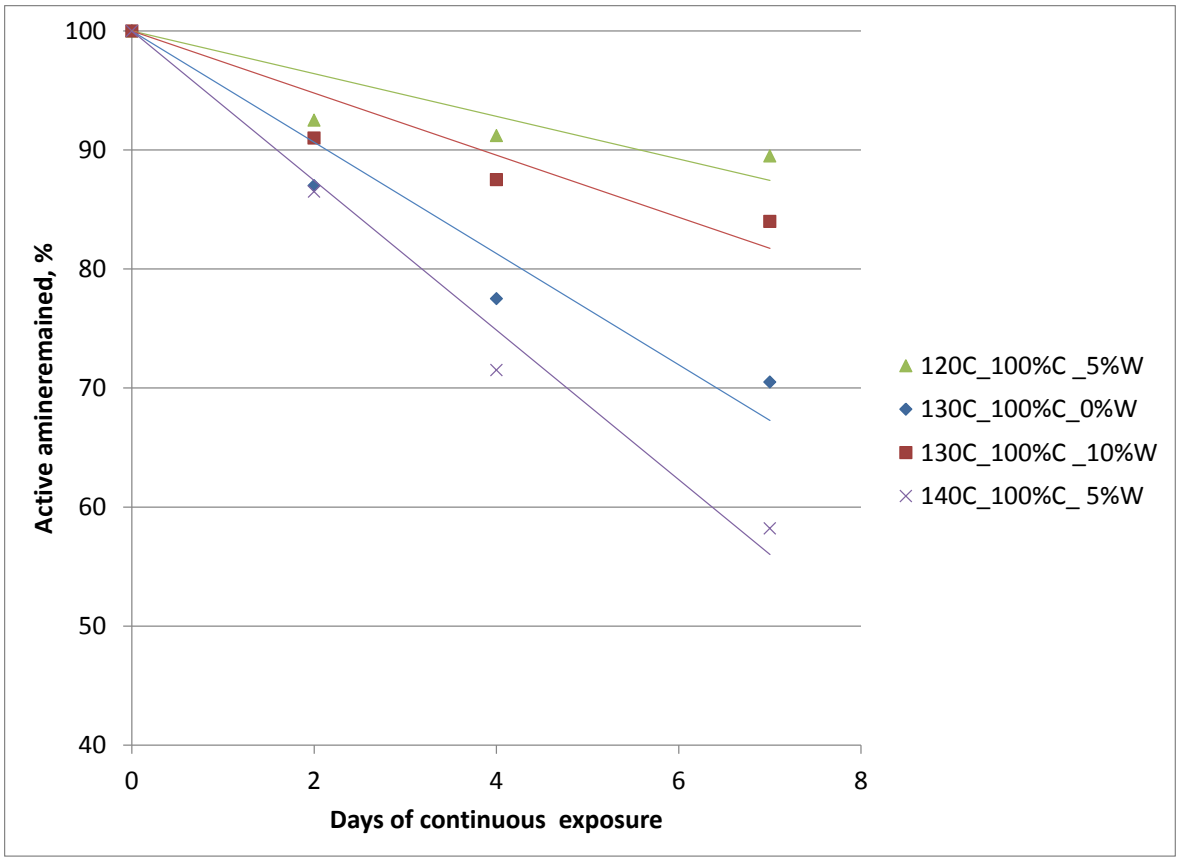

Figure 28. Summary of thermal degradation performance of GAP-0 as a function of carbamate and water loading.

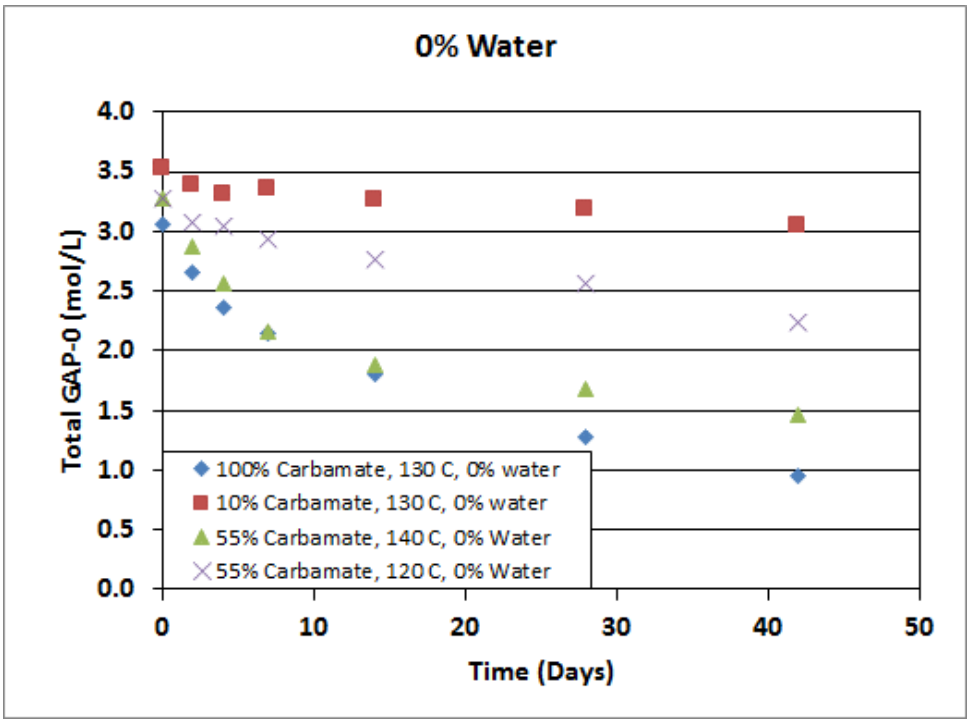

Figure 29. GAP-0 concentration as a function of time.

For this analysis, the form of the rate expression for GAP-0 decomposition was assumed to take the form in Equation 4.

Equation 4. Rate expression for GAP-0 thermal decomposition

$$r_d = k_f[GAP0]^x[GAP0carb]^y - k_r[Urea]^m[water]^n$$

where:

$r_d = rate\ of\ decomposition\ (\frac{mol}{L \cdot s})$

$k_f = forward\ rate\ constant$

$k_r = reverse\ rate\ constant$

$[GAP0] = total\ GAP0\ concentration\ (\frac{mol}{L})$

$[GAP0carb] = GAP0\ carbamate\ concentration\ (\frac{mol}{L})$

$[Urea] = urea\ concentration\ (\frac{mol}{L})$

$[water] = water\ concentration\ (\frac{mol}{L})$

In order to determine the value of k_f, the initial, linear portion of the data for each of the dry experiments, shown in Figure 29, was isolated and fit to a straight line, as shown in Figure 30. The slope of the line for each fit corresponds to the initial rate of decomposition of GAP-0 at each condition.

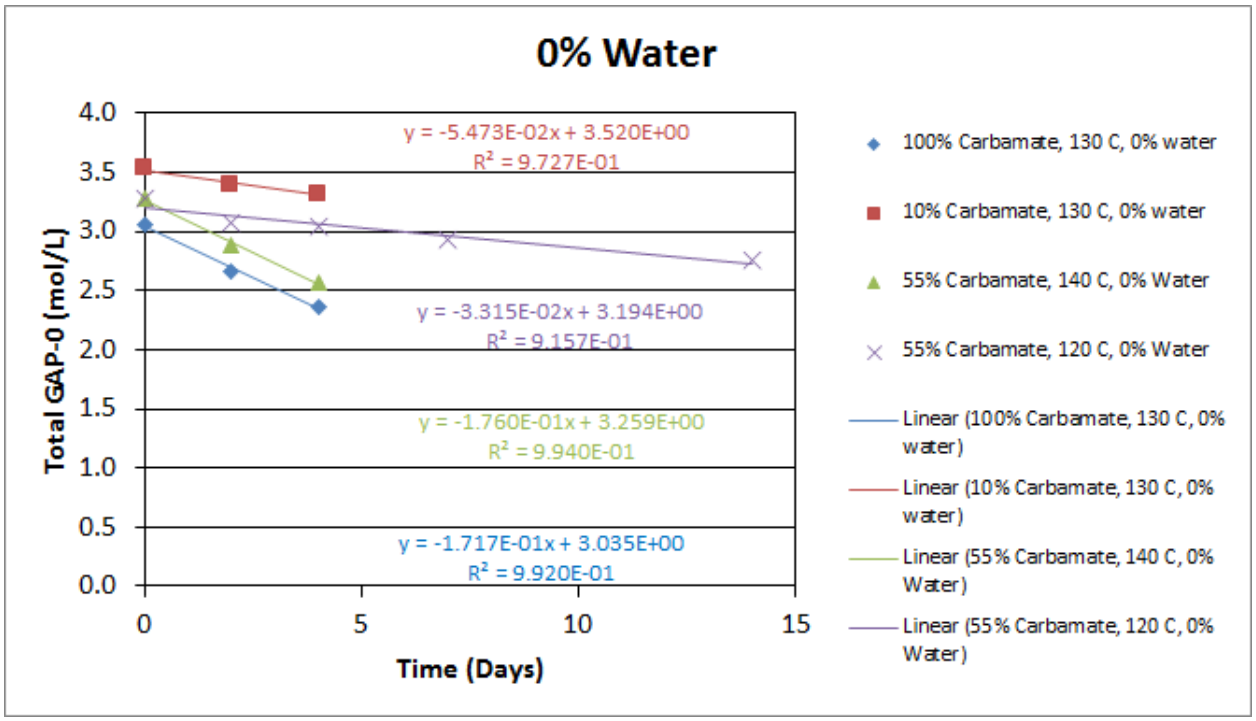

Figure 30. Linear fit of the initial, linear portion of the decomposition data for each of the dry experiments.

Since little decomposition had occurred, and therefore little urea or water had been formed, the reverse reaction term in Equation 4 could be ignored. Since r_d was known from the linear fit, and [GAP0] and [GAPcarb] were known from NMR and the initial compositions loaded in the reactors, it was possible to calculate k_f if the order of reaction for GAP-0 (x) and GAP-0 carbamate (y) were assumed. A range of values for x and y were assumed and the resulting Arrhenius plots were evaluated. The best fit was found to correspond to x = 1 and y = 0.5, shown in Figure 31. This resulted in a pre-exponential factor of 2.68×10^8 and an activation energy of 116 kJ/mol. However, the R-squared value for the linear fit was somewhat unsatisfactory at 0.8193.

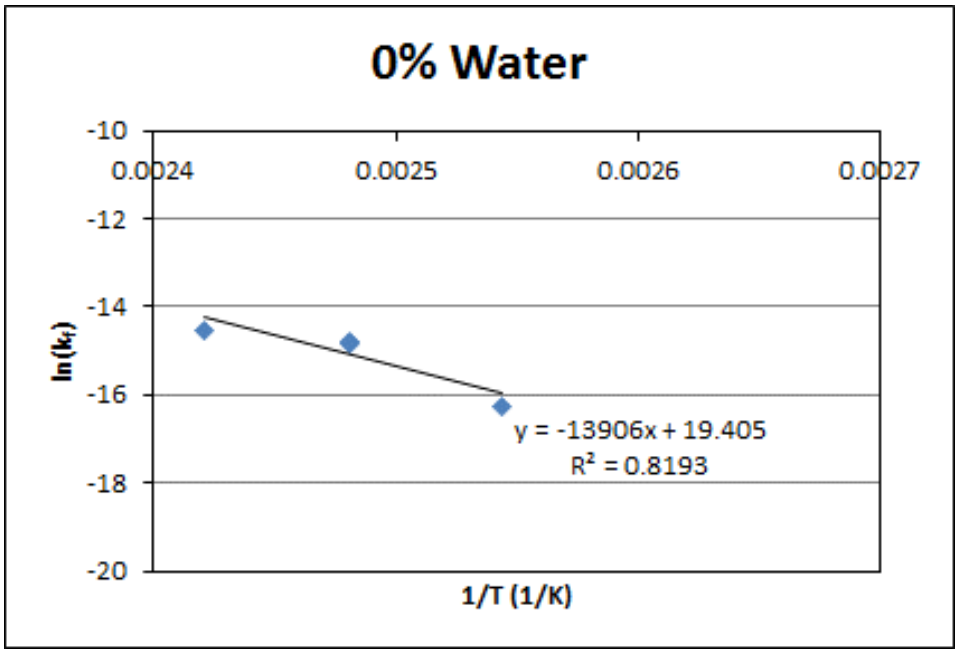

Figure 31. Arrhenius plot of k_f.

In order to calculate k_r, the complete set of decomposition measurements for each set of conditions was fit to a second order polynomial, as shown in Figure 32. The slope of each fit was calculated as a function of time, giving the rate of decomposition for each condition as a function of time. Using the calculated rates, the values calculated for k_f, and the concentrations of total GAP-0, GAP-0 carbamate, water, and urea, it was possible to calculate k_r for each set of conditions, assuming values for m and n and using Equation 4. A range of values for m and n were assumed and the resulting Arrhenius plots were evaluated. However, no values for m or n were found that resulted in an Arrhenius plot with an acceptable R-squared value for a linear fit. It was therefore impossible to calculate values for k_r.

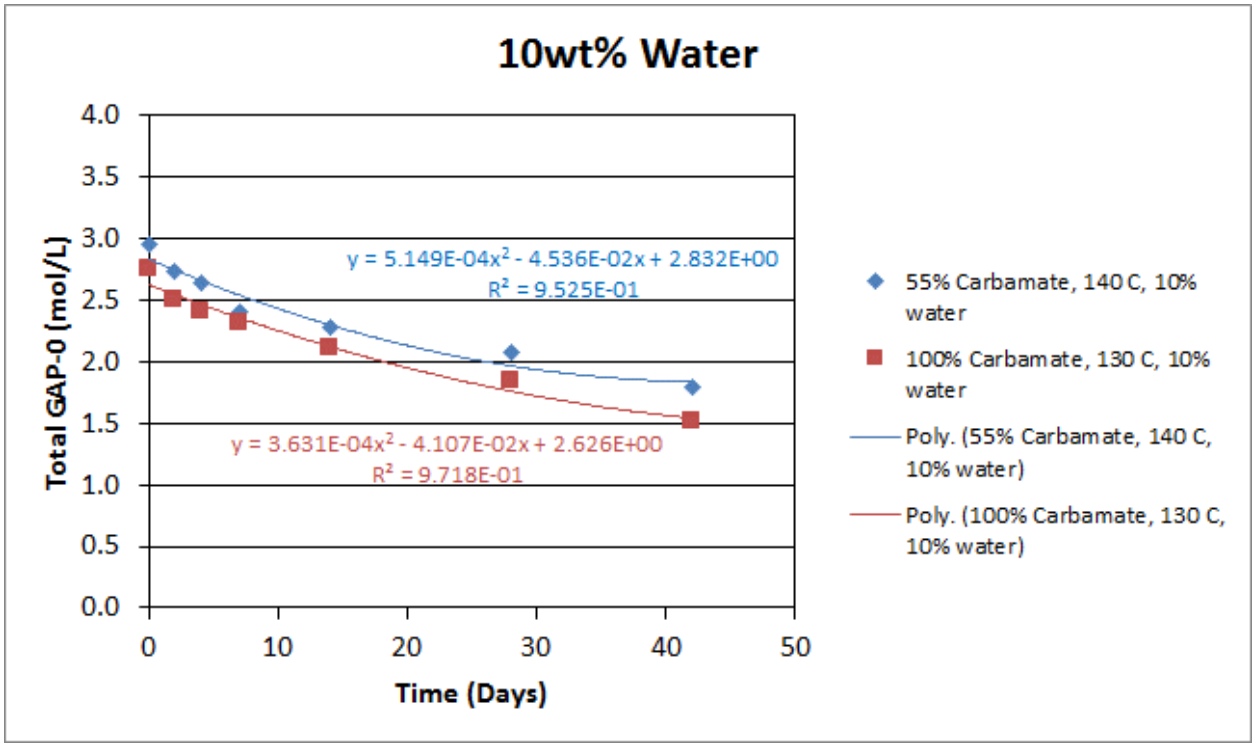

Figure 32. Polynomial fit for data sets with initial water loadings of 10 wt%.

In this experiment, thermal degradation of GAP-0 through the urea formation mechanism was confirmed by NMR analysis. As shown in Figure 28, the amine content of GAP-0 declined within the first week of continuous exposure. The rate of amine loss was reduced at lower temperature and in the presence of water. These results suggested that desorber temperature should be minimized to avoid thermal degradation of the solvent. As indicated by the GAP-0 absorption/desorption isotherms (Figure 36), high temperatures (>140°C) are needed to desorb CO_2 at elevated pressure. As a result, the two-stage desorber design described in Task 3.3 was abandoned in favor of a single-stage, atmospheric pressure desorber for the bench scale system.

Atmospheric Pressure Desorber Batch Experiments

The goal of atmospheric pressure desorption (polisher) experiments was to determine the optimal operating conditions to maximize solvent regeneration. The effects of carbamate/liquid flow rate, vessel temperature, agitation rate, and residence time on the extent of desorption were evaluated. The ranges of these parameters studied are shown in Table 16.

Table 16. Ranges of parameters to be studied in desorber unit operation testing.

Parameter	Polisher Range
Temperature (°C)	120-140
Pressure (psig)	0
Agitation Rate (% of maximum rpm)	0-100%
Rich solvent flow rate (mL/min)	30-360
Residence Time (min)	19-36

Desorber performance was quantified using the methods shown in Table 17. The extractables method used to evaluate the liquid outlet composition is described above. Online and offline IR systems were used to measure the composition of the liquid effluent from the desorber. Calibration of the FT-IR unit to differentiate between GAP-0 and GAP-0 carbamate was challenging because as solvent CO_2 loading increases the solvent solidifies (in the absence of water).

Table 17. Measurement methods for performance parameters evaluated in desorber unit operation testing.

Parameter	Measurement Method
% Carbamate Conversion (mol%)	Calculated from gas outlet and liquid outlet compositions and flow rates
Gas Outlet Flow rate (slm)	Mass flow meter
Gas Outlet Composition	Mass spectrometer (online) CO_2 analyzer (online)
Liquid Outlet Composition	Extractables measurement (offline) FT-IR (online/offline)

The FT-IR probe was calibrated using a series of samples with different carbamate concentrations. Table 18 summarizes the samples used to prepare the calibration curve. The carbamate concentrations were determined based on the extractables content. The range of the calibration curve focused on lower concentrations of carbamate to ensure that the mixture remained a liquid during testing. The calibration curve was completed at room temperature.

Table 18. Samples used for FT-IR probe calibration

Sample name	Carbamate concentration (% wt)
F2390-007 A, B	5% ± 0.4
F2390-007 G	7.2%
F2390-007 E	8.7%
F2390-007 F	11.3%
F2390-007 C	17.4% ± 1.6

The calibration curves for 5 different wavelengths were analyzed in the FT-IR software. The wavelengths used and corresponding R^2 values are summarized in Table 19. The R^2 values indicate that the calibration curves were linear for all of the wavelengths selected. Additional testing will be completed to assess calibration stability over time.

Table 19. Summary of R^2 values for different wavelengths.

Wavelength (cm^{-1})	R^2 value
1304	0.995
1410	0.991

1441	0.994
1467	0.995
1588	0.996

Batch mode experiments demonstrated operability of the atmospheric pressure desorber system and desorption of carbamate consistent with the equilibrium isotherms. System commissioning confirmed that temperature and agitation rate could be controlled within the ranges of interest. After system commissioning, batch mode experiments were completed at three temperatures using a batch of carbamate previously produced in the spray absorber and containing 95wt% carbamate. Experiments were conducted at 120°, 130°, and 140°C at 150rpm agitation speed.

Data from these experiments, including temperatures, gas flowmeter readings, and liquid sample collection times, are provided in Figure 33, Figure 34, and Figure 35. Flowmeter readings fluctuated during the experiment and were not logged continuously. The maximum value observed at each time point when values were recorded was used for the graphs. All liquid samples were analyzed by IR, and some samples were also analyzed for extractables content.

Table 20 summarizes the results for the liquid analysis. For very highly loaded samples that were difficult to characterize by IR, the carbamate content was measured using the extractables method. As can be seen from the data, carbamate content as predicted by the preliminary IR calibration curve was not consistent with that measured based on extractables content. Further development of the IR probe for this application was not pursued. In subsequent experiments, the extractables method was used to characterize all lean and slurry samples produced.

Table 20. Liquid analyses obtained from batch desorber experiments.

Liquid Sample	Temperature in desorber when collected (°C)	Wt % carbamate based on IR (1530 to 1600 cm^{-1} range)	Wt % carbamate based on liquid extractables content
1	117	83.8	65.2
2	120.1	79.2	59.4
3	121.3	71.4	51.8
4	121.6	64.6	49.9
5	125.7	64.3	43.9
6	130.9	20.2	
7	131.5	14.6	
8	133.7	10.1	
9	139.7	4.3	
10	141.4	3.5	

During these experiments, CO_2 desorption was evident from the gas flowmeter readings shown in Figure 33, Figure 34, and Figure 35. After several minutes, this flow

rate declined to near zero, indicating that equilibrium had been reached at that operating temperature. Continuous datalogging of this flow meter will allow for more accurate integration of such curves to support desorber mass balance calculations. The carbamate used in this series of experiments was 95% carbamate. The data in Table 20 shows that 95% conversion of GAP-0 carbamate is possible in the desorber at atmospheric pressure at 140°C. This data, in combination with the absorber GAP-0 conversion data summarized in Table 9, shows entitlement to achieve 25-160g CO_2/kg solvent in net working capacity.

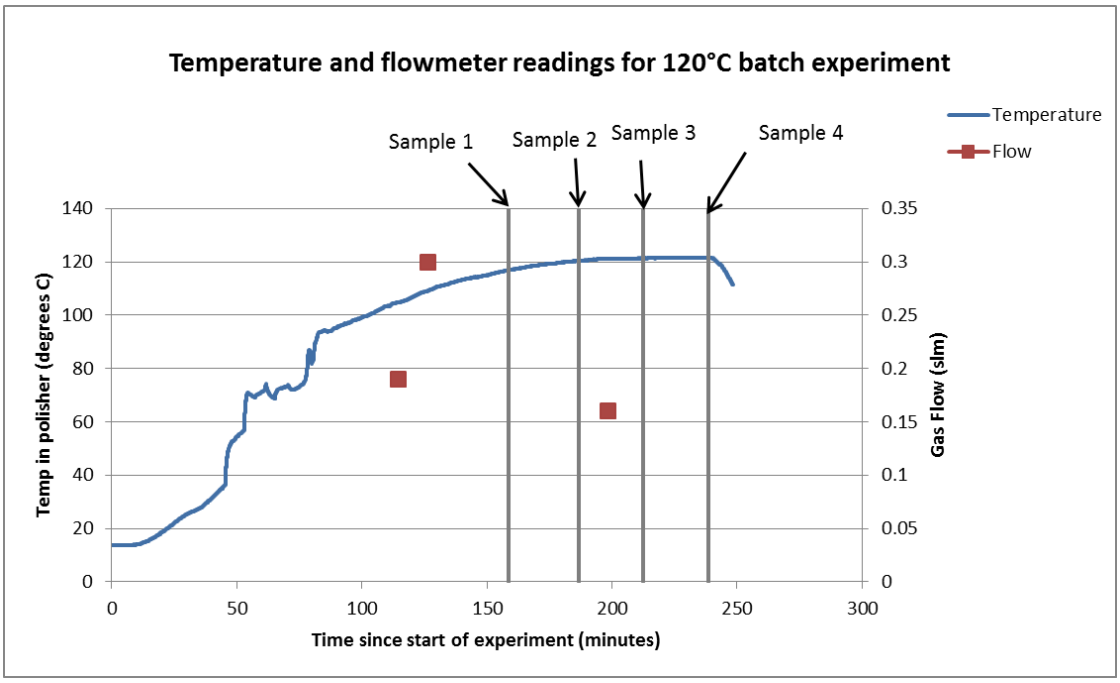

Figure 33. Temperature, flowmeter readings, and sample collection times for 120°C experiment.

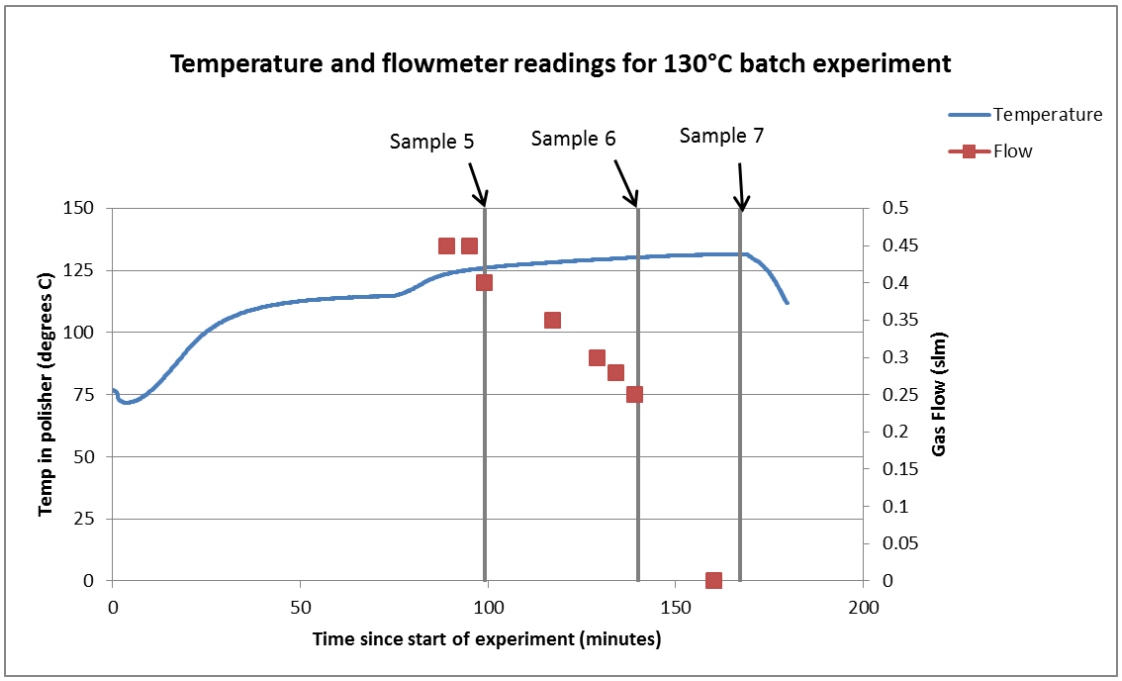

Figure 34. Temperature, flowmeter readings, and sample collection times for 130°C experiment.

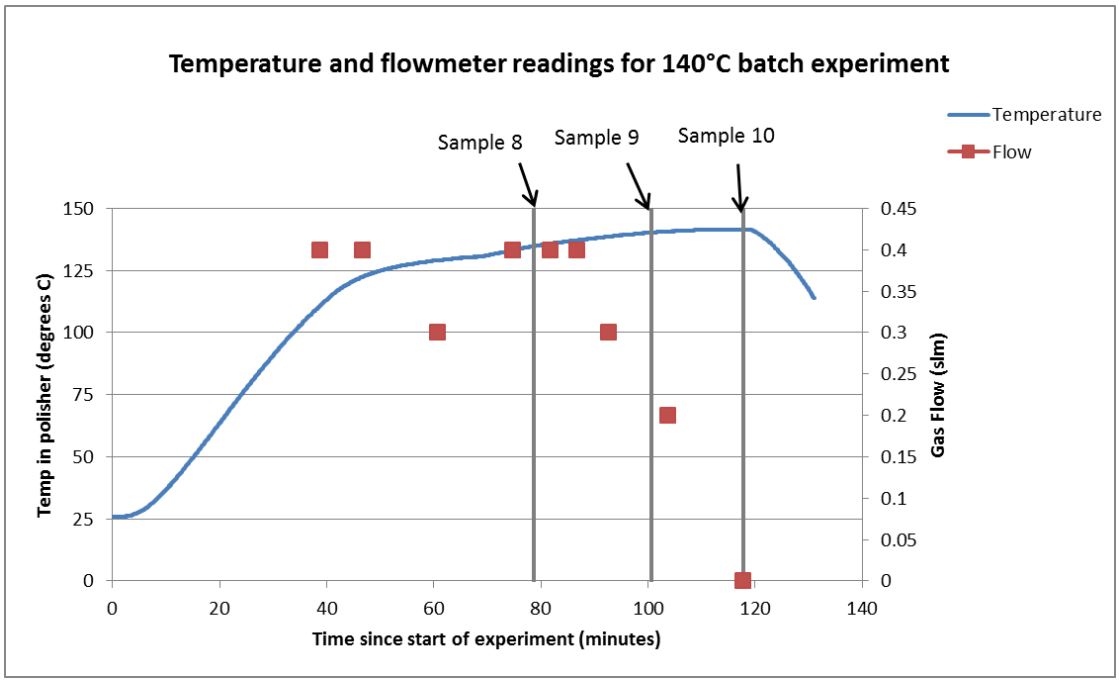

Figure 35. Temperature, flowmeter readings, and sample collection times for 140°C experiment.

The data points from each experiment corresponding to equilibrium (Samples 4, 7, and 10) are compared to the equilibrium desorption isotherms in Figure 36. The experimental data is in reasonable agreement with the desorption isotherms.

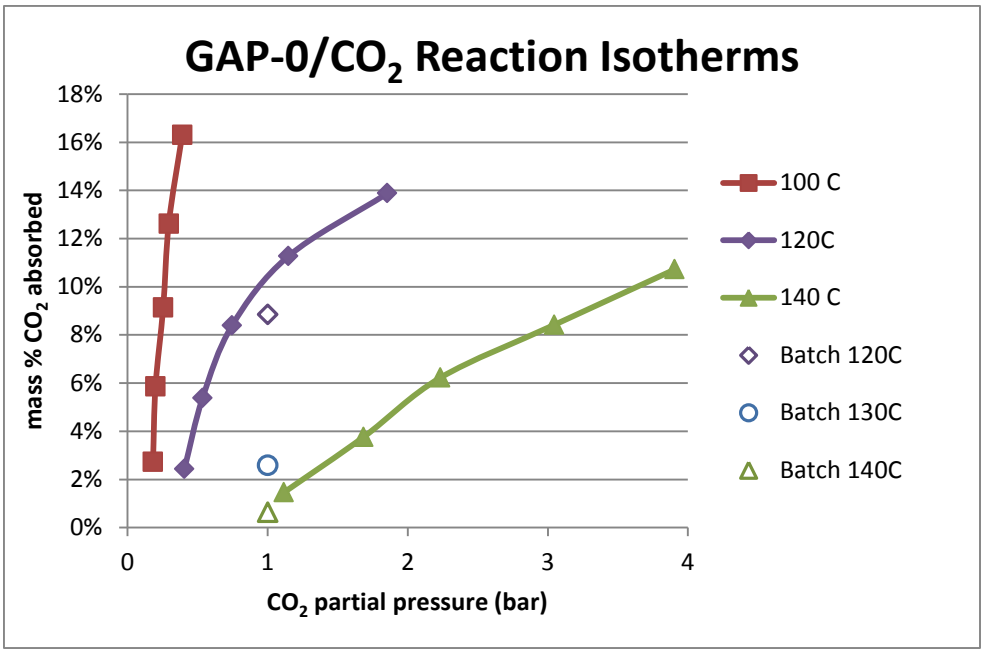

Figure 36. Desorber batch experiments compared to equilibrium isotherms.

Task 4.3 Determine scale-up effects

Previous efforts to develop a lab scale spray absorber for the phase-changing aminosilicone solvent were focused on two main systems: a semi-batch mode spray dryer and a continuous spray tower. The similarities and differences between these systems and the bench scale absorber are summarized in Table 21.

Table 21. Summary of absorber scale up effects.

		Yamato spray dryer	ARPA-e continuous spray absorber		Bench scale spray absorber	
Gas Flow Rate	slm	23.5	20	20	100	150-200
CO2 loading	mol%	16%	16%	58%	50%	16%
Liquid Flow Rate	mL/min	40	35	50	200	270-360
GAP-0:CO2	mol:mol	1.00	0.90	0.35	0.35	1.00
Absorber volume	L	7	22	22	400	400
Est. gas residence time	min	0.30	1.10	1.10	4.00	2-2.7
Est. gas velocity	m/s	0.030	0.010	0.010	0.004	0.005-0.007
GAP-0 conversion	mol%	82%	30%	90%	94%	67-76%
Solids consistency	-	dry, flowable	viscous liquid	dry, flowable	dry, flowable	dry, flowable

Compared to the lab scale spray dryer and continuous spray absorber, the bench scale spray absorber has longer average gas residence time and lower estimated gas velocity, as a result of the increased size and volume of the bench scale vessel compared to the previous vessels. The bench scale absorber generates comparable GAP-0 conversion at constant GAP-0 : CO_2 feed ratio and constant CO_2 feed concentration to each of the lab scale absorbers.

The extruder performance observed at the bench scale was consistent with expected performance based on the lab scale extruder experiments conducted in a previous project[12]. The bench scale extruder was operated at the lower end of its feed rate range. As a result, the torque observed during operation at desorption temperatures was near the low end of its operable range. When operated at lower temperatures, extruder torque was within the middle of the operable torque range.

GAP-0 conversion in batch mode experiments was consistent with that dictated by the equilibrium desorption isotherms, as shown in Figure 36. A comparison of the desorber size and possible residence time for the lab scale and bench scale units is shown in Table 22.

Table 22. Comparison of lab- and bench-scale desorber parameters.

	Lab scale	Bench scale
Desorber volume (mL)	220	5000 mL
Avg. residence time at 50% fill	11 min	15 min
Avg. residence time @ 75% fill	17 min	22 min

Task 4.4 Determine suitable materials of construction

Materials of construction experiments were completed for conditions simulating the absorber and extruder inlet under dry conditions and the absorber and atmospheric pressure desorber (polisher) under wet conditions. Coupons of C1010 carbon steel and 304L stainless steel were exposed to GAP-0 carbamate according to the conditions shown in Table 23. Samples were exposed continuously for 6 weeks. After exposure, samples were cleaned according to the procedure listed in ASTM G1-03[14], using the solvents defined in Table A1.1 (carbon steel – designation C3.5; stainless steel – designation C7.1). Coupons were exposed to the appropriate cleaning solution, rinsed with deionized water, dried, and weighed. The cleaning procedure was repeated until the slope of the weight loss vs. cleaning cycle curve matched that of the control samples. This procedure is consistent with that detailed in a previous report[15]. Coupon mass loss was then used to calculate the estimated corrosion rate in terms of mm/year erosion of equipment wall thickness.

Table 23. Exposure conditions for materials of construction experiments.

Unit Operation	Temperature (°C)	Pressure (bar)	Gas Composition	Liquid/Solid Composition	Water loading
Absorber	60	~1.1	16% CO_2/N_2	GAP-0 carbamate (solids)	0
Absorber	60	~1.1	16% CO_2/N_2	GAP-0 carbamate (solids)	5wt%
Extruder inlet	60	~1.1	air	GAP-0 carbamate (solids)	0
Desorber	140	2-3	CO_2	GAP-0 & GAP-0 carbamate (liquid/solid mixture)	5wt%

The corrosion coupons used for desorber conditions are a different shape than those used for absorber and extruder inlet conditions because a pressure-capable vessel is required. The arrangement of the desorber coupons compared to that of the absorber and extruder inlet coupons is shown in Figure 37.

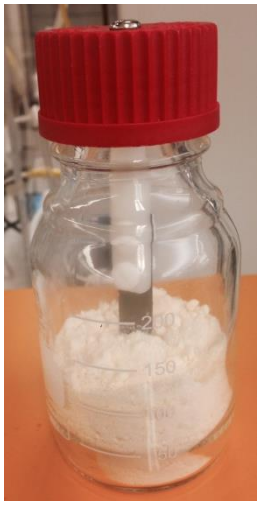
a)

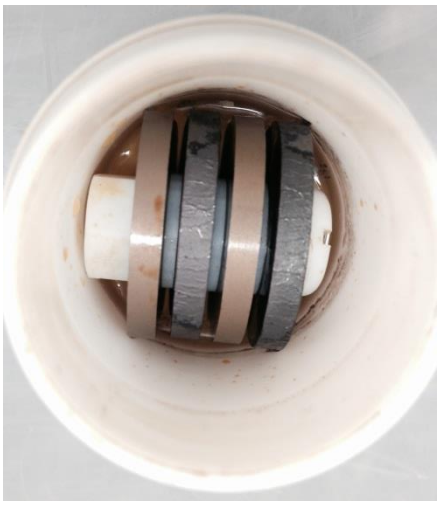
b)

Figure 37. Coupon exposure arrangement for a) absorber and extruder inlet and b) desorber conditions.

Coupon mass loss after the third cleaning cycle for all exposure conditions as a function of exposure time is shown in Figure 38 and Figure 39 for carbon steel and Figure 40 for stainless steel. It is evident that carbon steel was more susceptible to corrosion than stainless steel at the conditions tested. The absorber and extruder inlet conditions were the mildest, and wet desorber conditions were the most aggressive. Figure 39 shows the data in Figure 38 excluding the most aggressive condition (wet desorber).

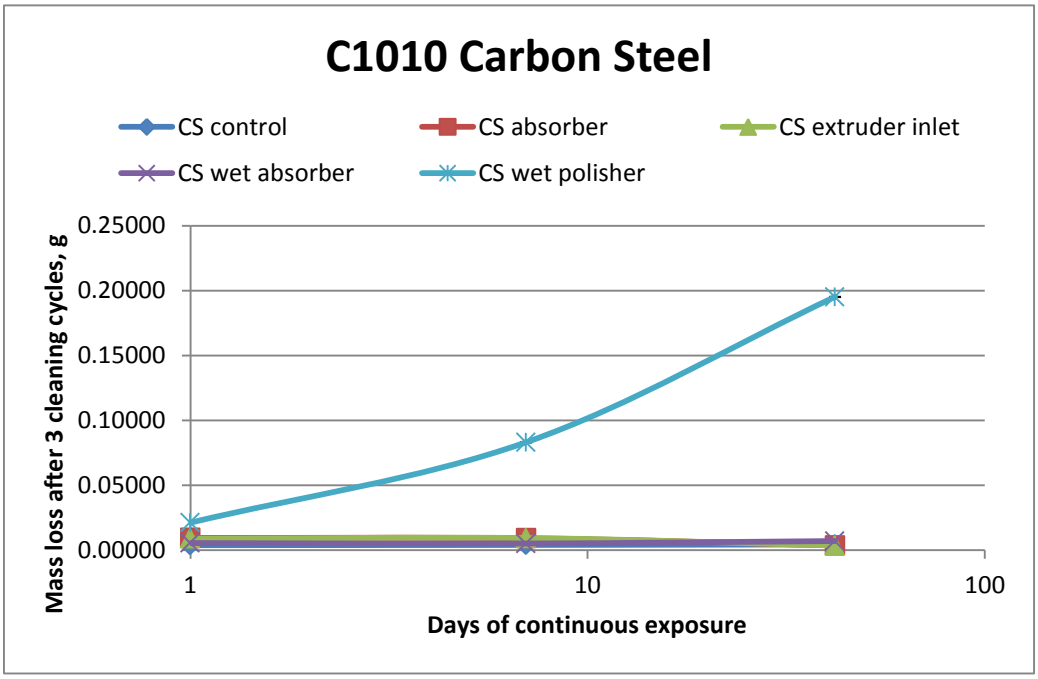

Figure 38. Carbon steel mass loss during 6 weeks of exposure.

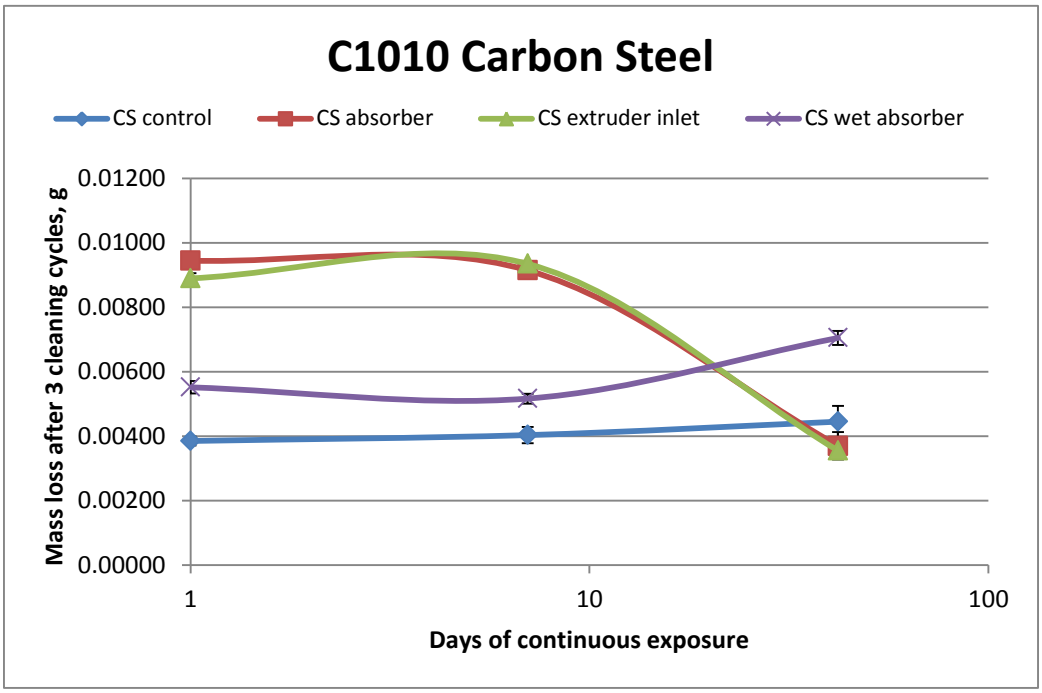

Figure 39. Carbon steel mass loss during 6 weeks of exposure (excluding wet polisher).

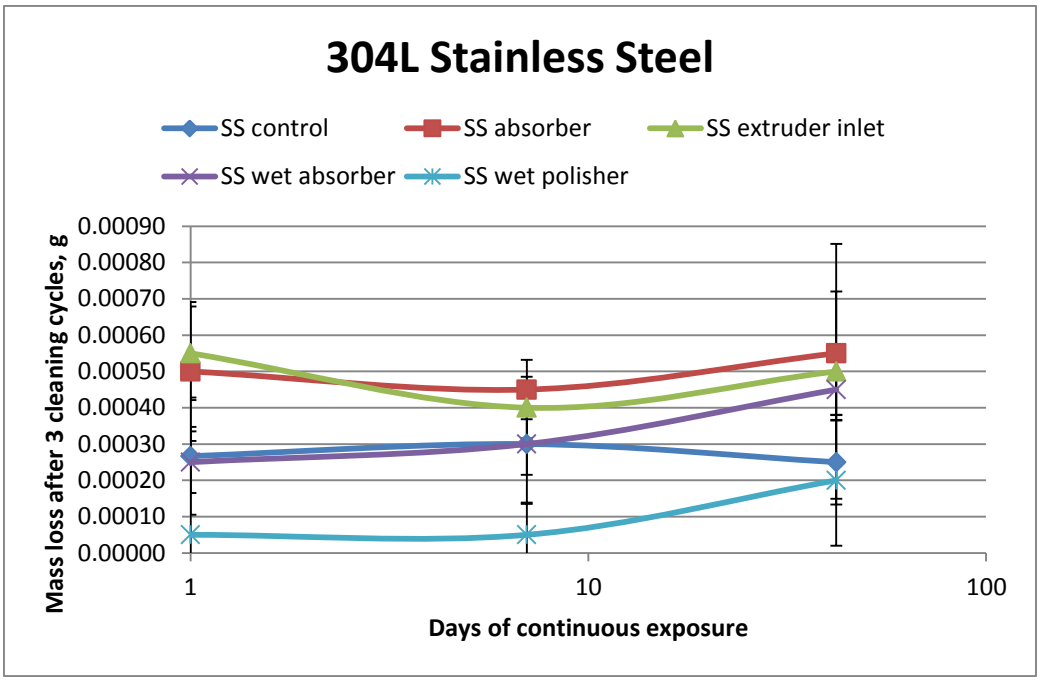

Figure 40. Stainless steel mass loss during 6 weeks of exposure.

Photos of cleaned coupons after 6 weeks exposure to desorber conditions are shown in Figure 41. Color change is visibly evident in the carbon steel coupon, and the stainless steel coupon is indistinguishable from the control. SEM images of these samples and the samples exposed to the wet absorber conditions are shown in Figure 42 and Figure 43. Changes in surface morphology are evident in the carbon steel samples exposed to desorber conditions (Figure 42).

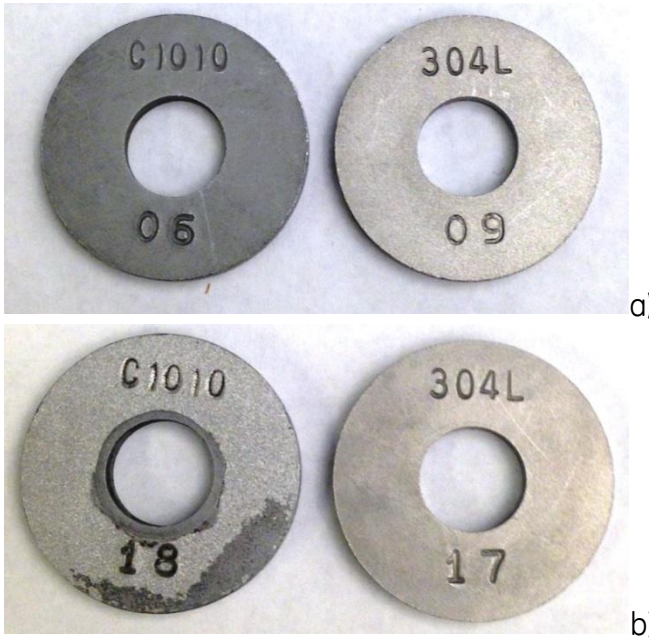

Figure 41. Carbon steel and stainless steel coupons after 6 weeks of exposure to a) control conditions and b) desorber conditions.

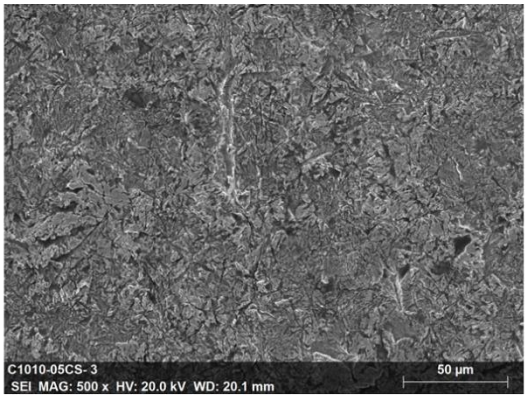

6 weeks control C1010

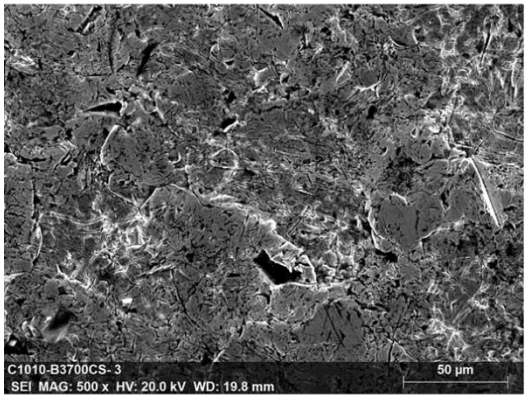

6 weeks wet absorber C1010

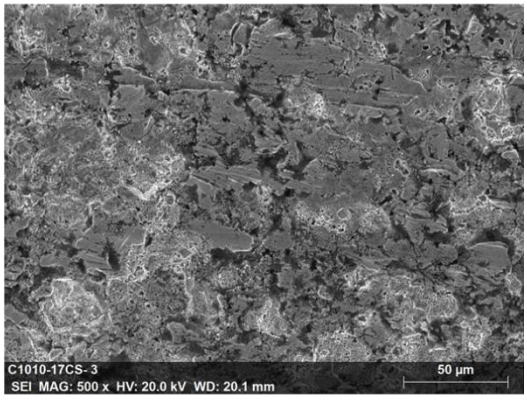

6 weeks wet polisher C1010

Figure 42. SEM images of carbon steel samples after 6 weeks exposure to control, wet absorber, and wet polisher (desorber) conditions.

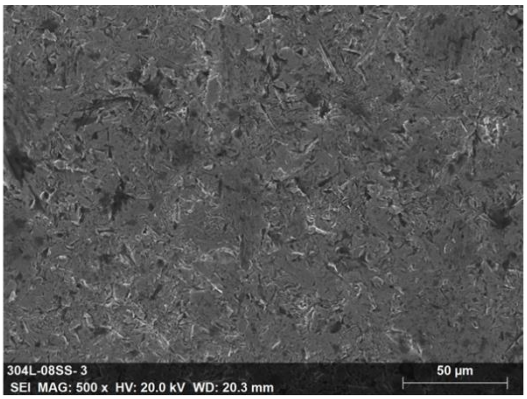

6 weeks control 304L SS

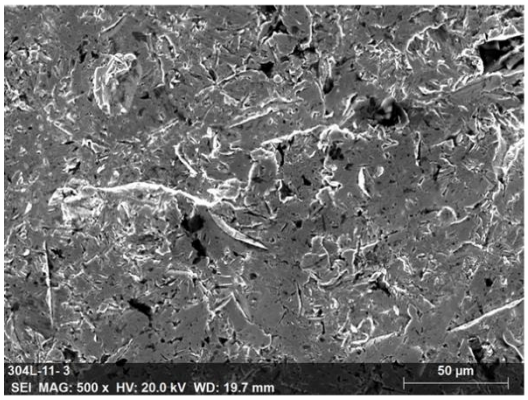

6 weeks wet absorber 304L SS

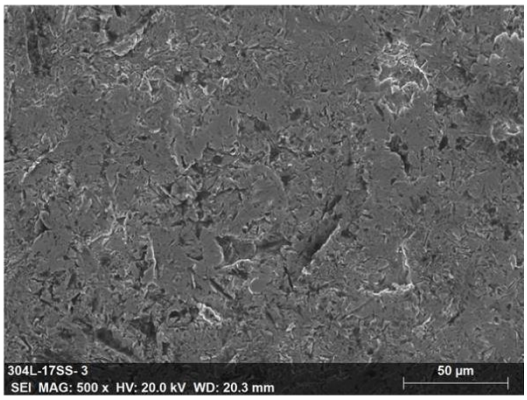

6 weeks wet polisher 304L SS

Figure 43. SEM images of stainless steel samples after 6 weeks exposure to control, wet absorber, and wet polisher (desorber) conditions.

Figure 39 illustrates the unexpected result that the carbon steel coupons exposed to the dry absorber and extruder inlet conditions experienced significant mass loss after 1 day and 1 week of exposure, but no more than the control samples after 6 weeks' exposure. This result may be the effect of the formation of a protective passivation layer on the surface of the coupons that is stabilized over time. To explore this, a set of carbon steel samples were exposed for 6 weeks under dry absorber conditions. Half of these samples were washed according to the ASTM acid etching cycle, and half were rinsed with deionized water. Both sets were submitted for XPS surface analysis in an attempt to detect the presence and composition of such a passivation layer. These results are shown in Figure 44, and suggest that the ASTM acid washing procedure appears to remove oxidized carbon species, in particular carbonate, that are typical passivation products for carbon steel as described in the literature.

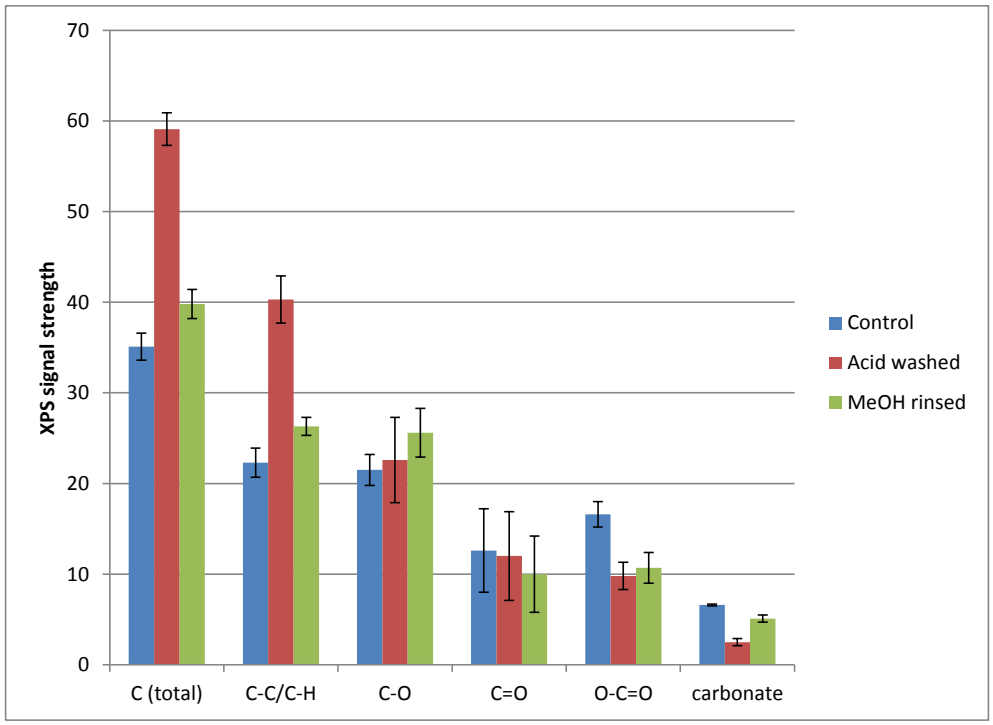

Figure 44. XPS results of control, acid-washed, and methanol-rinsed carbon steel coupons exposed to dry absorber conditions.

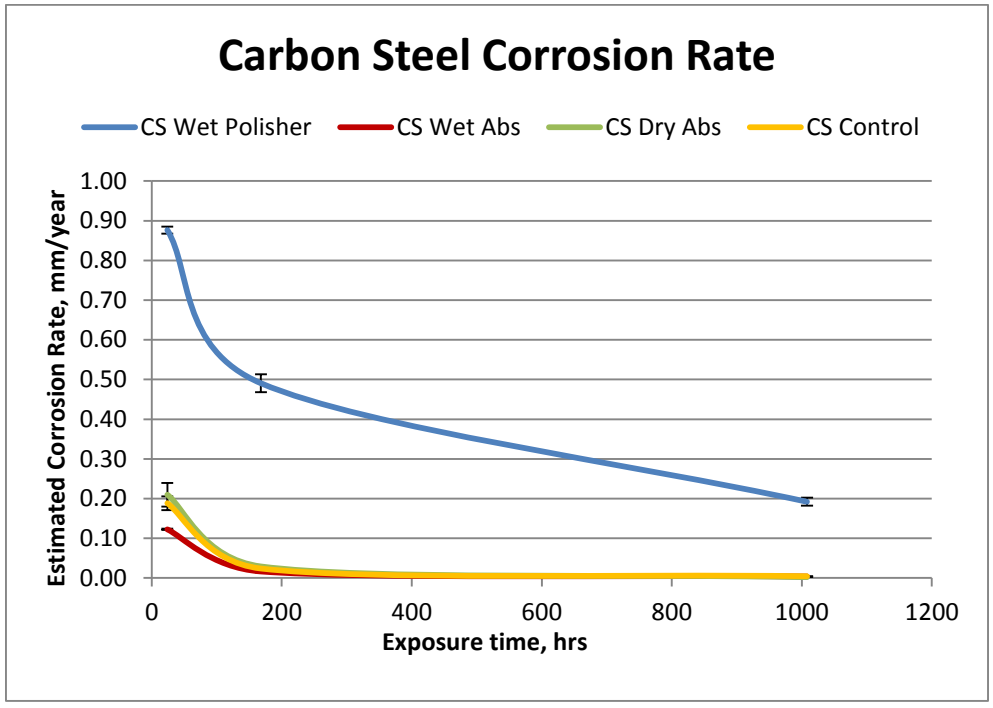

Figure 45. Estimated corrosion rate of carbon steel in conditions of the phase-changing CO_2 capture process unit operations.

The corrosion coupon mass loss data shown above corresponds to the estimated annual corrosion rate data shown in Figure 45 and Figure 46. The corrosion rate of stainless steel is approximately an order of magnitude lower than that of carbon steel, on the order of tens of microns per year compared to hundreds of microns per year. Initial corrosion rates are consistently high, and decline to a lower corrosion rate. This suggests that over time the development of corrosion products on the surface inhibits mass transfer of the reactants to the metal surface. For carbon steel, the condition having the highest corrosion rate was the wet polisher, with corrosion rates on the order of 0.2-0.9mm/year. All other conditions tested had carbon steel corrosion rates that were indistinguishable from the control condition and on the order of 5-200microns/year. For stainless steel, all of the conditions tested had corrosion rates that were indistinguishable from the control condition. This data supports the selection of carbon steel materials of construction for process units operating at low temperature. Carbon steel may be employed in high temperature process units with the use of a suitable corrosion inhibitor.

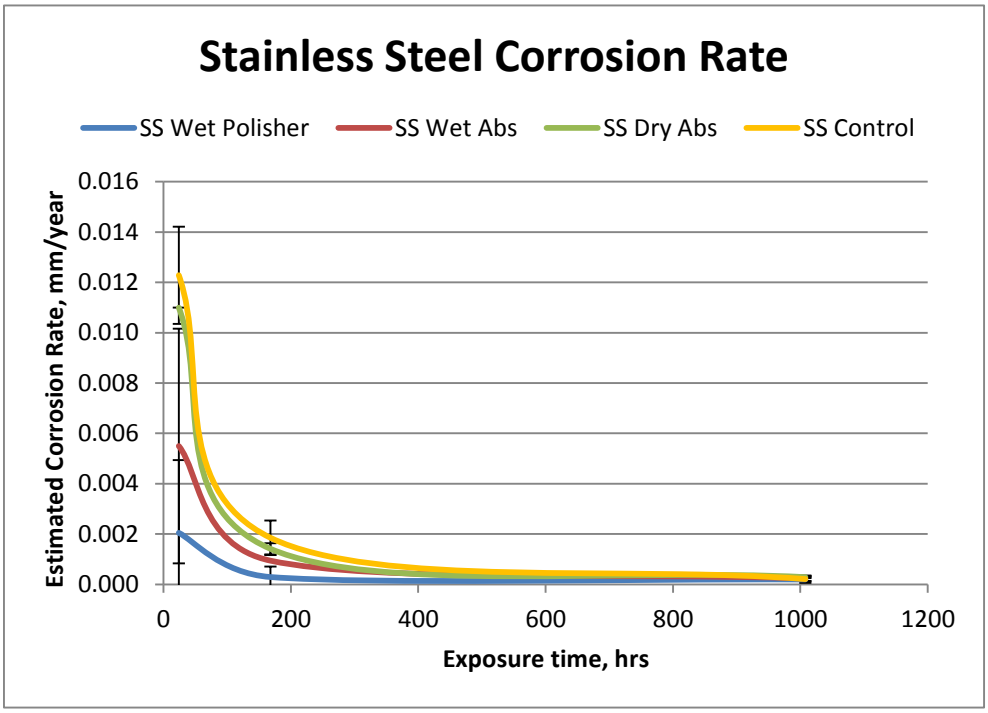

Figure 46. Estimated corrosion rate of stainless steel in conditions of the phase-changing CO_2 capture process unit operations.

In order to justify the use of carbon steel materials of construction for process units operating at high temperatures, a suitable corrosion inhibitor must be employed. A screening experiment to determine the efficacy of corrosion inhibitors was conducted.

A survey of the open literature identified the seven materials shown in Figure 47, which have been used to reduce corrosion of carbon steel for aqueous CO_2 capture solvents. These include four inorganic materials: sodium metavanadate[16,17,18] ($NaVO_3$), copper(II) carbonate[1,2,19,20] ($CuCO_3$), sodium molybdate[21] (Na_2MoO_4) and sodium thiosulfate[3,22]

($Na_2S_2O_3$); as well as three organic materials: myrisitc acid[23] ($CH_3(CH_2)_{12}CO_2H$), 2-mercaptobenzimidazole[24] ($C_7H_6N_2S$) and tetradecylamine[8] ($CH_3(CH_2)_{13}NH_2$). Each of these materials was tested at an inhibitor concentration of 1000 ppm, which is a concentration frequently employed in the literature.

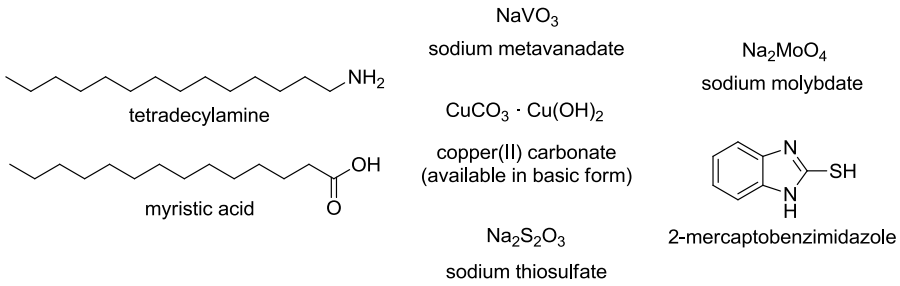

Figure 47. Corrosion inhibitors used in screening experiments.

Since the 304L stainless steel samples did not show significant corrosion rates under these conditions, the current experiments focused only on C1010 carbon steel coupons. Each Teflon® lined stainless steel pressure vessel was loaded with 4 g of GAP-0 carbamate, 0.2 g of H_2O, three C1010 coupons separated by Teflon® gaskets, and 1000 ppm of inhibitor, and the headspace was purged with 16% CO_2 in N_2 and then sealed. The vessels were placed in a 140°C oven for a period of 6 weeks. All inhibitors were used in pure form except for copper(II) carbonate, which is only available commercially in basic form as $CuCO_3{\cdot}Cu(OH)_2$. In this instance, the inhibitor was added at a concentration to give 1000 ppm $CuCO_3$. After the designated exposure time, a solid organic material was removed and the coupons were rinsed with methanol to remove any residual organic material as shown in Figure 48. The coupons were cleaned according to the procedure listed in ASTM G1-03[25], using the solvent designated C3.5 as defined in Table A1.1 (500 mL HCl, sp gr 1.19, 3.5 g hexamethylene tetramine, reagent water to make 1000 mL). The coupons were exposed to the cleaning solution for 10 minutes, rinsed with deionized water, dried in a vacuum oven at 100°C for 30 minutes, and weighed. The cleaning procedure was repeated until the slope of the weight loss vs. cleaning cycle curve matched that of control samples reported in a previous report[26] as shown in Figure 49.

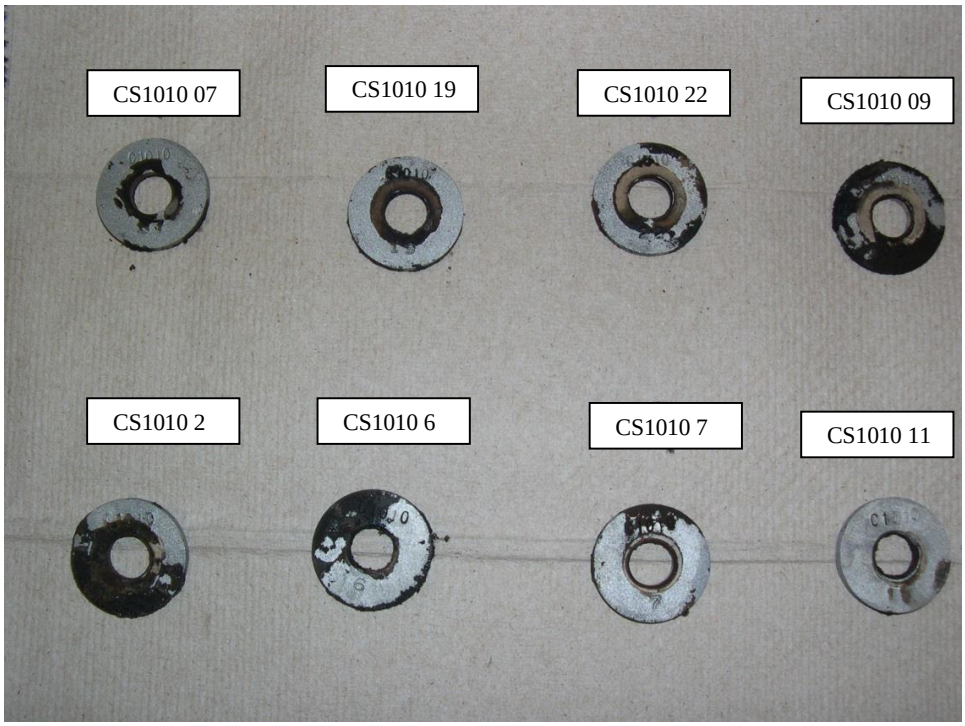

Figure 48. Photograph of coupons C1010 07 (no inhibitor), C1010 19 ($NaVO_3$), C1010 22 ($CuCO_3 \cdot Cu(OH)_2$), C1010 09 (Na_2MoO_4), C1010 2 ($Na_2S_2O_3$), C1010 6 (2-mercaptobenzimidazole), C1010 7 (myristic acid) and C1010 11 (tetradecylamine) before the acid cleaning procedure.

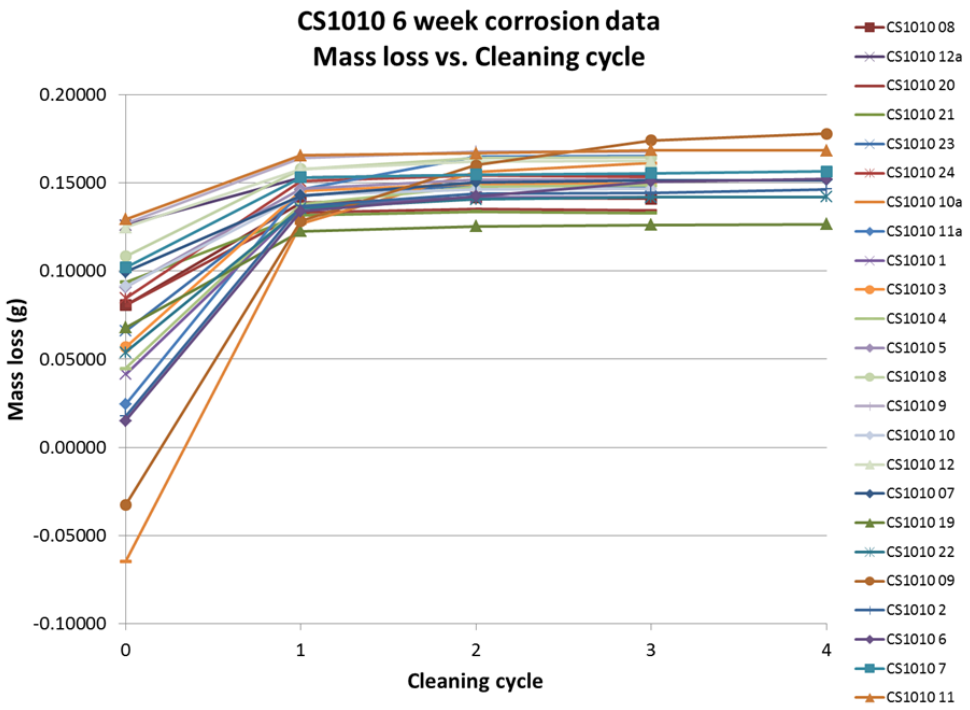

Figure 49. Mass loss vs. cleaning cycle for C1010 coupons exposed to wet polisher conditions in the presence of 1000 ppm inhibitor for 6 weeks.

One cleaning cycle was sufficient for most coupons examined, however coupons C1010 07, C1010 10 and C1010 11a required two cleaning cycles while coupons C1010 09 and C1010 6 required three cleaning cycles to remove corrosion products. Based on this mass loss data, corrosion rates have been calculated and are presented in Figure 50 as a function of corrosion inhibitor. Most of the corrosion inhibitors examined ($CuCO_3$, $Na_2S_2O_3$, 2-mercaptobenzimidazole and tetradecylamine) showed no significant impact on corrosion rates. Myristic acid and Na_2MoO_4 appear to have increased the rate of corrosion when compared to the control experiment containing no corrosion inhibitor. Sodium metavanadate is the only material that displayed a marginal improvement of approximately 13% to the observed corrosion rate compared to the control experiment with no inhibitor. The corrosion rates shown in Figure 50 are lower than typical additive-free carbon steel corrosion rates for aqueous amines reported in the literature[17,23,27,28].

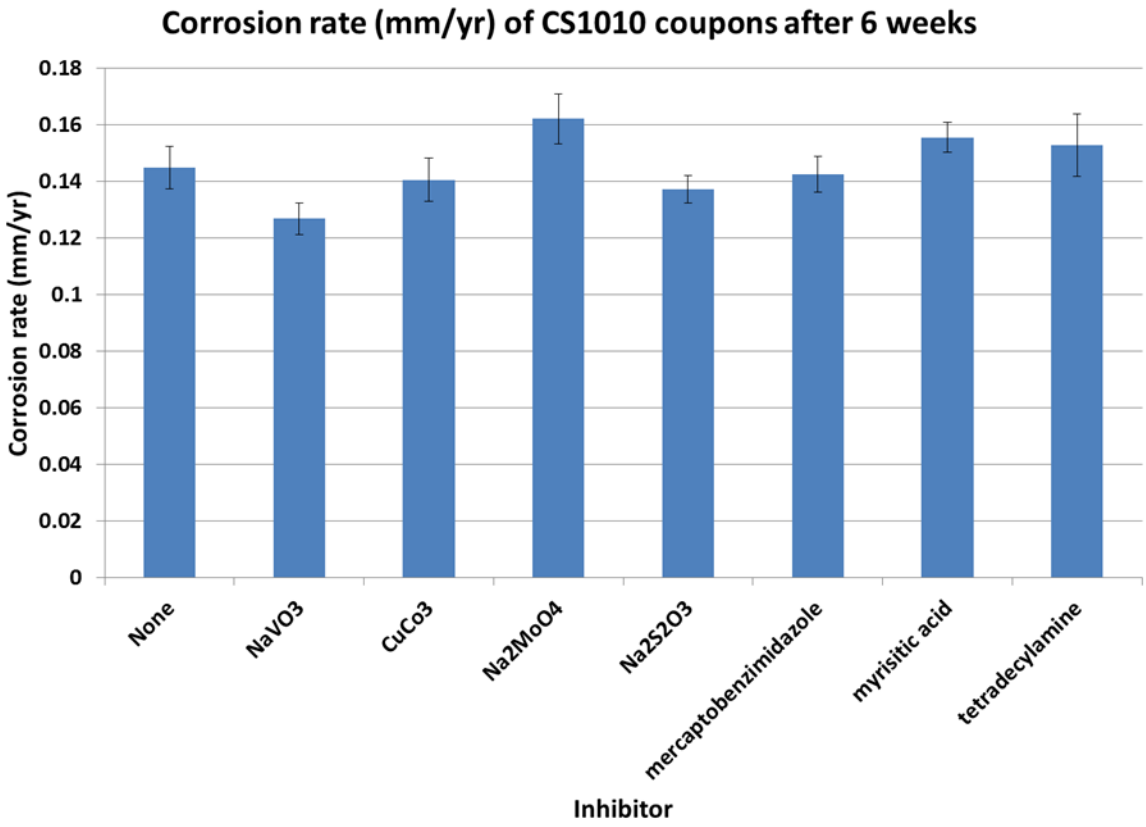

Figure 50. Corrosion rate (mm/yr) for CS1010 coupons after 6 weeks at wet polisher conditions as a function of inhibitor.

Aliquots from the liquid samples recovered from the Teflon® lined stainless steel vessels and from the solid material scraped from the coupons were analyzed by ^{1}H NMR to assess the integrity of the GAP-0 solvent after the 6 week exposure period. The liquid samples were completely soluble in the methanol-*d*4 used to record the ^{1}H NMR spectra and in general showed the presence of 45-55% urea (with the remainder being starting GAP-0 amine), as the result of thermal degradation of the GAP-0 solvent over the course of 6 weeks at 140°C. Despite a filtration to remove bulk insoluble material, fine particulates were present in each of the NMR samples generated from the solid organic residue scraped from the coupons. As a result, these ^{1}H NMR spectra were much broader. However sufficient resolution was available to establish that the methanol-*d*4 soluble portion of the organic residue scraped from the coupons also contained 45-55 % urea (with the remainder being starting GAP-0 amine) as the result of thermal degradation.

Task 4.5 Assemble components into continuous system

Slurry Pump Selection and Commissioning

As a result of the humid absorption experiments described in Task 4.2, the bench scale system was reconfigured for a carbamate/water slurry, rather than dry carbamate

solids. Instead of the dry transfer methods identified to integrate the bench scale absorber with the extruder, a bench scale pump designed for viscous slurries or pastes was employed to transfer carbamate/water slurry from the absorber to the desorber.

Viscosity of carbamate/water slurries was measured to inform selection of a suitable bench scale slurry pump. These slurries were prepared by mixing GAP-0 carbamate solids with water ("synthetic" slurries), which more closely resembles a heterogenous slurry as described in Task 3.4. This approach was used because such synthetic slurries were expected to represent an upper limit on the viscosity of slurries produced in the spray absorber. As shown in Figure 51, the viscosity of such carbamate/water slurries increased with decreasing water content, and could be as high as 20,000cP at low water loading and low temperature. A more complete study of GAP-0/carbamate/water mixtures is discussed in Task 6.1.

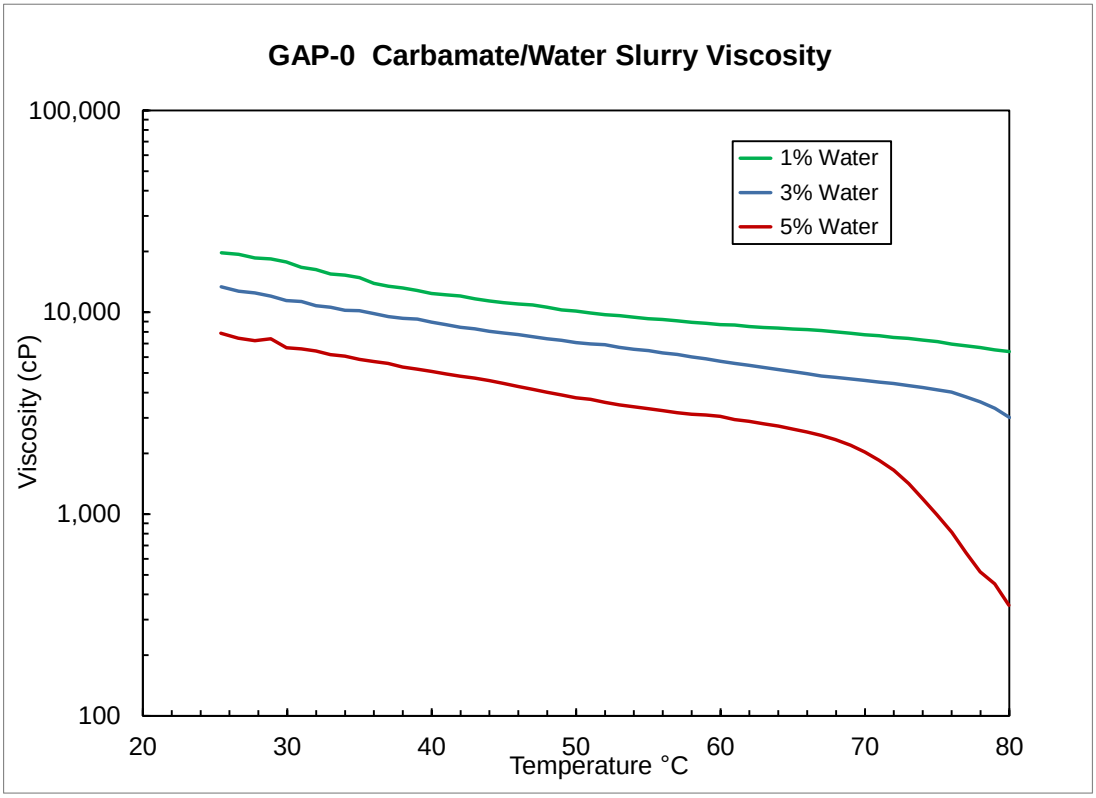

Figure 51. Viscosity of GAP-0 carbamate/water slurries as a function of temperature and water loading.

Given these results, a Seepex progressive cavity pump was purchased for installation in the bench scale system. Progressive cavity pumps utilize a rotating auger to transport and pressurize viscous pastes and slurries. The pump selected for this application can process fluids having viscosities up to 20,000 cP.

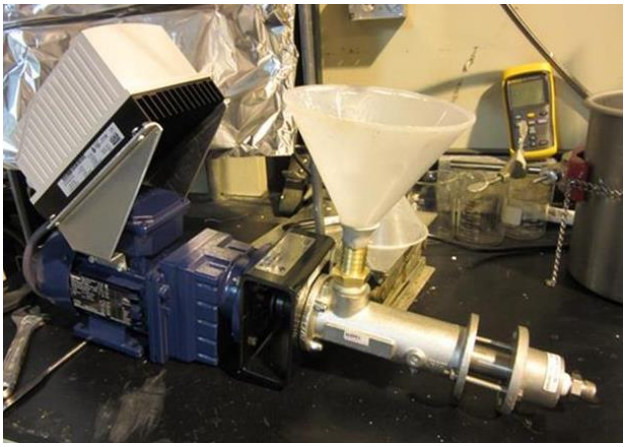

Figure 52. Bench scale progressive cavity pump.

Figure 53. Pump control panel.

Upon receipt of the pump, experiments were completed to confirm pumpability of GAP-0/carbamate/water slurries using the bench scale progressive cavity pump. The progressive cavity pump is shown in
Figure 52, and the control panel for the pump is shown in
Figure 53.

A funnel was added to the inlet of the pump to allow for slurry to be added during testing. A flexible line was connected to the pump discharge to recirculate slurry to the pump inlet. The experiments were completed using a synthetic slurry made with carbamate solids produced in the absorber on 5/13/15. The first test of the pump was completed with slurry containing 56.7% carbamate, 40.9% GAP-0, and 2.4% water. The pump successfully pumped the slurry. Figure 54 shows the slurry being poured into the funnel. Figure 55 shows the slurry being pumped through the flexible recirculation line and back into the inlet funnel.

Figure 54. 56.7% carbamate slurry being poured into funnel at pump inlet.

Figure 55. Pumping of 56.7% carbamate slurry into inlet funnel.

The slurry was returned to the container used for mixing and allowed to stir overnight. Additional carbamate and water were added to the slurry the next day, yielding a slurry comprised of at least 66.2% carbamate, 29.1% GAP-0, and 4.7% water. Some material was lost in the system during pumping on the first day so the carbamate content may have been slightly higher for this experiment.

The pump was able to pump the higher carbamate content slurry, as shown in Figure 56. During pumping, a small scoop of powder was added to the inlet funnel, to simulate

slurry coming from the absorber that could contain chunks of solid carbamate. The slurry could still be pumped, but there was some clogging in the funnel inlet that needed to be dislodged. This observation informed the design of the pump inlet for integration with the bench scale absorber.

Figure 56. Pumping of 66.2% carbamate slurry into inlet funnel.

Control and Data Acquisition System

A control and data acquisition system was built and installed to the phase-changing CO_2 capture system. The system is split into two major sections: the absorber and the desorber. The system was built based on a single GE 90/30 Programmable Logic Controller (PLC) and a PC running Cimplicity, a GE Intelligent Platforms software product that provides visualization, data storage, and a custom user interface.

The absorber control system consists mainly of collecting temperature, pressure, moisture and flow values from the absorber gas and liquid feed system. The simulated flue gas is controlled and measured, mixing N_2 and CO_2 to meet the desired flow rate and composition. The system can also control the humidity of the gas feed with a humidifier and controllable water feed system. The inlet and outlet gas pressures are measured. The discharged CO_2-rich slurry will be pumped out of the absorber through a temperature controlled line to the desorber system. The flow rate, density, and temperature of the slurry will be measured via an Endress and Hauser coriolis meter. The CO_2 content of the exit gas is measured by an online CO_2 analyzer. Exit gas flow is currently measured via a pitot tube, due to solids interference with a more sophisticated thermal type flowmeter. With the shift to a slurry-based system, we hope to be able to use thermal type flow meter. The gas feed and liquid feed (lean solvent) are in open loop control. The user interface is shown in Figure 57.

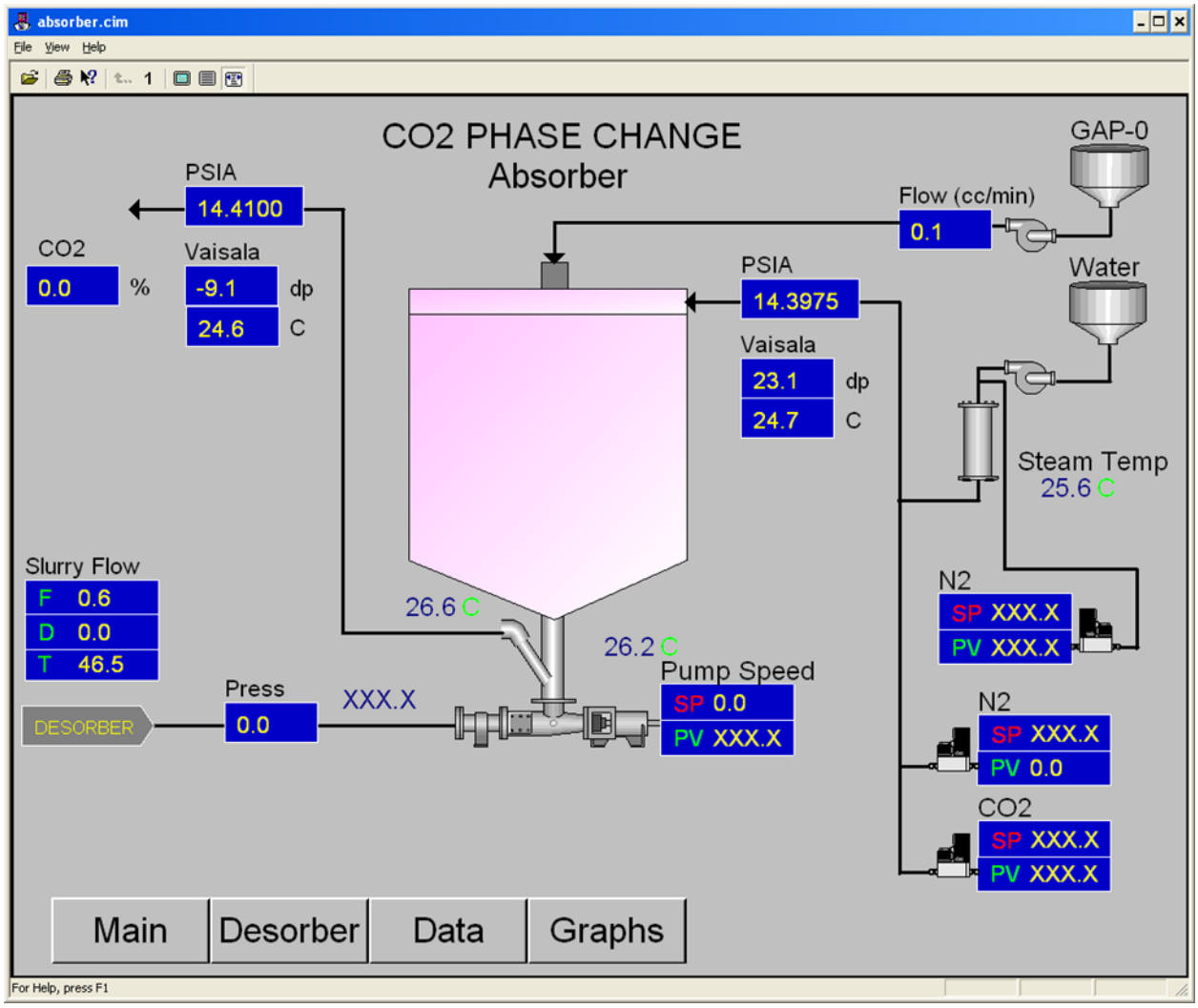

Figure 57. Absorber control system user interface.

The desorber control system consists mainly of data acquisition of temperature of the rich feed and the temperatures of the desorber and oil heat system. The CO_2 gas effluent is measured for flow rate and moisture content. The lean solvent is removed from the desorber via a pump that is controlled from the measured level in the desorber. This pump can also be controlled for flow rate from the lean solvent flow meter. Since heat input is critical to this sub-system, the hot oil supply and return temperatures to the desorber are measured. The user interface is shown in Figure 58.

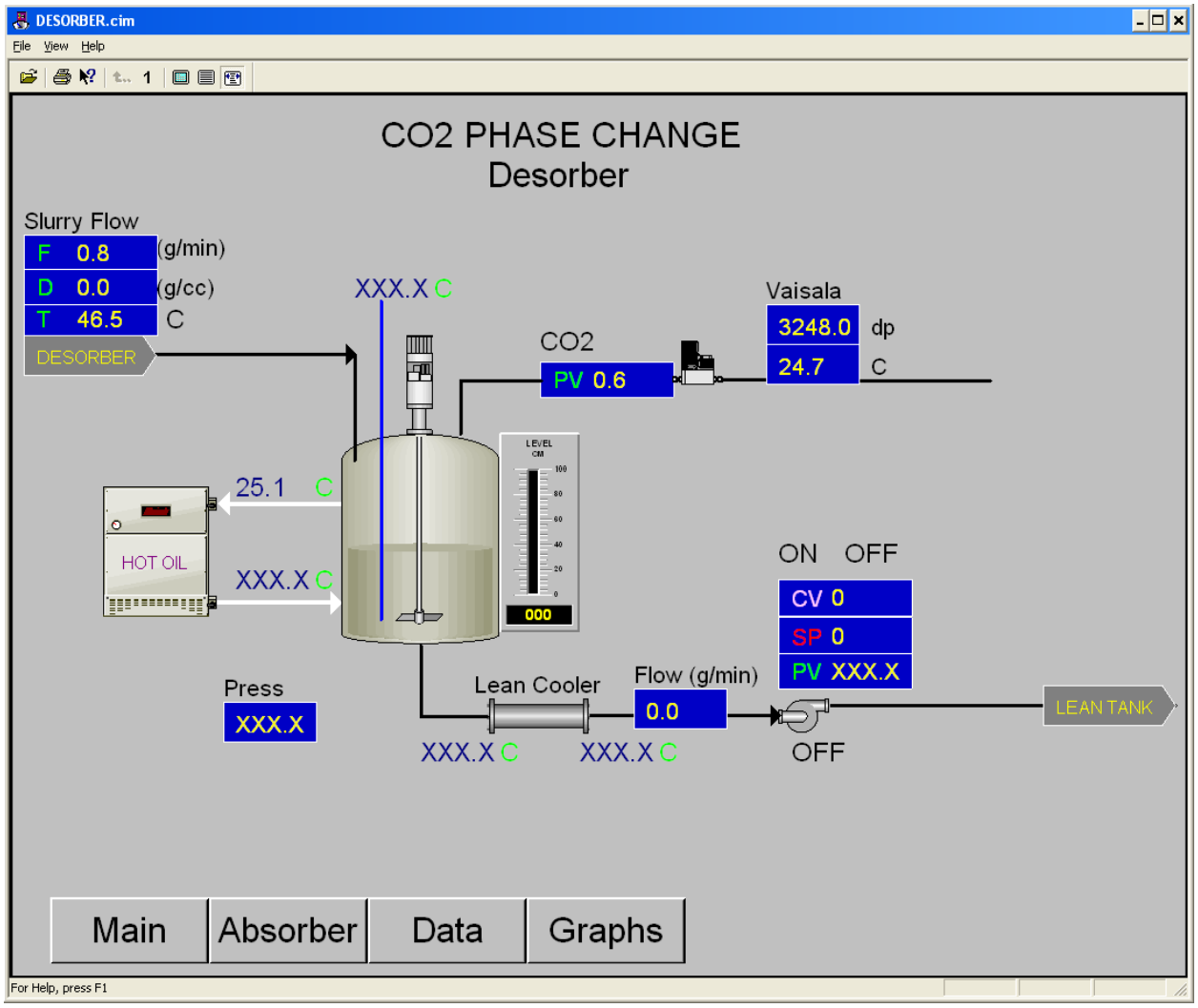

Figure 58. Desorber control system user interface.

Data from this system is logged continuously into a database and can be easily exported to Excel for manipulation and analysis.

Task 5 – Perform technology assessments

Task 5.1 – EH&S Risk Assessment

An EH&S risk assessment was performed to determine the impact of the process on human health and the environment. This report is included in DOE's OSTI database, report number DOE-GEGR-0013687-3.

Task 5.2 – Update capture cost model

The capture cost model was updated to reflect the shift in focus from dry CO_2-rich solids to a CO_2-rich carbamate/water slurry. This analysis yielded cases that met the target of $45/tonne CO_2 captured, which was the goal defined for the second budget period of the project.

Task 5.3 – Update process model to include integrated system performance

The phase-changing aminosilicone process configurations considered in Task 5.3 are summarized in Table 24 and Figure 60. The lean solvent enters the absorber at 40°C (104°F) and chemically reacts with CO_2 contained in the flue gas, forming a dry, friable solid or a slurry depending on the water content of the CO_2 stream. The absorber for this process is a spray absorber, since the rich solvent leaves the absorber in a solid or slurry form. The exothermic CO_2 absorption reaction increases the temperature of the solvent. The absorber is operated at 40-82°C (104-180°F) and at atmospheric pressure. The rich solvent from the absorber is fed to an extruder (Cases 6-6C) or slurry pump (Cases 6D-6I), which feeds the slurry into a pressurized desorber (Case 6) or an atmospheric pressure desorber (Case 6A-6I), wherein the solids are heated to 130-150°C (266 to 302°F) to produce a stream of CO_2 and a regenerated stream of solvent. The hot vapor products from the desorber, which consist primarily of CO_2, are cooled in heat exchangers utilizing water. Entrained solvent is removed from the cooled gas streams and returned to the desorber. The gas stream is further cooled to remove the entrained water, which is sent to the waste water treatment plant. The cooled CO_2 gas is delivered to the CO_2 product compressor. The lean solvent exiting the desorber is cooled before recycle to the absorber. In the commercial process, this cooling step would be part of a rich/lean heat exchange arrangement, to maximize heat management around the desorption system.

Table 24. Summary of major cases considered for the phase-changing aminosilicone CO_2 separation system.

Case	# of desorbers	Desorber Temperature (°C)	Desorber Pressure (psia)	Rich/Lean U (BTU/hr/ft²/F)	Rich Solvent	Rich pump	550MW net w/ capture
6	2	150	1st – 63 2nd - 15	25	Solid	Pump	N
6A	1	150	15	25	Solid	Extruder	N
6B	1	140	15	25	Solid	Extruder	N
6C	1	130	15	25	Solid	Extruder	N
6D	1	140	15	75	50 wt% GAP-0	Slurry Pump	N
6E	1	130	15	75	50 wt% GAP-0	Slurry Pump	N
6F	1	140	15	75	5 wt% H_2O	Slurry Pump	N
6G	1	130	15	75	5 wt% H_2O	Slurry Pump	N
6H	1	140	15	75	5 wt% H_2O	Slurry Pump	Y
6I	1	140	15	75	5 wt% H_2O	Slurry Pump	Y

Schematic sketches of the phase-changing CO_2 capture process concepts are shown in Figure 59.

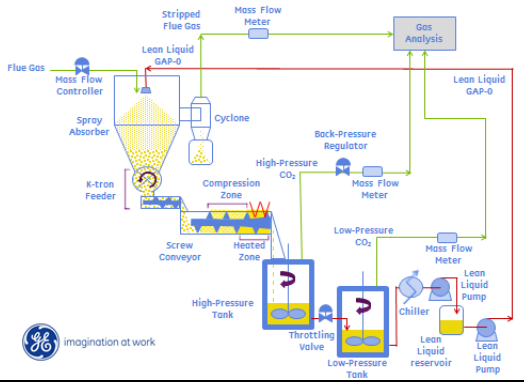	Case 6 – Extruder used to feed 2-stage (pressurized + atmospheric pressure) desorber
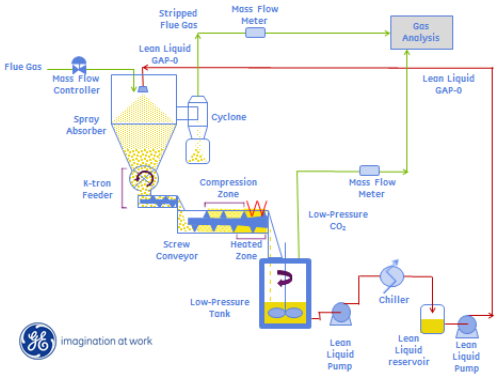	Case 6A-Case 6C – Extruder used to feed single stage atmospheric pressure desorber
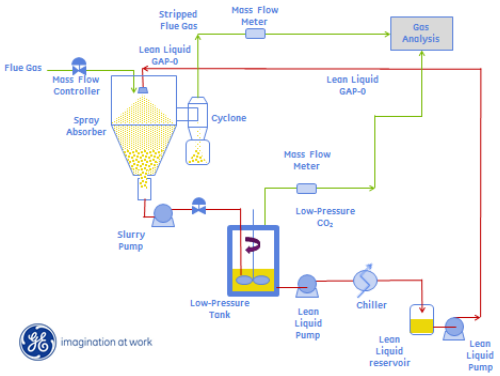	Case 6D-Case 6I – Slurry pump used to feed single stage atmospheric pressure desorber

Figure 59. Conceptual designs for the phase changing aminosilicone CO_2 capture process.

Task 5.4 – Determine solvent manufacturability

A solvent manufacturability study was prepared, in which synthetic pathways to GAP-0 were reviewed and cost estimates were prepared for commercial scale manufacture of the GAP-0 solvent. This report is included in Appendix A of this document.

Task 6 – Continuous system testing

Task 6.1 – System integration

Continuous Absorber Testing and Slurry Pump Integration

Four experiments were completed to determine the effect of liquid flowrate and gas CO_2 concentration on slurry composition. A summary of the experiments is provided in Table 25.

Table 25. Summary of absorber runs.

Run ID	Liquid flow rate setpoint (mL/min)	Gas flow rate (slm)	Gas composition (mol% CO2 in N2)	GAP0/CO2 molar ratio	Slurry water content per KFT (wt%)	Extractables (wt% carbamate)	mol% GAP-0 conversion (per extractables)	mol% CO2 conversion (per extractables)	% CO2 conversion per CO2 analyzer
2016-05-09	160	150	16%	0.59	3.3	78.1	75.2%	44.4%	49.9%
2016-05-19	270	150	16%	1.00	3	72	68.6%	68.4%	77.9%
2016-06-13 A	30	150	2%	0.89	12.2	78.9	76.1%	67.4%	68.0%
2016-06-13 B	40	150	2%	1.18	8.1	76.4	73.3%	86.7%	67.3%

All of the experiments were completed with a total gas flowrate of 150 slm and a dew point in the range of 38-40°C, and pumpable slurry was formed in each experiment. The carbamate and water contents of the slurries are provided in Table 25. Carbamate content was measured directly using the extractables method described above. Water content was measured via Karl-Fischer titration, using methanol as the solvent. CO_2 capture efficiency was calculated using both the gas and liquid side composition data, and the two metrics were generally in agreement. As expected, the water content increased significantly as the lean liquid flow rate was decreased for the 2% CO_2 runs. The slurry produced during these runs appeared to have significantly lower viscosity than previous experiments.

In these experiments, it was observed that CO_2 capture efficiency was comparable in wet and dry flue gas conditions for varying GAP-0 : CO_2 mole ratios. As shown in Figure 60, the presence of water did not appear to inhibit CO_2 absorption by the phase-changing solvent. The conditions shown in Figure 60 are 150slm gas flow rate containing 16% CO_2 (blue, orange) and 2% CO_2 (green), and liquid flowrates commensurate with 0.6 GAP-0 : CO_2 mole ratio (blue) and 1 GAP-0 : CO_2 mole ratio (orange, green).

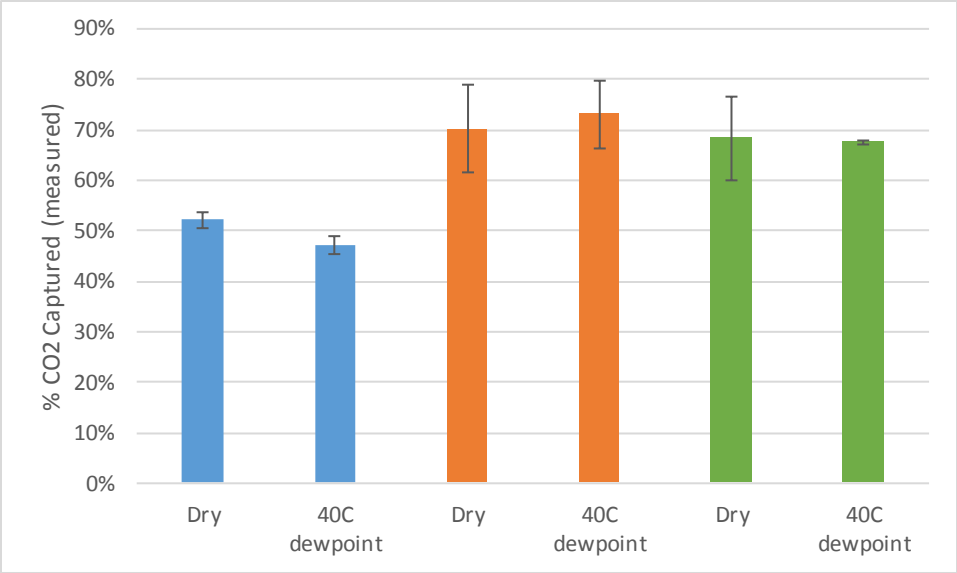

Figure 60. Comparison of CO_2 capture efficiency for dry vs. wet flue gas for a range of absorber operating conditions.

Three absorber experiments were completed to evaluate the effect of carbamate and water content in the liquid feed to the absorber. Though all three experiments were completed using the same liquid flowrate setpoint, the liquid flowrates for the 8/23/16 and 8/24/16 experiments were significantly lower than the setpoint due to clogging observed in the filter on the liquid line feeding the absorber. The buildup of carbamate on this filter is suspected to be due to solids precipitation in the material used to feed the absorber. This issue was not observed during the 9/9/16 run after the filter was changed, nor was it observed in later experiments wherein solvent was immediately circulated from the desorber to the absorber. Solvent sample analysis data from these experiments is summarized in Table 26.

Table 26. Lean solvent and slurry composition from absorber experiments.

Date	Sample Type	GAP-0 carbamate (wt %)	Water (wt %)	GAP-0 (wt %)
8/23/16	Absorber lean feed solvent	4.5	2.3	93.2
	Absorber slurry effluent	84	5	11
8/24/16	Absorber lean feed solvent	24.9	5.5	69.7
	Absorber slurry effluent	84.4	6.7	8.9
9/9/16	Absorber lean feed solvent	14.1	3.1	82.8
	Absorber slurry effluent	85.5	7.7	6.8

During the 9/9/16 absorber experiment, carbamate buildup was observed on the outside of the absorber due to leakage through the lid. The gasket around the lid was replaced with EPDM foam after this experiment, and clamps were added around the lid to further decrease the potential for leaks. It also appeared that some GAP-0 may have gotten into the air motor for the rotary atomizer. This issue was confirmed on 9/20/16 when a piece of tubing was attached to the compressed air outlet on the atomizer and directed to a collection container. A significant amount of liquid was observed in that tubing as soon as GAP-0 flow reached the atomizer, which indicated that the rotary atomizer was not functioning properly. Repair and replacement of the rotary atomizer is costly and requires a long lead time. As a result, the pneumatic atomizer was installed to the absorber and was used for all subsequent testing.

These absorber experiments demonstrated that the absorber system was robust to the presence of carbamate and water in the lean solvent, up to at least 25wt% carbamate and 7.7% water. Pumpable slurry was produced in each of these experiments.

Viscosity of GAP-0/Carbamate/Water Mixtures

Characterization of GAP-0/carbamate mixtures as described in Task 3.4 focused on water-free mixtures. Given the reconfiguration of the bench scale process for carbamate slurries, the effect of water content on viscosity needed to be studied. Further, the addition of water to GAP-0/carbamate mixtures allowed for study of higher carbamate loadings than attainable in dry (water-free) mixtures.

Mixtures containing carbamate loadings of 0% - 80% and water concentrations of 0% - 15% were prepared. Each carbamate concentration was prepared in a similar manner to that employed in Task 3.4. GAP-0 and GAP-0 carbamate solid were mixed in a three-neck flask fitted with an overhead stirrer and nitrogen inlet. The mixtures were heated to 100°C under a blanket of nitrogen until a single-phase solution was obtained, at which point the solution was divided into separate containers and Millipore water was added to obtain the desired water content. Extractables measurements for each carbamate solution prepared in this way showed minor deviations in carbamate concentration from the targeted value, as a result of CO_2 absorption or desorption during heating. Samples containing 72% carbamate showed a tendency to precipitate/crystallize on standing at room temperature. As a result, these samples were stored at 80°C prior to viscosity measurements as a preventative measure to ensure the samples remained homogeneous (see Table 27). The 72% carbamate samples with <10% water did not remain homogeneous solutions even if stored at 80°C and therefore no viscosity measurements were performed.

Table 27. GAP-0/GAP-0 carbamate solution concentrations and storage temperatures.

Solution	% Carbamate per extractables method	Storage temperature (°C)
GAP-0	0	25
F2356-137	19	25
F2414-11	45	25
F2414-12	66	25
F2356-154	72	80

The viscosity of each solution was measured over a range of shear rates (1 – 150 s^{-1}) and temperatures (25 – 80°C). Because viscosity was found to be independent of shear rate, the results are shown below for a shear rate of 25 s^{-1} in Figure 61 through Figure 65. Interestingly, both the GAP-0 (Figure 61) and 19% GAP-0 carbamate (Figure 62) solutions exhibit an increase in solution viscosity as water is added. This observation is reversed at higher carbamate concentrations as depicted in Figure 63 through Figure 65 for the 45%, 66% and 72% GAP-0 carbamate solutions. It was observed that the 72% carbamate solutions with 10% and 15% water remained homogenous down to 30°C, enabling viscosity measurements to be performed at these temperatures.

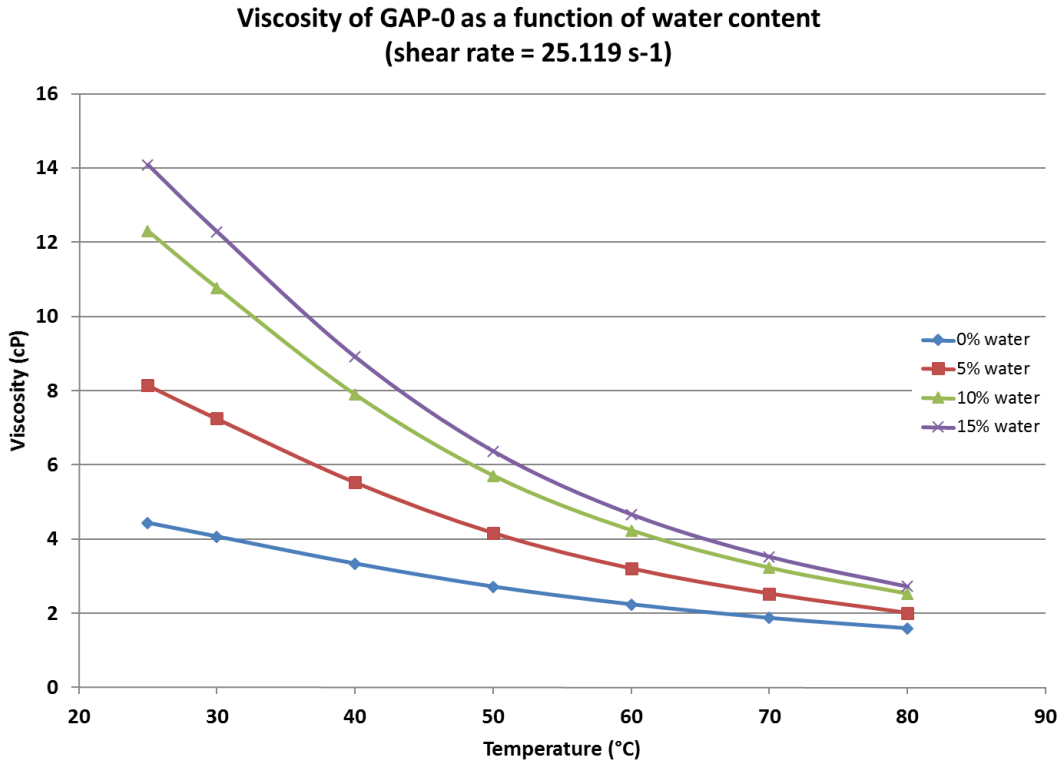

Figure 61. Viscosity of GAP-0 as a function of water content.

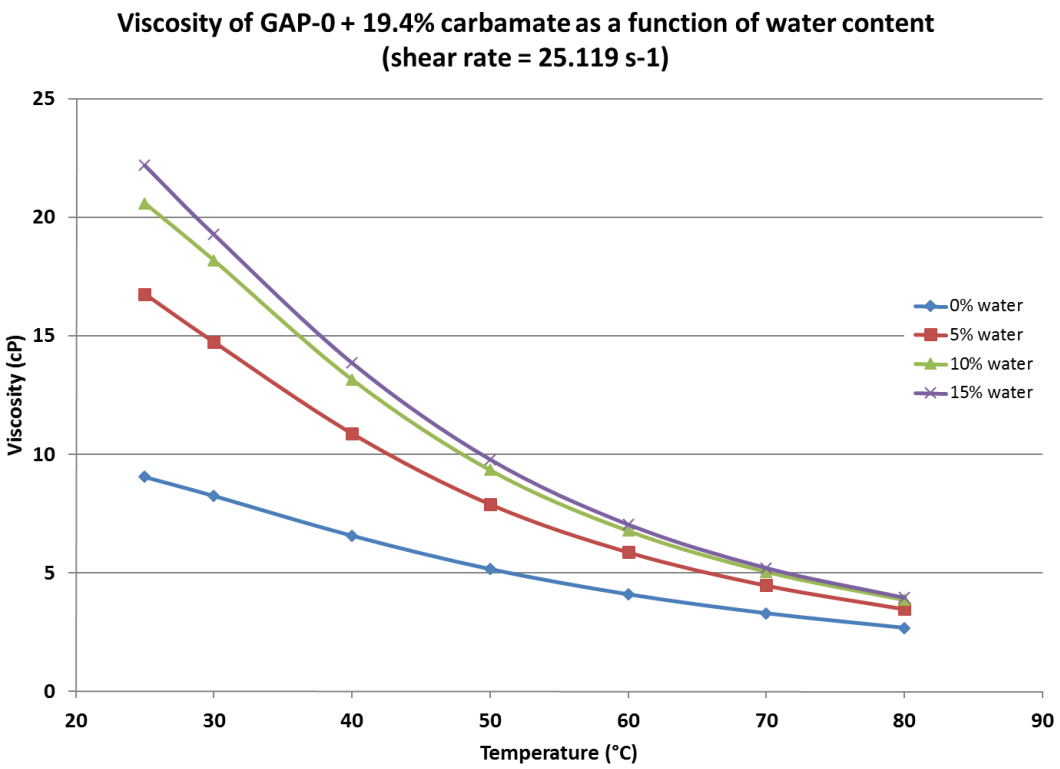

Figure 62. Viscosity of 19% GAP-0 carbamate as a function of water content.

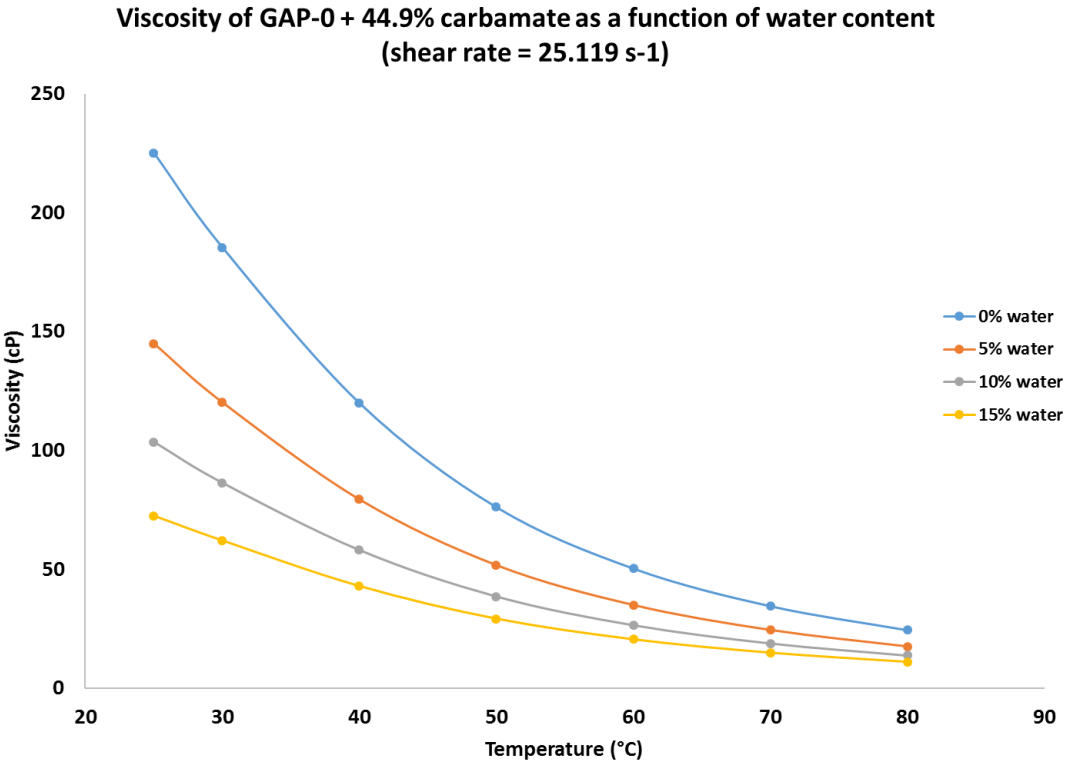

Figure 63. Viscosity of 45% GAP-0 carbamate as a function of water content.

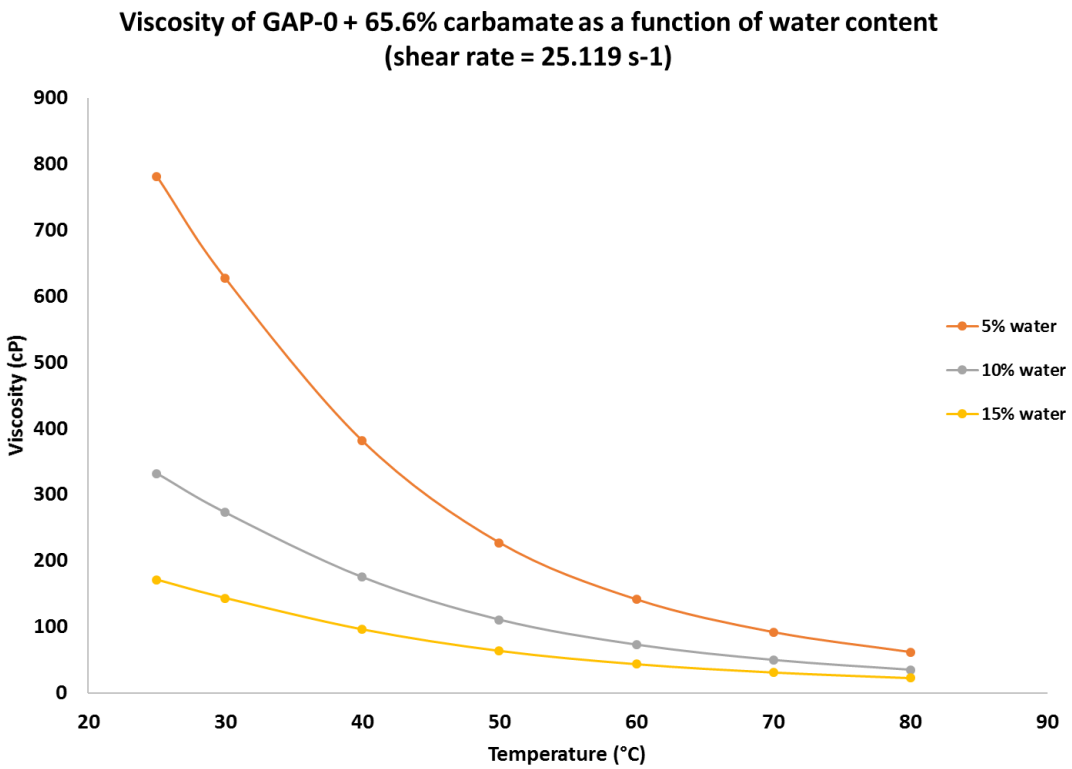

Figure 64. Viscosity of 66% GAP-0 carbamate as a function of water content.

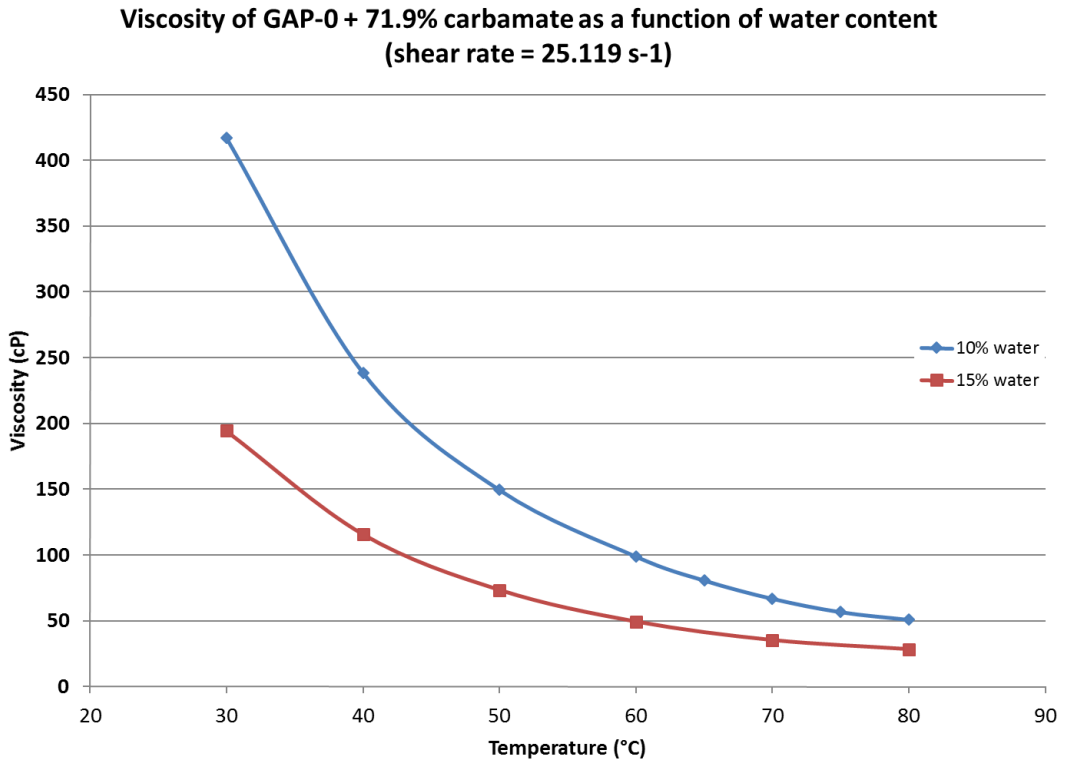

Figure 65. Viscosity of 72% GAP-0 carbamate solution as a function of water content.

This more complete data set relating viscosity to slurry composition was used to develop a model relating slurry viscosity to slurry composition, which was incorporated into the Aspen process model for process optimization and economic analysis. Development of this model is discussed in more detail in Task 7.2.

Continuous Desorber Experiments

Continuous mode desorber experiments were initiated before the bench scale slurry pump was installed. During this period, a peristaltic pump was used to feed a GAP-0/GAP-0 carbamate slurry to the desorber. Norprene peristaltic pump tubing was used because it has been shown to be resistant to aminosilicones. This arrangement successfully pumped GAP-0/GAP-0 carbamate slurries containing up to 51% carbamate and 3% water at flow rates of 20-100mL/min. Slurries were produced in a continuously stirred tank (shown in Figure 66) having a discharge port mounted at the bottom of the tank.

Figure 66. Slurry holding tank having continuous agitation.

After demonstration of successful pumping with this apparatus, the slurry was continuously stirred overnight. The following morning, the slurry was still pumpable in the peristaltic pump arrangement. The pump was then used to add slurry continuously to the desorber, which contained solvent from a previous batch mode experiment discussed previously. The pump was set at a flowrate of 20 mL/min. The temperature during this experiment is provided in Figure 67**.** A temperature decrease was observed in the desorber when slurry addition started, and thereafter the vessel temperature rebounded to the desired setpoint. This effect suggested that additional heat transfer

capacity was needed in the polisher to maintain temperature at the desired operating conditions.

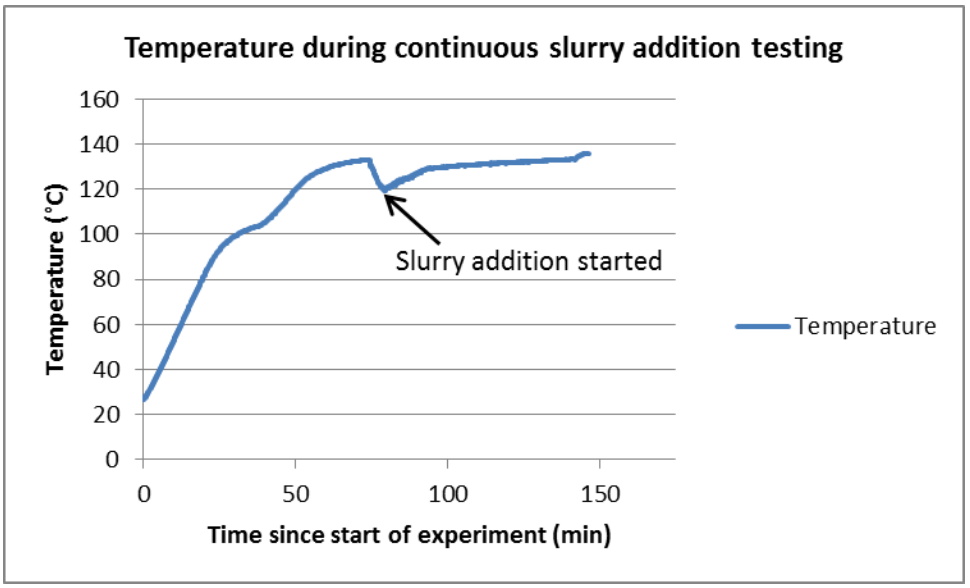

Figure 67. Desorber temperature during continuous slurry addition at 20mL/min.

Several continuous desorber experiments were completed using slurries that were prepared manually to controlled composition. In this way, operability of the desorber could be de-risked before integration of the spray absorber and slurry pump. These experiments are summarized in Table 28.

Table 28. Summary of desorber experiments

Date	Slurry Composition	Slurry Feed Rate (mL/min)	CSTR Temp. (deg C)	Recirculation HX?	Notes
4/6/2016	48.1% carbamate, 3.1% water	35	136	N	Confirmed need for HX upgrade
6/2/2016	50.3% carbamate, 3.1% water	40	133	Y	
6/14/2016	77.7% carbamate, 8-13% water		~130	Y	Demonstrated need for improved pressure relief.
6/27/2016	45.6% carbamate, 6% water	50-75	130	Y	Demonstrated need for increased gas condenser

					capacity.
7/15/2016	44% carbamate, 3% water	50-100	130	Y	Demonstrated stable temperature control.
7/18/2016	46.3% carbamate, 5.9% water	50-150	130	Y	

The first experiment (conducted on 4/6/16) was intended to confirm the heat transfer performance of the CSTR for a carbamate/water slurry when operated with continuous slurry addition. Because the bench scale system was initially designed for a two-stage desorption process and for low levels of water, it was necessary to determine if the atmospheric pressure CSTR was undersized.

A slurry comprised of 48.1 wt% carbamate and 3.1 wt% water in lean GAP-0 was prepared in a stainless steel container. The slurry was continuously mixed during the experiment, and the container was heat traced to 45°C to ensure that the mixture could be pumped easily.

The experiment started with an inventory of lean liquid in the CSTR, which was heated to 136°C prior to slurry addition. The slurry was pumped into the reactor at a setting of 35 mL/min on the peristaltic pump. This corresponded to a flowrate of approximately 50 g/min according to a Coriolis flowmeter.

The temperature in the polisher decreased significantly to 123.7°C after approximately 23 minutes of slurry addition. The slurry feed was then turned off to allow the reactor temperature to increase before flowing liquid through the lines on the outlet of the polisher. This observation led to the decision to implement a recirculation loop heat exchanger to increase the heat transfer to the desorber.

After allowing the reactor to heat for approximately 17 minutes, the flow was turned on again to the 35 mL/min setting on the peristaltic pump. The lean pump on the outlet of the polisher was turned on at a flowrate of approximately 31 g/min. Attempts were made to increase the flowrate of lean liquid on the outlet of the polisher. However, operation of the pump created a vacuum in the lines after the polisher, and the flowrate leaving the polisher was observed to decrease over time.

After this experiment, the lean cooling heat exchanger was replaced to see if this resolved the issue with the vacuum in the lines. The recirculation loop with a heat exchanger (Figure 68) was integrated into the desorber to improve heating given the significant decrease in temperature that was observed during continuous slurry addition.

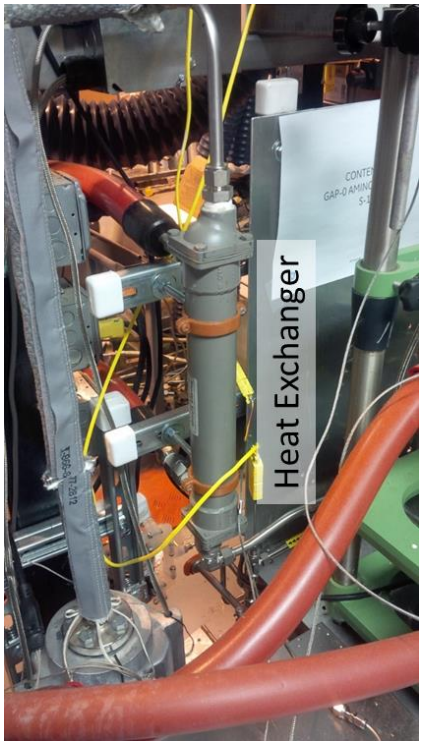

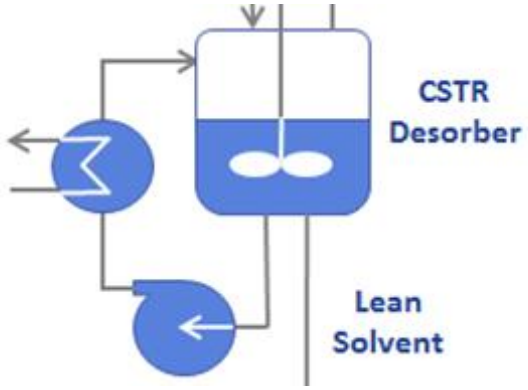

Figure 68. Heat exchanger for desorber recirculation loop.

The purpose of the second experiment (6/2/2016) was to test the new heat exchanger on the recirculation loop and to determine if the issue with vacuum in the outlet lines for the polisher was resolved. In this experiment, a slurry comprised of 50.3 wt% carbamate and 3.1 wt% water in lean GAP-0 was prepared in the heated stainless steel container. The container was heat traced to 50°C during this experiment.

The reactor was heated to approximately 133°C before slurry flow started. Then slurry was pumped into the reactor at a setting of 40 mL/min, which corresponded to the 75-96 g/min according to the flowmeter. However, there continued to be issues with vacuum in the outlet lines from the polisher so the flowrate leaving the polisher reached a maximum of only 36 mL/min and was unable to maintain a consistent level of solvent in the polisher during the experiment. Figure 69 shows the decrease in temperature that was observed during slurry addition and corresponding increase in temperature after the slurry pump was turned off. Given that issues were still observed with vacuum in the liquid line after the polisher, the lean solvent pump was moved from its position after the flowmeter to directly before the flowmeter after this experiment.

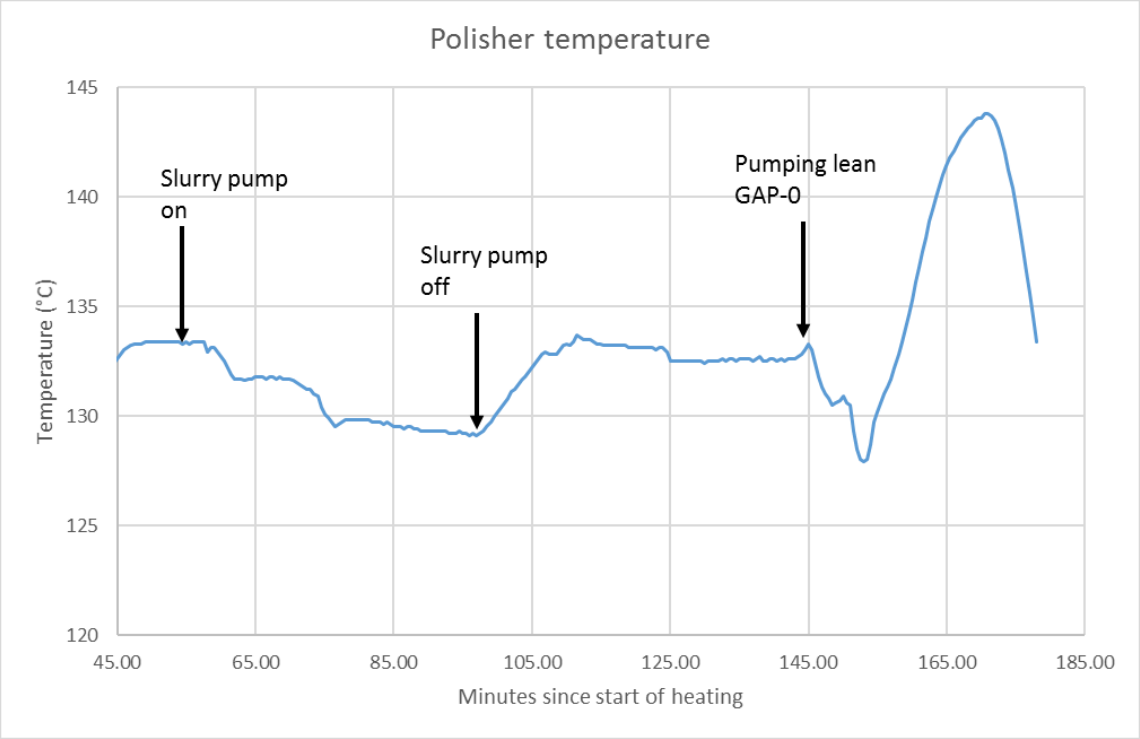

Figure 69. Polisher temperature during 6/2/16 experiment.

The purpose of the third experiment (6/14/2016) was to demonstrate operation with slurry having higher carbamate and water concentration. Slurry produced during the 6/13/16 absorber run was used for this experiment. The water content of the slurry from the absorber runs ranged from approximately 8-13 wt% water, which is significantly higher than previous runs in the polisher. In addition, the carbamate concentration was higher, and was more typical of carbamate loading of slurries produced in the spray absorber. The polisher was observed to cool significantly during slurry pumping as a result of the high water content and higher liquid flowrate.

A pressure build-up in the polisher was also observed that caused the glass fitting on the gas outlet of the reactor to lift out of place and the balloon used for pressure relief to fully inflate. A significant pressure drop across the flowmeter on the lean liquid line was also observed that limited the maximum flowrate that could be achieved on the outlet of the polisher.

The purpose of the fourth experiment (6/27/2016) was to continue to increase the feed flowrate to the desorber, with the aim of demonstrating operation at slurry flow rates that are more consistent with spray absorber operation. A slurry comprised of 45.6 wt% carbamate and 6 wt% water in lean GAP-0 was prepared in the heat traced stainless steel container. The container was heat traced to 50°C during pumping.

The lean flowmeter was not yet exchanged with the new unit before this experiment, so this experiment was completed with the lean flowmeter bypassed to avoid the issues with high pressure drop in the desorber liquid discharge lines. The pressure

gauge located after the flowmeter showed a very low pressure indicating that the current lean flowmeter is the source of at least some of the pressure drop between the desorber and the lean solvent storage tank.

Flow started at a setpoint of 50 mL/min on the peristaltic pump, which corresponded to approximately 56 g/min on the slurry flowmeter. As expected the temperature in the desorber initially decreased, so the hot oil temperature was increased in an attempt to keep the reactor temperature at about 130°C. The flowrate was later increased to a setpoint of 75 mL/min, which corresponded to 105-125 g/min on the flowmeter. Significant fluctuations in flowrate were observed according to the flowmeter during the experiment.

Figure 70 shows the effect of slurry addition on the polisher temperature in this experiment. As previously mentioned, significant temperature decreases were observed during slurry addition. A build-up of pressure in the polisher, as evidenced by the fully inflated balloon, was also observed. This limited how much the hot oil temperature could be increased, and, as a result, it could not be determined if the polisher could be adequately heated at higher hot oil temperatures. Subsequently, a manometer pressure relief device was installed to the desorber to eliminate this limitation.

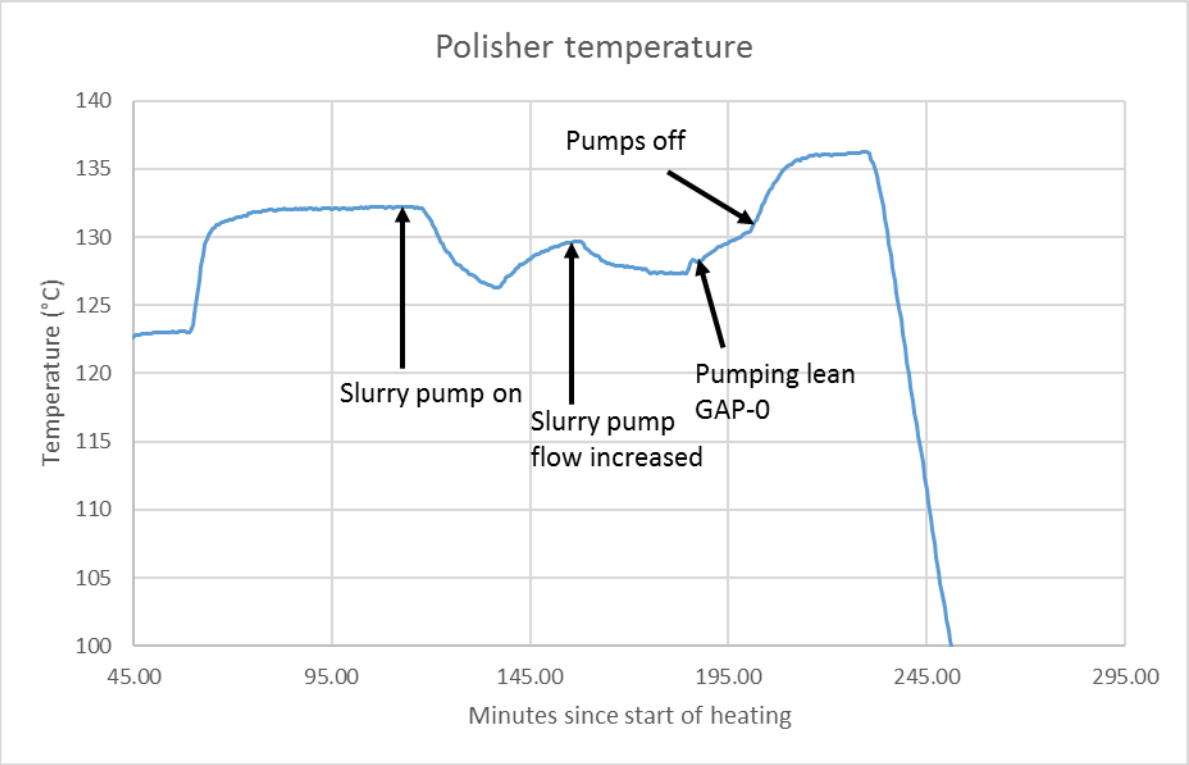

Figure 70. Polisher temperature during 6/27/16 experiment.

The purpose of the 7/15/2016 and 7/18/2016 experiments was to confirm that the manometer installed on the gas outlet of the unit was working properly and to test how well the desorber temperature and level could be controlled at different slurry

flowrates. Table 29 summarizes the compositions of the slurries used for the two experiments.

Table 29. Synthetic slurry and lean solvent compositions used in desorber experiments.

Date	Sample Type	GAP-0 carbamate (wt %)	Water (wt %)	GAP-0 (wt %)
7/15/16	Synthetic slurry feed	44	2.95	53.05
	Lean solvent product	10	2.5	87.5
7/18/16	Synthetic slurry feed	46.3	5.9	47.8
	Lean solvent product	7.7	2.8	89.5

Both experiments showed that a temperature of approximately 130°C could be maintained in the reactor, though fluctuations were observed when slurry flowrates to the reactor were increased. The temperatures of the hot oil units were adjusted accordingly to compensate for this during the experiments. These experiments showed that at 130°C approximately 77-83% of carbamate fed to the reactor was converted to GAP-0, and that a measurable portion of the water contained in the slurry remained in the liquid desorber effluent. These results informed the next set of absorber experiments, which were designed to evaluate the effect of lean solvent carbamate and water concentration on absorber performance.

During the 7/18/2016 desorber experiment, water was observed to be dripping out of a vent line on the discharge side of the desorber gas flowmeter. This prompted the addition of a peristaltic pump to the condenser on the gas line to continuously remove water from the system. This was first utilized during the integrated experiment on 7/25/2016 and was used in all subsequent experiments.

Integrated System Experiments

After demonstrating continuous operation of the absorber/slurry pump and desorber subsystems for a range of slurry compositions, the two subsystems were connected, forming an integrated system. Virgin GAP-0 was sprayed into humid simulated flue gas in the spray absorber, and the resulting slurry was pumped into the desorber inlet. In these experiments, lean liquid from the desorber was collected in separate containers. This intermediate step allowed for evaluation of desorber performance while mitigating the risk of any negative impact of lean solvent carbamate loading on the absorber. Sample analysis data from these experiments is summarized in Table 30.

Table 30. Slurry and lean solvent composition from integrated experiments.

Date	Sample Type	GAP-0 carbamate (wt %)	Water (wt %)	GAP-0 (wt %)
7/20/16	Absorber slurry effluent	60.1	1.9	38
	Desorber lean solvent effluent	9.3	1.2	89.5
7/25/16	Absorber slurry effluent	No samples taken	No samples taken	No samples taken
	Desorber lean solvent effluent	17.4	1.6	81
7/27/16	Absorber slurry effluent	80.2	12.5	7.3
	Desorber lean solvent effluent	11.3	1.3	87.4
8/4/16	Absorber slurry effluent	80.8	1.9	17.3
	Desorber lean solvent effluent	18.5	0.8	80.7
9/23/16	Absorber slurry effluent	82.8	4.9	12.3
	Desorber lean solvent effluent	11.6	2.5	85.9

Four of these experiments were completed with the rotary atomizer. Only the 9/23 run utilized the pneumatic atomizer. The 9/23 run demonstrated that pumpable slurry could be formed using the pneumatic atomizer. For the pneumatic atomizer set-up, the humidified portion of the simulated flue gas was fed to the atomizer, serving as the atomizing gas, and the balance of the CO_2 and N_2 gas mixture was fed through the lid of the absorber as in the rotary atomizer configuration.

For the first integrated experiment on 7/20, the experiment was started with the progressive cavity pump discharging into a stainless steel container so the appearance and consistency of the slurry could be monitored during the experiment. A peristaltic pump was then used to transfer the slurry from that container into the desorber. After observing that the slurry could be pumped through the system using this setup, the intermediate slurry collection step was bypassed. In the remainder of this experiment and in all subsequent experiments, the progressive cavity pump discharged directly to the desorber.

The integrated experiment completed on 7/25 was the only experiment completed at the higher liquid flowrate of 120 mL/min. It was challenging to maintain higher temperatures in the desorber at this flow rate due to the slurry water content. It was also more challenging to recover from minor system upsets during a run at this higher

flowrate. Therefore, the GAP-0 liquid flowrate was fixed at 90 mL/min for remaining experiments, allowing for exploration of other process variables.

It was observed during these early integrated experiments that it was challenging to run the slurry flowmeter without observing significant variations in flowrate. This was thought to be due to periodic pump starvation and entrainment of gas bubbles in the slurry pump discharge lines. The 7/27 integrated experiment was run at a lower progressive cavity pump flowrate to see if this issue would be resolved. However, this resulted in overflow of the slurry pump inlet, causing solvent to carry over into the absorber gas effluent lines. Ideally, the pump should be operated such that the inlet is flooded, but the head of liquid at the inlet should be minimal to limit solvent carryover with the gas exhaust. To improve our ability to monitor this liquid level and detect solvent carryover, the flexible hose that connected the absorber to the gas exhaust lines was replaced with a clear hose.

Throughout the desorber experiments and culminating in the 8/4/2016 integrated experiment, pressure built up several times in the desorber. This resulted in the agitator fitting lifting out of the lid of the desorber. These episodes of presure rise in the desorber were due to significant clogging of the CO_2 flowmeter on the desorber gas effluent line. As small amounts of GAP-0 were carried out of the desorber, they accumulated in the CO_2 flowmeter. Because this flowmeter was near room temperature and in a CO_2-rich environment, this entrained GAP-0 solidified in the flowmeter. After the 8/4/2016 experiment, this flowmeter was bypassed to eliminate future episodes of pressure rise in the desorber.

Task 6.2 - Steady state testing

Demonstrate continuous steady-state operation

Following succesful operation of the integrated system, continuous closed-loop testing commenced. In these experiments, lean liquid from the desorber was pumped directly back to the absorber. These experiments were run for at least four hours each. All experiments were completed at a GAP-0 flowrate of 90 mL/min. GAP-0 : CO_2 molar ratios were varied by changing the total gas flowrate and/or the % CO_2 concentration. Desorber temperature was controlled to 130-140°C. A summary of the experiment conditions conducted in continuous mode is shown in Table 31. Sample analysis results from these experiments are summarized in Table 32.

Table 31. Continuous system experiment conditions.

Date	GAP-0 flowrate (mL/min)	Total gas flowrate (SLM)	% CO_2 in feed gas (mol%)	Desorber temp (°C)	GAP-0 : CO_2 molar ratio (measured)
9/28/16	90	100	16	130	0.31
9/30/16	90	100	16	135	0.31
10/5/16	90	100	16	140	0.41
10/11/16	90	100	16	130	0.32

10/13/16	90	100	16	140	0.44
10/21/16	90	100	9	130	0.62
10/21/16	90	100	9	140	0.68
10/24/16	90	150	9	130	0.39
10/24/16	90	150	9	140	0.40
10/27/16	90	150	16	130	0.23
10/27/16	90	150	16	140	0.21
10/31/16	90	100	6	130	0.98
10/31/16	90	100	6	140	0.93
11/2/16	90	150	4	130	0.87
11/2/16	90	150	4	140	0.76
11/8/16	90	100	4	130	1.43
11/8/16	90	100	4	140	1.23
11/30/16	90	150	9	130	0.41
11/30/16	90	150	9	140	0.38
12/8/16	90	100	6	130	1.00
12/8/16	90	100	6	140	0.86

Table 32. Slurry and lean solvent sample compositions for the experiments listed in Table 31.

Run ID	CSTR T (deg C)	Slurry GAPC (wt%)	Slurry Water (wt%)	Lean GAPC (wt%)	Lean Water (wt%)
2016-09-28	130	77.8	4.3	18.1	3.2
2016-09-30	135	79.5	4.3	11.4	3.8
2016-10-05	140	82.9	3.1	8.5	1.4
2016-10-11	130	80.7	4.6	17.6	2.7
2016-10-13	140	82.8	3.3	10.7	0.9
10/21/2016 A	130	78.6	3.5	17.4	2.0
10/21/2016 B	140	78.7	4.3	1.3	2.7
10/24/2016 A	130	80.6	4.3	18.9	2.4
10/24/2016 B	140	79.1	6.7	1.1	3.9
10/27/2016 A	130	81.9	5.5	13.2	2.6
10/27/2016 B	140	77.0	7.2	1.3	4.5
10/31/2016 A	130	62.3	5.1	11.0	2.2
10/31/2016 B	140	52.0	6.8	0.9	3.7
11/2/2016 A	130	51.3	7.8	2.4	4.3
11/2/2016 B	140	48.1	10.1	0.4	6.2
11/30/2016 A	140	83.0	4.1	19.3	2.1
11/30/2016 B	140	79.8	6.9	2.5	4.5
11/8/2016 A	130	36.5	5.9	6.2	2.9
11/8/2016 B	140	30.8	8.5	0.1	5.2
12/8/2016 A	140	73.8	4.0	12.2	2.0
12/8/2016 B	140	70.2	6.9	0.6	4.6

Liquid samples from both the slurry feed to the desorber and the lean stream leaving the desorber were collected at approximately 30 minute intervals for the duration of each experiment. To determine how long the system needed to get to steady state, all of the liquid samples collected during the 10/11/16 experiment were analyzed, as shown in Figure 71. After reviewing these results, it was determined that two hours after the desorber reached the target temperature was sufficient for the system to

reach steady state. This allowed for two experimental conditions to be completed in one day; most typically, two different desorber temperatures were tested in each run.

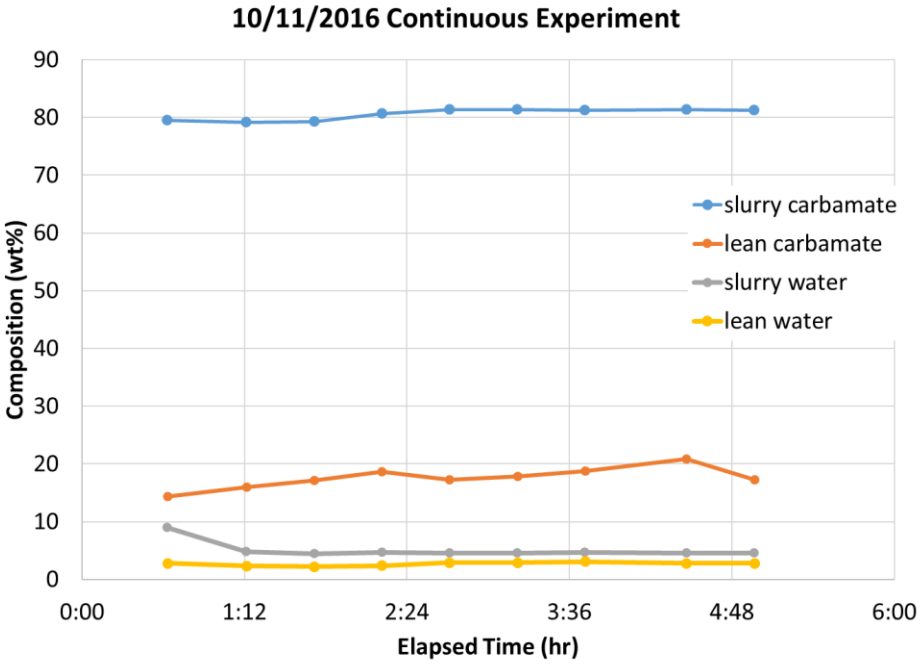

Figure 71. Slurry and lean solvent carbamate and water content results for 10/11/16 experiment.

Figure 72 shows the CO_2 capture rate vs. the GAP-0 : CO_2 molar ratio for the experiments completed this quarter. The CO_2 capture rate was based on the liquid analyses due to issues with the CO_2 analyzer for the gas phase. As expected, the lower GAP-0 : CO_2 molar ratio experiments showed significantly lower CO_2 capture rate. For molar ratios up to 0.8 mol GAP-0 : mol CO_2, near-stoichiometric CO_2 capture was demonstrated. For excess GAP-0 conditions, no significant increase in CO_2 capture was observed, and only the 12/8 experiments, which will be discussed later, showed CO_2 capture rate above 80%.

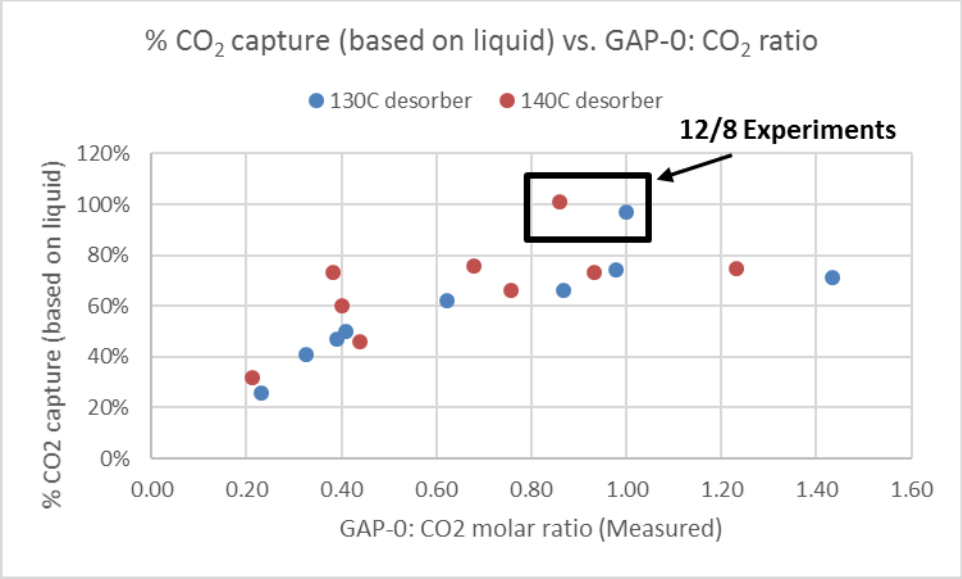

Figure 72. CO_2 capture rate vs. GAP-0: CO_2 molar ratio.

Material and Energy Balance for Continuous Bench-Scale System

Material and energy balances were calculated for the continuous bench scale system runs. Online process data, including flow rates and temperatures, were combined with slurry and liquid sample analyses to calculate CO_2 capture and desorption rates and estimate heat duty required for desorption. An example of one of these calculations is shown in Figure 73.

	measured	12/8/2016 run data							
Absorber									
	% CO2 Capture	91%							
	L/G (mol GAP-0/mol CO2)	1.2							
	Gas								
		Inlet				Outlet			
	Temperature (deg C)	40				55			
	Pressure (barg)	0.1				0.1			
	Flow rate (slm)	100.0				103.5			
		g/min	wt%	mol/min	vol% dry	g/min	wt%	mol/min	vol%
	N2	107.6		3.8	94%	107.6		3.8	
	CO2	10.8		0.25	6%	0.9		0.02	
	H2O	9.0		0.5		6.6		0.37	
	Total	127.4				115.2			
	Liquid								
		Inlet				Outlet			
	Temperature (deg C)	25				63			
	Flow rate (mL/min)	97.6				114.3			
		g/min	wt%	mol/min	mol%	g/min	wt%	mol/min	mol%
	GAP-0	73.6	85.8%	0.3		22.9	22.2%	0.1	
	GAPC	10.5	12.2%	0.04		76.0	73.8%	0.26	
	H2O	1.7	2.0%	0.1		4.1	4.0%	0.2	
	Total	85.8				103.0			

CSTR Desorber									
	% CO2 Desorbed	89%							
	Gas								
		Inlet				Outlet			
	Temperature (deg C)					130			
	Pressure (barg)					1			
	Flow rate (slm)					15.9			
						g/min	wt%	mol/min	vol%
	CO2							0.2	35.7%
	H2O							0.42	64.3%
	Total							0.6	
	Liquid								
		Inlet				Outlet			
	Temperature (deg C)	80				130			
	Flow rate (mL/min)	114.3				73.6			
		g/min	wt%	mol/min	mol%	g/min	wt%	mol/min	mol%
	GAP-0	22.9	22.2%	0.1		56.9	85.8%	0.2	
	GAPC	76.0	73.8%	0.26		8.1	12.2%	0.03	
	H2O (slurry)	4.1	4.0%	0.2		1.3	2.0%	0.1	
	Total	103.0				66.3			

Slurry Preheater			
	Flow rate (mL/min)	114.3	
		g/min	Cp (J/g/C)
	GAP-0	22.9	2.26
	GAPC	76.0	2.25
	H2O	4.1	4.18
	Total	103.0	
	Inlet Temperature (deg C)	63	
	Outlet Temperature (deg C)	80	
	Sensible Heat (kW)	0.1	

Recirculation HX						
		Inlet	Outlet			
	Temperature (deg C)	80	130			
	Flow rate (mL/min)	114.3				
		g/min	Cp (J/g/C)			
	GAP-0	22.9	2.26			
	GAPC	76.0	2.25			
	H2O	4.1	4.18			
	Total	103.0				
	Sensible Heat (kW)		0.2			
	Water vapor fraction		1.00	0.75	0.50	0.25
	Heat of Vaporization (kW)		0.2	0.1	0.1	0.0
	Heat of Reaction (kW)		2.7			
		min	max			
	Total Duty (kW)	3.0	3.1			

Figure 73. Heat and material balance of bench scale system.

State-Point Data Table

The updated State-Point Data Table is shown in Table 33.

Table 33. State-point data table.

	Units	Measured/Estimated Performance	Projected Performance
Pure Solvent			
Molecular Weight	g/mol	248.51	248.51
Normal Boiling Point	°C	258.7	258.7
Normal Freezing Point	°C	< 0	< 0
Vapor Pressure @ 15°C	bar	1.8E-05	1.8E-05 (GAP-0) / 0.017 (water)
Working Solution			
Concentration	kg GAP-0/kg working solution	1	0.9
Specific Gravity (15°C/15°C)	-	0.891	0.891 (GAP-0) / 1.0 (water)
Specific Heat Capacity @ STP	kJ/kg-K	2.29	2.29 (GAP-0) / 4.18 (water)
Viscosity @ STP	cP	4.4	12.3 (10% water, 90% GAP-0)
Surface Tension @ STP	dyne/cm	25.4	25.4 (GAP-0) / 72.8 (water)
Absorption			
Pressure	bar	1	1
Temperature	°C	30	40-60
Equilibrium CO2 Loading	gmol CO2/kg	3.61	2.60
Heat of Absorption	kJ/kg CO2	-2577	-2577
Solution Viscosity (@ 40°C)	cP	N/A	235 (10% water, 90% GAP-0/carbamate)
Desorption			
Pressure	bar	7	1
Temperature	°C	160	130
Equilibrium CO2 Loading	gmol CO2/kg	1.36	0.91
Heat of Desorption	kJ/kg CO2	-2577	-2577

Task 6.3 – Process optimization

Starting in early October, a significant amount of liquid carryover was observed in the gas exhaust line from the absorber. This increase is coincident with the change from the rotary atomizer to the pneumatic atomizer, and it is believed that the increased

carryover is due to decreased droplet size generated by the pneumatic atomizer. In an attempt to mitigate this issue, cooling was added to the collection container and gas lines directly after the slurry pump before the 10/21/16 experiments. Copper tubing was wrapped around the collection container and around the line leading to the cyclone, and cooling water was pumped through the copper tubing (Figure 74). This did not result in a significant increase in the amount of liquid collected in these areas.

Figure 74. Additional cooling lines on absorber gas exhaust.

Stainless steel wool was also packed in the cyclone and the filter housing to function as a demister to remove more entrained liquid from the exhaust gas. This resulted in some increase in the amount of liquid collected, but liquid was still observed at the end of the gas exhaust lines.

An additional heat exchanger was added, which was cooled with water (Figure 75). This was installed downstream of the cyclone and filter between the 11/8/16 and 11/30/16 experiments and was used during experiments completed on 11/30/16 and 12/8/16. A significant amount of liquid was collected in the tank below this heat exchanger, and the humidity in the gas outlet was observed to decrease on both days, compared to earlier replicates of the experimental conditions. However, droplets were still visually observed in the gas phase leaving the exhaust line at the back of the hood. Buildup of solid carbamate has been observed at the end of this exhaust line, which indicates that the exhaust gas does still contain some GAP-0. Additional options for removing entrained liquid from the absorber gas exhaust will be explored in 2017.

Figure 75. Heat exchanger added to absorber gas exhaust line.

An additional condenser was also installed on the desorber gas exhaust line (Figure 76). This was installed prior to the 11/30/16 experiment. This resulted in an increase in the amount of condensate collected and a corresponding decrease in absolute humidity in the exhaust gas leaving the coolers in comparison with replicate experiments.

Figure 76. Condensers on desorber gas exhaust line.

SO_2/CO_2 Absorption/Desorption Experiments. Several laboratory scale experiments were run to determine the fate of ppm levels of SO_2 in the simulated flue gas. To this end, GAP-0 containing varying levels of water was exposed to a mixture of 50 ppm SO_2, 16% CO_2, with the balance being N_2, for 3 hours at temperature to assure equilibrium conditions were achieved. Figure 77 shows the apparatus employed, which consisted of a mechanically stirred absorption vessel with gas inlet and outlet tubes. The outlet gas was passed through a caustic scrubber before being vented in the fume hood to guarantee complete neutralization of the acid gas. Variation of both absorption temperature and water level allowed for bracketing of the expected operating parameters for the absorption process.

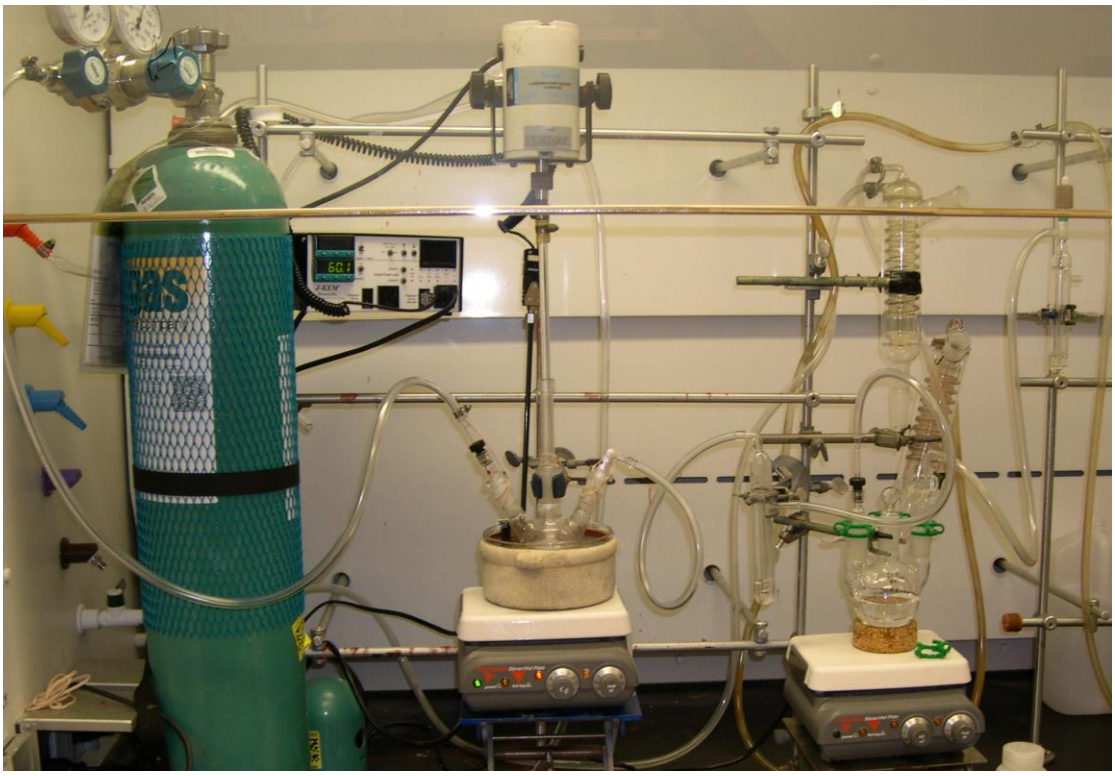

Figure 77. SO_2 Gas Absorption Apparatus.

At the highest water levels, a stirrable slurry was formed on reaction with the simulated flue gas. As the water level decreased, the carbamate that formed became a solid mass that needed to be manually broken up several times over the 3-hour reaction period to assure efficient reaction with CO_2 and SO_2. Table 34 shows the analyses performed on the carbamate product and desorbed GAP-0.

Table 34. GAP-0 Analyses from screening experiments.

Experiment	Water (wt %)	Temp (°C)	% Carbamate (extractables)	Water content	ppm S content (Absorption)	ppm S content (Desorption)
F2432-54	10	40	99.7	3.30	75 +/- 2	122 +/- 2
F2432-55	5	40	98.6	1.46	115+/- 5	194 +/- 3
F2432-58	1	40	96.4	0.93	43 +/- 3	52 +/- 2
F2432-59	10	60	99.4	2.15	60 +/- 1	121 +/- 2
F2432-62	5	60	99.2	1.04	177 +/- 4	263 +/- 7
F2432-63	1	60	99.1	1.24	236 +/- 11	246 +/- 3

In all cases, efficient formation of the carbamate was achieved as determined by the extractable values. Water analyses via Karl-Fischer titrations showed a general correlation of higher to lower water content that followed the initial water content apart from the F2432-63 experiment. In all cases the measured value was less than the original level because the reactive gas sweeping through the system removed

some of the water.

The highest-level result was that it appeared that SO_2 did react with the GAP-0. The general trend of higher sulfur content in desorbed samples versus the corresponding absorbed samples was expected. If the sulfur salts remained after CO_2 desorption, then the relative amount of sulfur in the sample would increase as is seen. However, the absolute amounts of sulfur detected varied considerably. This may have been due to a couple of factors including mass transfer of the SO_2 gas into the carbamate solid and the water content of the system. The mass transfer factor is supported by the fact that there was a greater amount of sulfur present in the 60°C samples than the 40°C samples and the higher temperature runs exhibited lower viscosities than those at lower temperatures.

One observation noted was that after desorption the recovered GAP-0 seemed to be hazy. One explanation is that the sulfur-containing heat stable salts that were presumably formed on reaction of SO_2 with GAP-0 may have been insoluble in the starting aminosilicone. To test this hypothesis, a separate, larger scale experiment was run in which GAP-0 with 10% water was treated with the mixture of 50 ppm SO_2 and 16% CO_2 at 40°C. The carbamate formed was desorbed and any solid that remained was isolated. Table 35 shows the results of the sample sulfur analyses.

Table 35. GAP-0 Analyses from larger scale experiment.

Experiment	Description	Sulfur content (ppm)					Mean S (ppm)
F2432-91-1	Carbamate	151	148	168	184	160	162 +/- 15
F2432-91-2	Desorbed liquid w/o filtering	123	126	124	117	-	123 +/- 4
F2432-91-3	Filtrate	120	122	118	-	-	120 +/- 2
F2432-91-4	Solid	1640	-	-	-	-	1640 +/- 70

The solid carbamate sample (91-1) contained ~ 160 ppm of sulfur. The desorbed (91-2) material had less sulfur; contrary to what was seen in Table 34. It is unclear why that is the case unless there was some surface-adsorbed SO_2 on the solid that escaped during heating in the desorption process. When the desorbed liquid was filtered to remove a small amount of solid that remained, the filtrate (91-3) showed no difference from the original desorbed material. However, the solid that was isolated contained a substantial amount of sulfur at 0.16 wt%; an order of magnitude greater than any of the other samples. Very little of the solid was isolated so no replicate testing was possible. Also, one would have expected the filtrate sample to be lower in sulfur than the desorbed liquid sample that contained the particles. But this was not the case but may have been because of small sample sizes. However, the solid (91-4) was 10x higher, suggesting that during thermal regeneration of the GAP-0 solvent it may be possible to remove at least some of the heat-stable sulfur salts from the recycle stream. To confirm this possibility, additional testing is required.

Task 7 – Economic and scale-up analysis

Task 7.1 – Develop scalable slurry pump and spray absorber concept and cost

Slurry pump concept. In order to specify a commercial scale slurry pump, knowledge of the viscosity of GAP-0/carbmate/water mixtures is needed. Experiments were conducted to collect this data, which was used to develop a new correlation for viscosity as a function of slurry composition (GAP-0, carbamate, and water) and temperature. This correlation was built into the Aspen Plus model. In previous versions of the model, viscosity of the carbamate was not included in the property set up. The challenge of including phase-changing solvent viscosity in the model was that pure GAP-0 carbamate is a solid, and therefore has an undefinable viscosity. In 2016, the phase-changing CO_2 capture process concept was modified to rely on a GAP-0 carbamate/water slurry as the rich solvent phase leaving the absorber. A thorough study of slurry viscosity was conducted[29], exploring the effects of temperature and composition. This data was regressed to be included in the Aspen Plus model to generate more rigorous estimates of slurry pumping power. The viscosity regression was performed with MATLAB and Aspen Plus using a similar approach to the Keq regression described above.

Experimental viscosity measurements were taken using a cup and bob viscometer. Multiple samples were prepared with compositions as presented in Table 1. Viscosity was measured for temperatures of 25-80°C and shear rates of 1-150s^{-1}. All viscosity data was found to be independent of shear rate, and the data for 25s^{-1} was used in the regression.

Table 36. Composition of samples for viscosity measurement.

Sample	*Water (wt%)*	*GAP-0 (wt%)*	*Carbamate (wt%)*
F2356-137-1	0.00	100.00	0.00
F2356-137-2	5.00	95.00	0.00
F2356-137-3	10.20	89.80	0.00
F2356-137-8	15.04	84.96	0.00
F2356-137-4	0.00	80.63	19.37
F2356-137-5	5.00	76.60	18.41
F2356-137-6	10.01	72.55	17.43
F2356-137-7	15.13	68.43	16.44
F2356-142-1	0.00	57.73	42.28
F2356-142-2	5.05	54.81	40.14
F2356-142-3	10.00	51.95	38.05
F2356-142-4	15.03	49.05	35.92
F2356-143-1	0.00	43.35	56.65
F2356-143-2	5.05	41.16	53.78

F2356-143-3	10.07	38.99	50.94
F2356-143-4	14.93	36.88	48.19
F2356-154-1	10.01	25.24	64.75
F2356-154-2	15.13	23.81	61.07

The equation that Aspen uses for mixture viscosity[30] is in the form shown in Equation 5.

Equation 5. Mixture viscosity expression used in Aspen Plus.

$$ln\mu^{l} = \sum X_i ln\mu_i^{*,l} + \sum k_{ij} X_i X_j ln\mu_{ij} + \sum X_i \left[\sum_{j \neq i} X_j (l_{ij} ln\mu_{ij})^{1/3} \right]^3$$

where X_i = mole fraction or weight fraction of component i
k_{ij} = symmetric binary parameter ($k_{ij} = k_{ji}$)
l_{ij} = antisymmetric binary parameter ($l_{ij} = -l_{ji}$)

The binary parameters k_{ij} and l_{ij} allow accurate representation of complex liquid mixture viscosity temperature dependence. Both binary parameters default to zero. Both binary parameters, k_{ij} and l_{ij}, must be specified for each component pair[1]. The first interaction parameter for the Andrade liquid viscosity model is fit to the following expression: $k_{ij} = A + B/T$[1]. The second interaction parameter for the Andrade liquid viscosity model is fit to the following expression: $m_{ij} = C + D/T$[1]. By default, these values are zeros, and they need to be specified. These parameters were regressed using MATLAB to match experimental data. The mixture viscosity equation shown in Equation 5 was modified for 3-component GAP-0/GAP-0 carbamate/water mixtures. Antisymmetric parameters (l_{ij}) were not used, and second binary interaction parameters were added. The final equation for which parameters were regressed is shown in Equation 6.

Equation 6. Mixture viscosity correlation for GAP-0/carbamate/water mixtures to be used in Aspen Plus.

$$\begin{aligned}\ln(\mu_{mix}) = {} & w_{GAP} * \ln(\mu_{GAP}) + w_{H2O} * \ln(\mu_{H2O}) + w_{CARB} \\ & * \left(a + \frac{b}{T}\right) + w_{GAP} * w_{H2O} * \left(c + \frac{d}{T}\right) + w_{GAP} * w_{CARB} \\ & * \left(e + \frac{f}{T}\right) + w_{H2O} * w_{CARB} * \left(g + \frac{h}{T}\right) + {w_{GAP}}^2 \\ & * {w_{H2O}}^2 * \left(j + \frac{k}{T}\right) + {w_{GAP}}^2 * {w_{CARB}}^2 * \left(l + \frac{m}{T}\right) \\ & + {w_{H2O}}^2 * {w_{CARB}}^2 * \left(o + \frac{p}{T}\right)\end{aligned}$$

To understand which coefficients in Equation 6 were important for the regression, a stepwise approach was used to find the best reduced model to fit the data. The result of this stepwise regression approach was a reduced model having 7 coefficients, which are presented in Table 37.

Table 37. Summary of regressed coefficients for viscosity correlation shown in Equation 6.

	Notation in equation	Notation in MATLAB	**Reduced model - FINAL MODEL**			
			Parameter #	**7**		
			Name	Value	p-value	AIC
GAPC/1	a	b1	b1	-6.72842	1.37E-22	-530.146
GAPC/2	b	b2	b2	5228.663	9.24E-62	
GAPC/3	c	b3				
GAP/H2O 1	d	b4	b3	18.09482	7.26E-28	
GAP/H2O 2	e	b5				
GAP/GAPC 1	f	b6	b4	-8.58493	1.17E-24	
GAP/GAPC 2	g	b7				
GAPC/H2O 1	h	b8	b5	-17.6739	1.06E-33	
GAPC/H2O 2	i	b9				
GAP/GAPC 3	j	b10	b6	27.16638	9.42E-16	
GAP/GAPC 4	k	b11				
GAP/H2O 3	l	b12	b7	-57.9421	1.78E-06	
GAP/H2O 4	m	b13				
GAPC/H2O 3	n	b14				
GAPC/H2O 4	o	b15				

Model predictions were validated with experimental data, and results fell within 20% error as shown in Figure 78 for the full range of viscosity values and in Figure 79 for the low end of the viscosity range. The coefficients shown in Table 37 were input into Aspen Plus for use in process model development, analysis, and scale up.

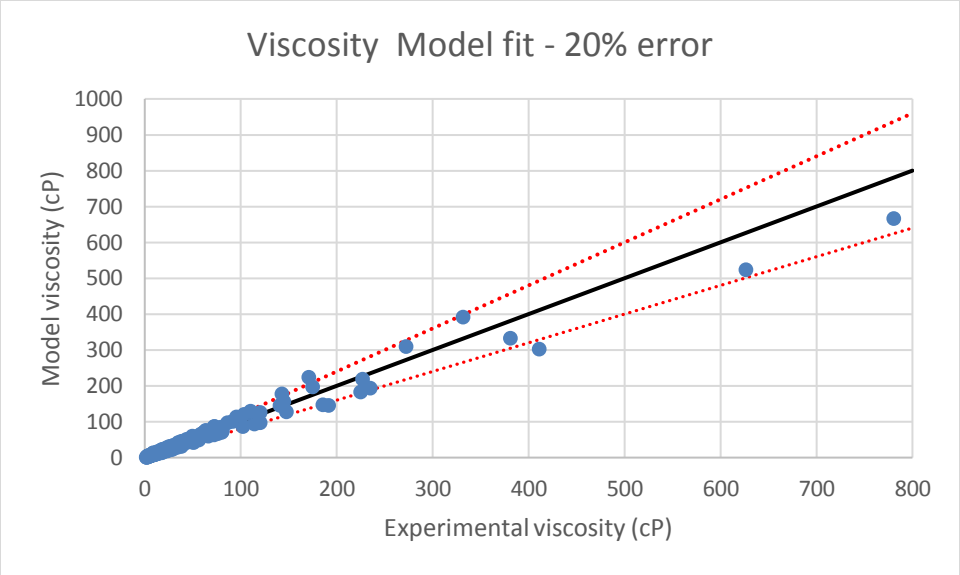

Figure 78. Comparison of Experimental viscosity data with regressed values.

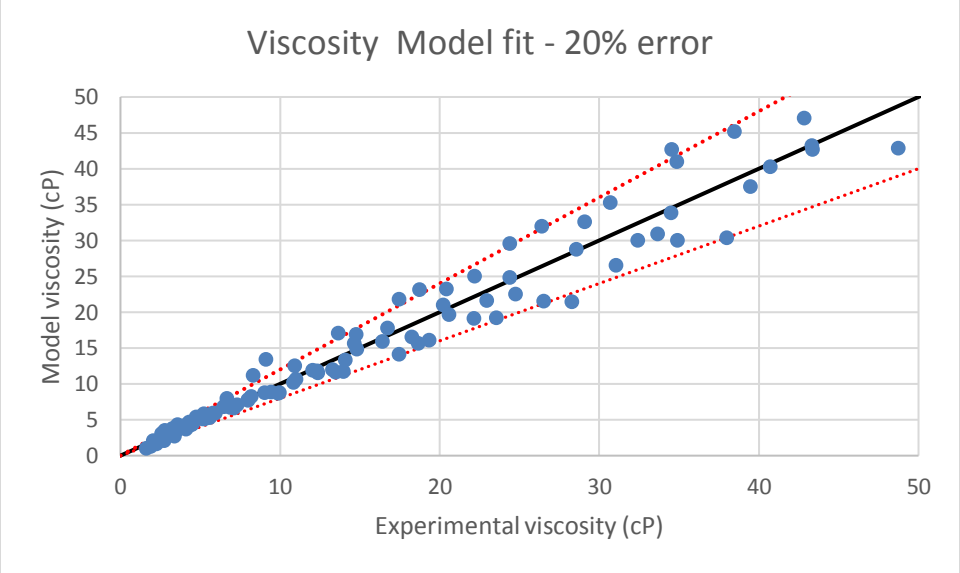

Figure 79. Comparison of experimental viscosity data with regressed values for low viscosity values.

In the techno-economic assessment, the slurry pump was modeled and costed as a centrifugal pump. Using the improved Aspen Plus model, the flow rate, temperature, and viscosity through the slurry pump were calculated. Additionally, a required pump head was calculated using approximated pipe sizes and lengths in addition to the pressure drops through the required equipment. This data was given to a pump supplier with a request to design and price an appropriate slurry pump. The pump supplier responded with a pump price and required motor size. This information was incorporated into the cost estimates for the techno-economic assessment

Absorber model development. In previous versions of the ASPEN model, the absorber

unit operation was modeled as a series of stoichiometric reactors with specified fractional conversion of CO_2 and heat of reaction. This setup was used because insufficient experimental data was available to be incorporated into the absorber model. In 2016, the continuous bench scale system was built, and experimental data was generated that allowed for development of a more rigorous absorber model. In this more rigorous model, the absorber is modeled as an equilibrium flash reactor that uses a globally-defined equilibrium chemical reaction constant K_{eq}. This approach allows for direct calculation of the absorber exit temperature and composition, whereas in previous versions of the model the absorber exit temperature was artificially limited by using a larger number of spray stages to achieve 90% capture overall.

Bench scale experimental data was used to regress the parameters of this equilibrium reaction using the expression in Equation 7.

Equation 7. Chemical reaction equilibrium constant correlation.

$$lnK_{eq} = A + \frac{B}{T}$$

A randomized portion of the continuous bench scale absorber data set was segregated to be used to validate the resulting regression. The rest of the data set was used to build the regression. The regression was executed using MATLAB in conjunction with ASPEN Plus. MATLAB automatically entered initial values for the equilibrium constant parameters A and B and absorber input parameters (defined in Table 38) into an absorber equilibrium flash reactor block in ASPEN. MATLAB executed the ASPEN simulation, calculated the residual error between the ASPEN calculations and experimental data for rich solvent temperature and carbamate loading, and selected values for the equilibrium constant parameters to use in the next iteration. This iterative regression was repeated to minimize the residual error between the ASPEN calculations and experimental data for rich solvent temperature and carbamate loading.

This regression yielded an ASPEN absorber model that predicts within 20% of the experimentally observed rich solvent carbamate loading and temperature, as shown in Figure 80 and Figure 81. In Figure 81 it is apparent that the absorber model overpredicts rich solvent temperature compared to the experimental data. This discrepancy is attributed to heat losses that are present in the bench scale spray absorber, which are not accounted for in the ASPEN model. Overall, it was concluded that regression of equilibrium constant parameters yielded good agreement of the model with experimental data, and this absorber model was used to scale the phase-changing aminosilicone process up to $550MW_{net}$.

Table 38. Summary of input and output parameters used in MATLAB/ASPEN regression of equilibrium constant parameters.

Stream	Parameter	Function
Lean Solvent In	Flow rate	Input into model, defined by experimental regression data set
	Temperature	Input into model, defined by experimental regression data set
	%Water	Input into model, defined by experimental regression data set
	%Carbamate	Input into model, defined by experimental regression data set
Gas In	Flow rate	Input into model, defined by experimental regression data set
	Temperature	Input into model, defined by experimental regression data set
	$\%CO_2$	Input into model, defined by experimental regression data set
Gas Out	$\%CO_2$	Output for comparison only
	Temperature	Output for comparison only
Rich Solvent Out	Flow Rate	Output for comparison only
	Temperature	Output for regression, algorithm minimizes the residual error of this result compared to experimental regression data set
	%Carbamate	Output for regression, algorithm minimizes the residual error of this result compared to experimental regression data set

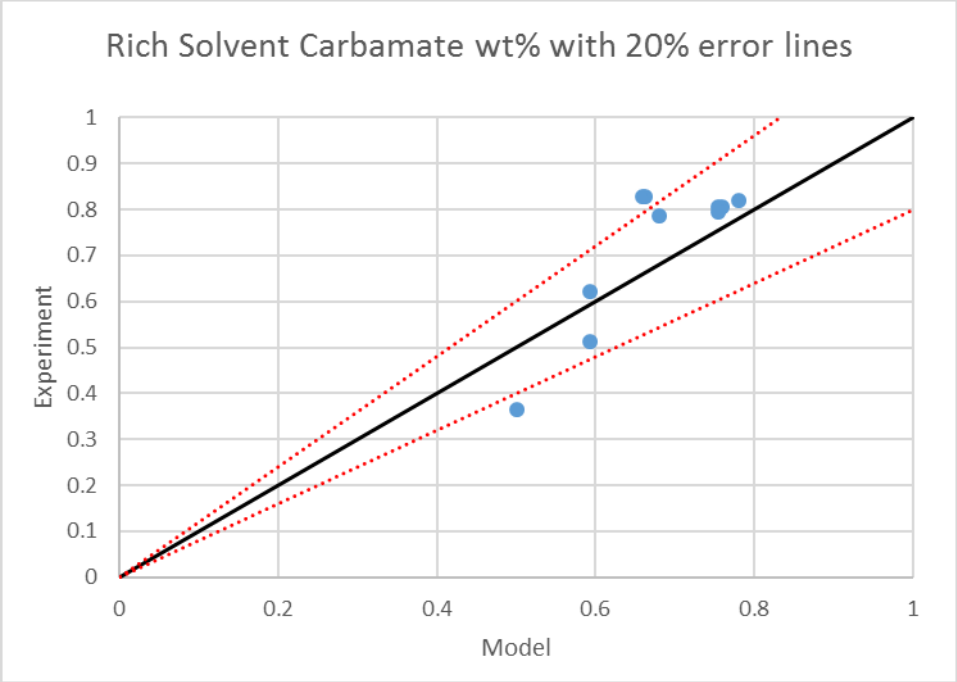

Figure 80. Comparison of rich solvent carbamate loading between experimental data and model prediction.

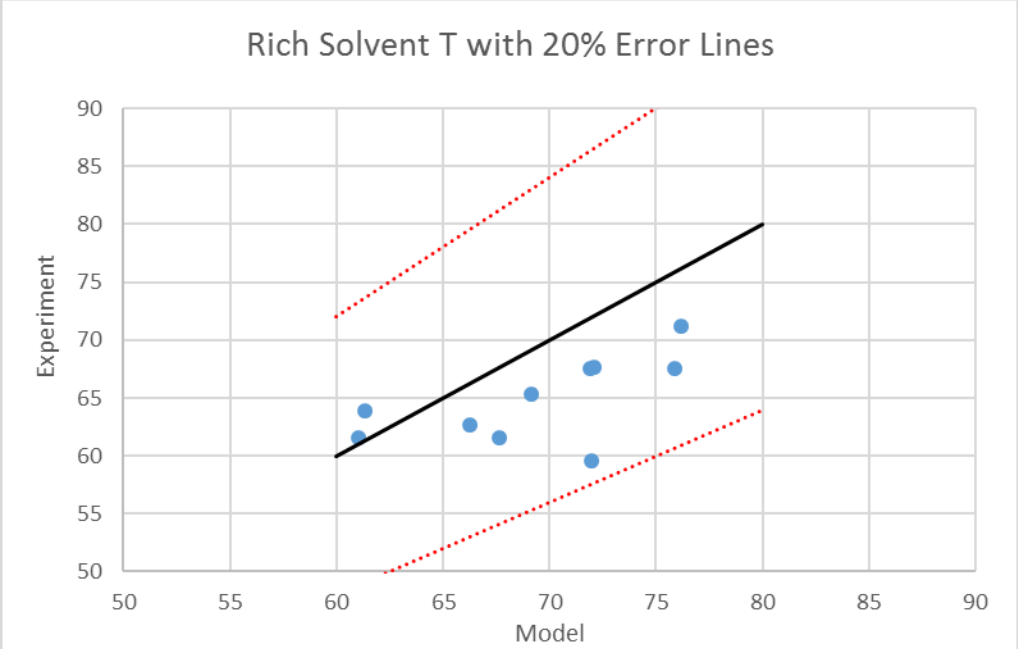

Figure 81. Comparison of rich solvent temperature between experimental data and model prediction.

Task 7.2 – Techno-Economic Assessment

Process and economic models of the CO_2 capture system were updated to reflect the best available data relating to solvent properties and system performance. Aspen chemical process simulation software was used to prepare the mass and energy balances for the system. Integration of the capture system with a coal-fired power plant was performed, using a power plant model developed with Thermoflow™ software. The power plant scale was defined by Case 11 in the DOE Bituminous Baseline report[31,32] (550MW net power without CO_2 capture). These models yielded an estimated CO_2 capture cost of $52.40/tonne for the CSTR process configuration excluding the cost impact of thermal degradation. The impact of solvent makeup due to thermal degradation was an increase of as much as $88/tonne, which confirms the need for a low temperature desorber. The analysis is detailed in the Techno-Economic Analysis report, which is included in DOE's OSTI database, report number DOE-GEGR-0013687-4.

In the process model, the absorber was specified as a cross-flow spray reactor with alternating absorption and cooling stages to manage the absorber temperature. As the result of a parametric study, the lean solvent was split evenly between each stage. In the best case, three absorption stages were needed to achieve 90% capture. Desorption was carried out in an atmospheric pressure CSTR desorber. Heat was recovered from the hot lean stream in a rich/lean heat exchanger. The lean liquid was further cooled prior to recycle to the absorber. Desorbed CO_2 was sent to a CO_2 compression train. An example of an Aspen Plus flowsheet developed for the CO_2 capture system is shown in Figure 82.

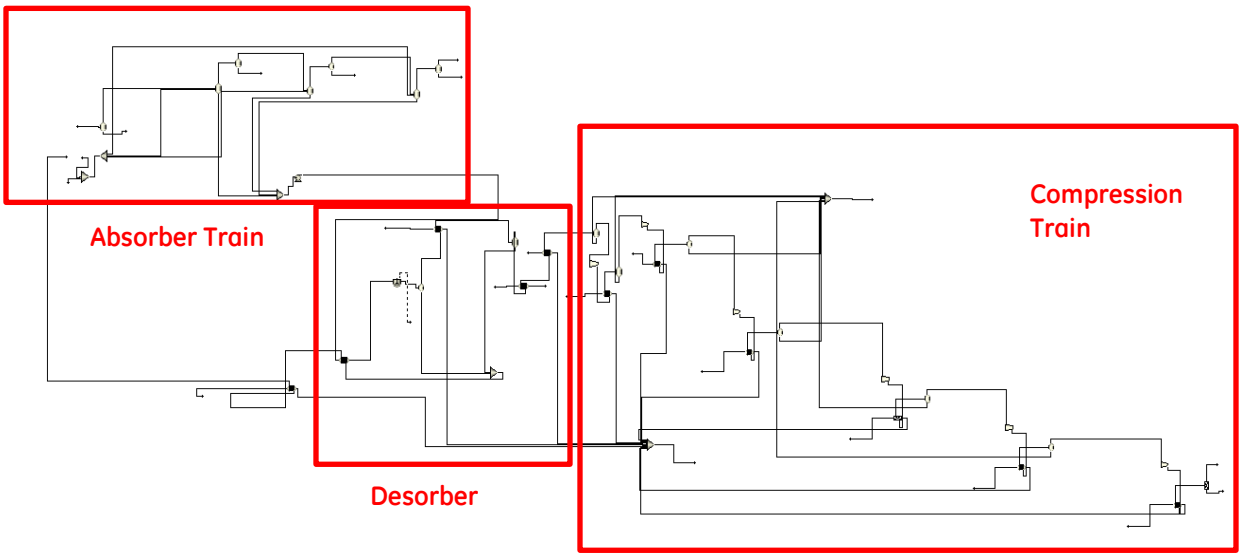

Figure 82. Example phase-changing CO_2 capture process model.

The best case described in the Preliminary Cost Study before scaling to $550MW_{net}$ (Case 6F) was the starting point for this analysis. Parametric studies were completed assuming constant power plant size per DOE Case 11[32] (550MW before carbon capture). This approach allowed for more efficient exploration of the effect of various

process configurations and operating parameters for the CO_2 capture system. Once a best case was identified for the carbon capture unit, the scale was adjusted to achieve 550 MW net power with carbon capture and the CO_2 capture system was heat integrated with the power plant.

Task 7.3 – Develop scale-up strategy

Scale-up of the phase-changing CO_2 capture process is dependent on addressing risks associated with solvent management. Due to the high cost of solvent makeup associated with thermal degradation, a low temperature desorption process is needed. Such a desorption process must also deliver high rates of desorption to maintain high CO_2 capture capacity of the solvent. Thermo-oxidative degradation of the solvent should be addressed to further minimize the potential for costly solvent replacement. Techno-economic assessment of the process utilizing the low-temperature desorber should be revisited to confirm that the reconfigured process is cost-competitive.

Bench-scale development of low-temperature desorption should be addressed in future work. For example, the bench-scale phase-changing CO_2 capture system could be retrofitted with a steam stripping column to evaluate this advanced desorber concept. The added functionality would allow sequential testing of CSTR and steam stripper regeneration to evaluate both desorption processes under similar process conditions. Designed experiments should explore the effects of water content in the rich solvent, GAP: CO_2 molar ratio in the rich solvent, and temperature of the reboiler. Thermal and hydrothermal degradation of the solvent and desorption efficiency of the column compared to the reboiler should be evaluated as a function of water content in the working solution.

Thermo-oxidative degradation of the phase-changing aminiosilicone solvent should also be evaluated at the bench-scale. A gas phase FTIR spectrometer should be connected to the exhaust of the bench-scale spray absorber to measure ammonia evolution rates as a function of absorber temperature, water content and solvent and flue gas flow rates.

Pending successful bench-scale demonstration of low-temperature desorption and acceptable cost performance of the new process configuration, pilot scale demonstration of the phase-changing CO_2 capture process with the low-temperature desorber should be pursued. The objective of a pilot demonstration would be to gain deeper understanding of the operational aspects of individual equipment and the overall CO_2 capture process, in order to optimize equipment sizes and process layout and improve prediction of performance and costs for a commercial scale system.

An additional objective of pilot demonstration is to accomplish a gradual, stepwise increase in the scale of operation from lab/bench scale to commercially relevant scales. One approach to this stepwise increase in scale is to establish target scale increments based on existing GE combustion products. An example of this approach is shown in Table 39. GE power generation equipment ranging from 1-110MWe gross

power output could be paired with CO_2 capture process equipment that is sized for the flue gas output.

Table 39. Scale up strategy.

	Bench scale	Pilot scale				Commercial scale
Time Frame	1/1/2014 - 9/30/2017	TBD	TBD	TBD	TBD	TBD
Location	GE Global Research Niskayuna, NY	TBD	TBD	TBD	TBD	TBD
Flue Gas	Simulated CO2, N2, H2O	NG-fired Waukesha engine	NG-fired LM1500 turbine	NG-fired LM2500 turbine	NG-fired LMS100 turbine	Pulverized coal boiler
Equivalent Power	0.004 MWe	1 MWe	10 MWe	30 MWe	110 MWe	550 MWe
Gas Flow Rate	10-20 kg/hr	~5,000 kg/hr	~100,000 kg/hr	~ 315,000 kg/hr	~846,000	~ 2,300,000 kg/hr
% CO2 in flue gas	2 - 16% (dry basis)	10% (dry basis)	7% (dry basis)	7% (dry basis)	7% (dry basis)	11 - 13% (wet basis)
SOx	-	1-5ppmv	1-5ppmv	1-5ppmv	1-5ppmv	1-5ppmv

The smaller of these GE turbine-driven systems may be of suitable size to be built in modular, transportable fashion for implementation at oil and gas production sites, allowing for demonstration of the CO_2 capture process and production of CO_2 for utilization in unconventional oil and gas projects. An example schematic of such a system is shown in Figure 83.

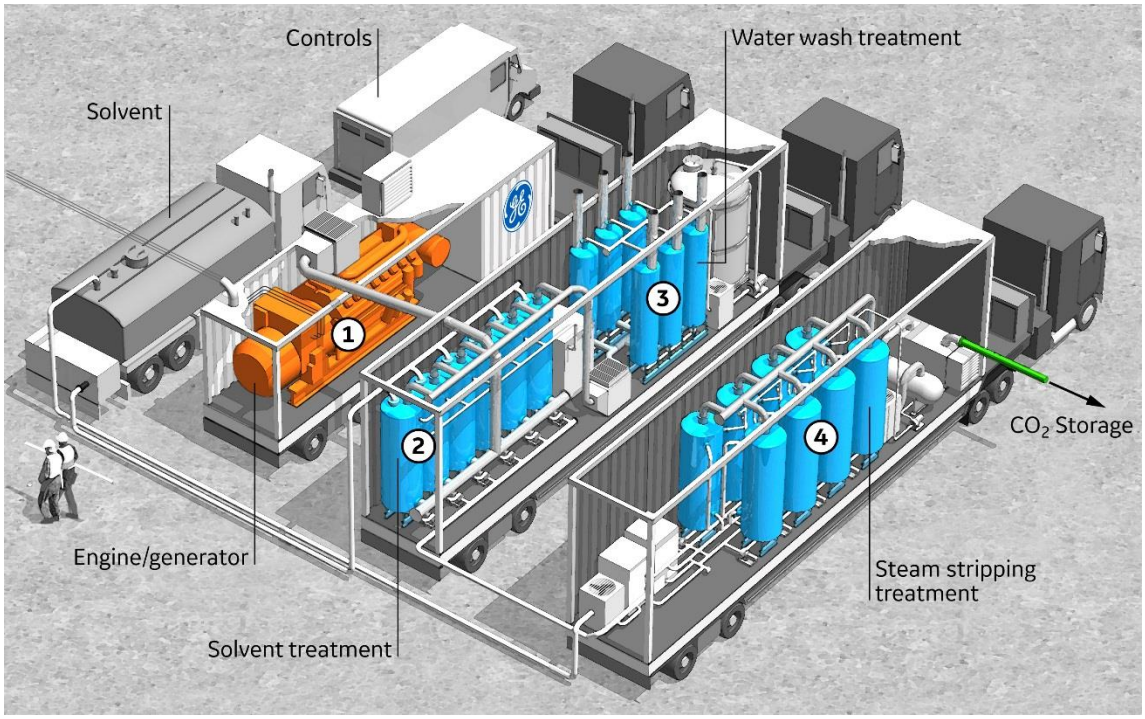

Figure 83. Conceptual sketch of 1MW engine-based CO_2 capture demonstration system.

Task 8 – Solvent management

Task 8.1 – Demonstrate bench-scale advanced desorber

Based on past experience with the phase-changing CO_2 capture system and the bench scale advanced desorber demonstrated in a parallel project[33], a mass balance was developed for use as a design basis for the bench scale advanced desorber for the phase-change process. The desorber was designed to process up to 500mL/min of CO_2-rich slurry and operate at reboiler temperature up to 125°C. This system was intended to be constructed of modular glassware components to allow for reconfiguration as needed, for example, variation of column height and diameter. The advanced desorber is intended to be installed in parallel to the existing CSTR desorber to allow for direct comparison of the two desorber units.

A design sketch for the bench scale advanced desorber is shown in Figure 84. The advanced desorber is a steam stripper style desorber. In this unit, rich solvent is introduced at the top of a packed column and flows downward to a collection vessel. A portion of the liquid from this vessel is heated via circulation through a heat exchanger. In this reboiler, a fraction of the aqueous portion of the working solution is vaporized and a fraction of the CO_2 contained in the solvent desorbs, and this vapor mixture flows upward through the column, heating the rich slurry that is flowing downward through the packing. In this way, the temperature of the richest solvent is limited, and CO_2 desorption rates are enhanced by steam dilution of the CO_2 vapor concentration in the column vapor phase. The vapor product passes through two condensers to remove entrained solvent and minimize the water vapor leaving the column. Condensate is returned to the column. The system will be fitted with temperature measurement instrumentation as well as ports to pull liquid samples in at various locations in the system.

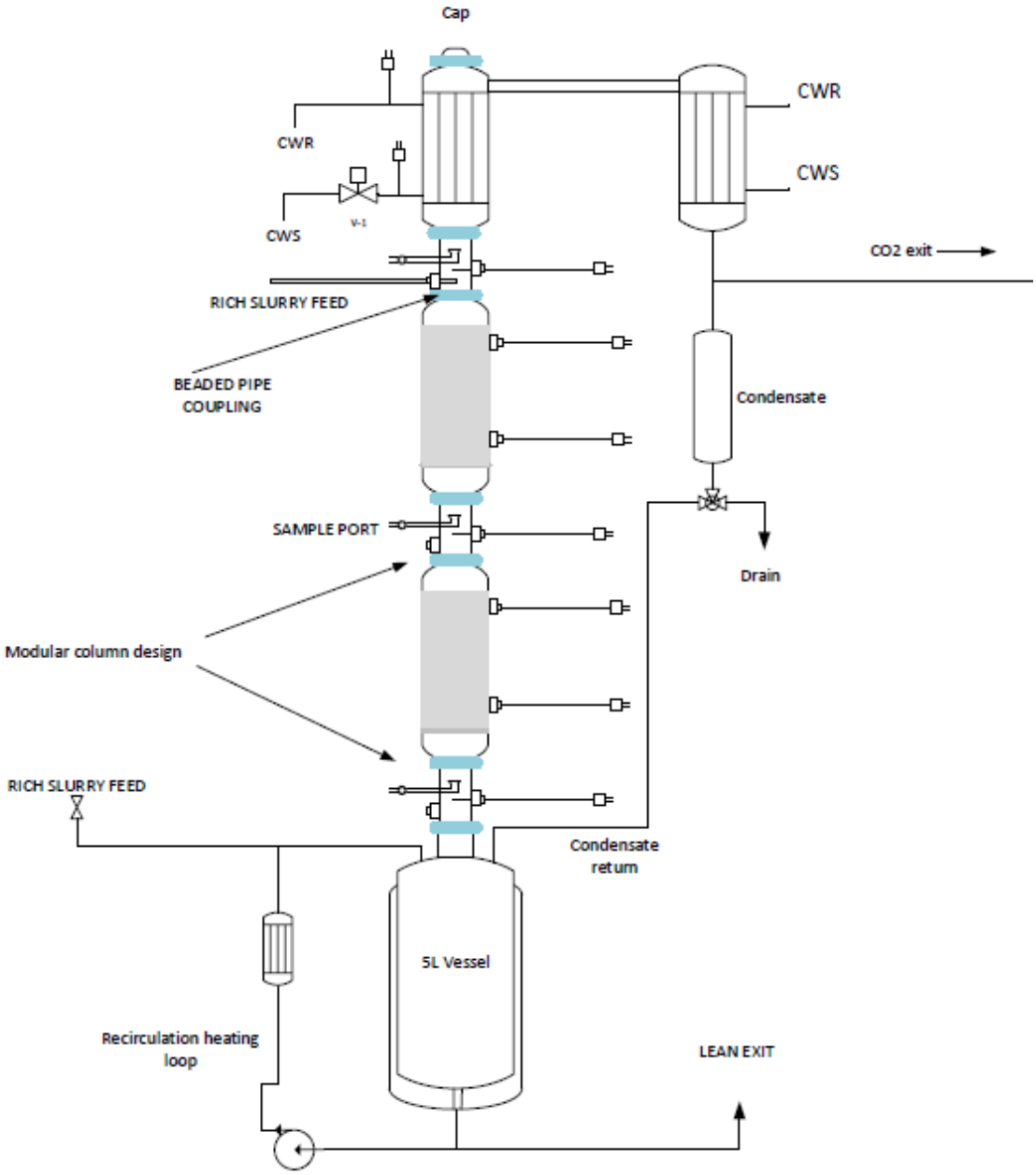

Figure 84. Design of bench scale advanced desorber.

Task 8.2 – Characterize properties of GAP-0/water mixtures

The project was ended prior to completion of these deliverables.

Task 8.3 – Study oxidative degradation

It is well established that ammonia production in aqueous amine solvents is indicative

of oxidative degradation of these CO_2 capture solvents. MEA has been most studied and the literature[34] suggests one pathway that is catalyzed by Fe^{+3} or other radical sources, leading to a volatile by-product.

Mass spectral analysis of head space samples in early experiments conducted in a different project showed ammonia was also present in thermally treated GAP-1 samples. To provide quantitative data on ammonia generation, an FT-IR spectrometer was installed in the CO_2 capture skid at the top of the absorber unit. A heated line ensured that condensation of volatile products did not occur (Figure 85).

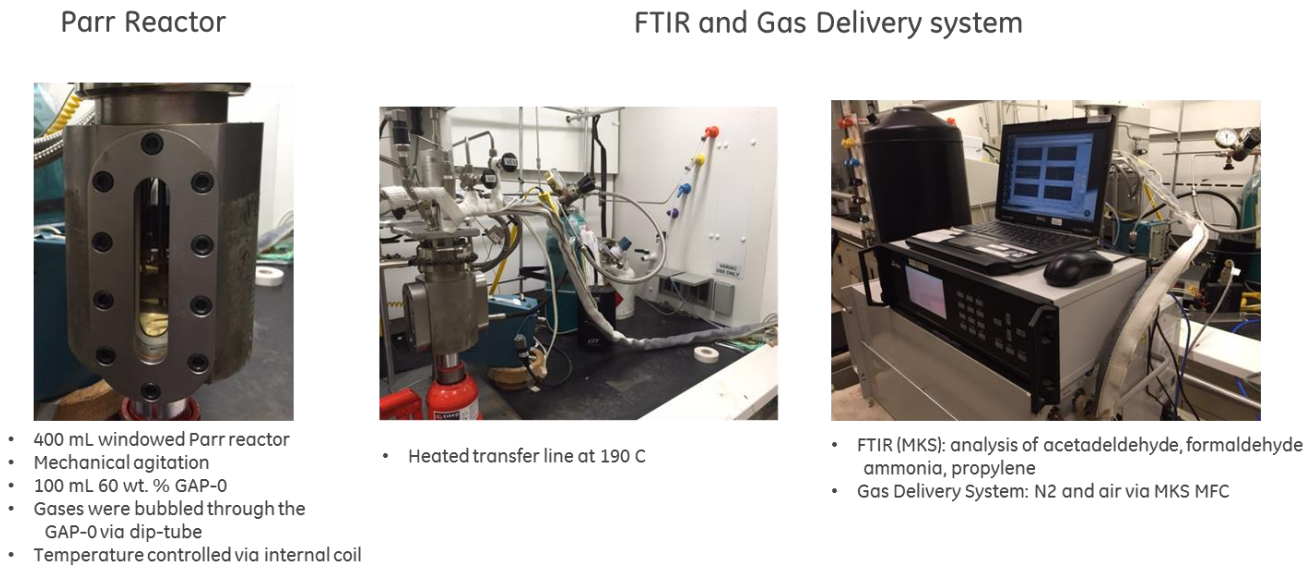

Figure 85. Bench Scale Apparatus to study oxidation of GAP-0 material

Baseline experiments for GAP-0 were performed in a 400 mL windowed Parr reactor with mechanical agitation. The desired gas (N_2 or air) was introduced below the solvent surface of the GAP-0 via a dip tube and the temperature was controlled via an internal heating coil. These experiments are similar to those conducted previously with a 60/40 wt% mixture of GAP-1/TEG and aqueous MEA under a different project.

Purging the virgin GAP-0 solvent at 50°C and 60°C with N_2 showed a large spike in ammonia concentration at seen in Figure 86. However, this rapidly dissipated and was likely due to ammonia already dissolved in the solvent from the manufacturing process or some degradation that occurred during shipping and storage. After 30 minutes, no ammonia was detected. Oxidative activity of GAP-0, GAP-1 / TEG (Sivance), and aqueous MEA (Aldrich) was evaluated by feeding air (1 SLM) into lean working solution (100 mL), under vigorous mixing, at 50°C, 60°C and 70°C for dry GAP-0, 10 wt% H_2O in GAP-0 and Fe^{2+} doped (2.5 mM) H_2O – GAP mixture. Ammonia concentration in the gas phase was measured by FTIR. Ammonia profiles (gas phase, FTIR) at 50°C, 60°C and 70°C are shown in Figure 87. Data is also summarized in Table 40. GAP-0 (dry and wet) exhibits similar ammonia generation to GAP-1 at 50 – 70°C. Spiking of Fe^{2+} salts was performed to simulate the conditions of an aged solvent containing corrosion

impurities. GAP-0 showed a significant increase in ammonia generation upon $Fe(OAc)_2$ spiking (2.5 mM). Similarly, ammonia generation for an aqueous MEA solution increased by more than 50% upon addition of $Fe(OAc)_2$. At 70°C in the presence of Fe^{2+}, the oxidation rate varied as following: GAP-1 < GAP-0 ~ MEA.

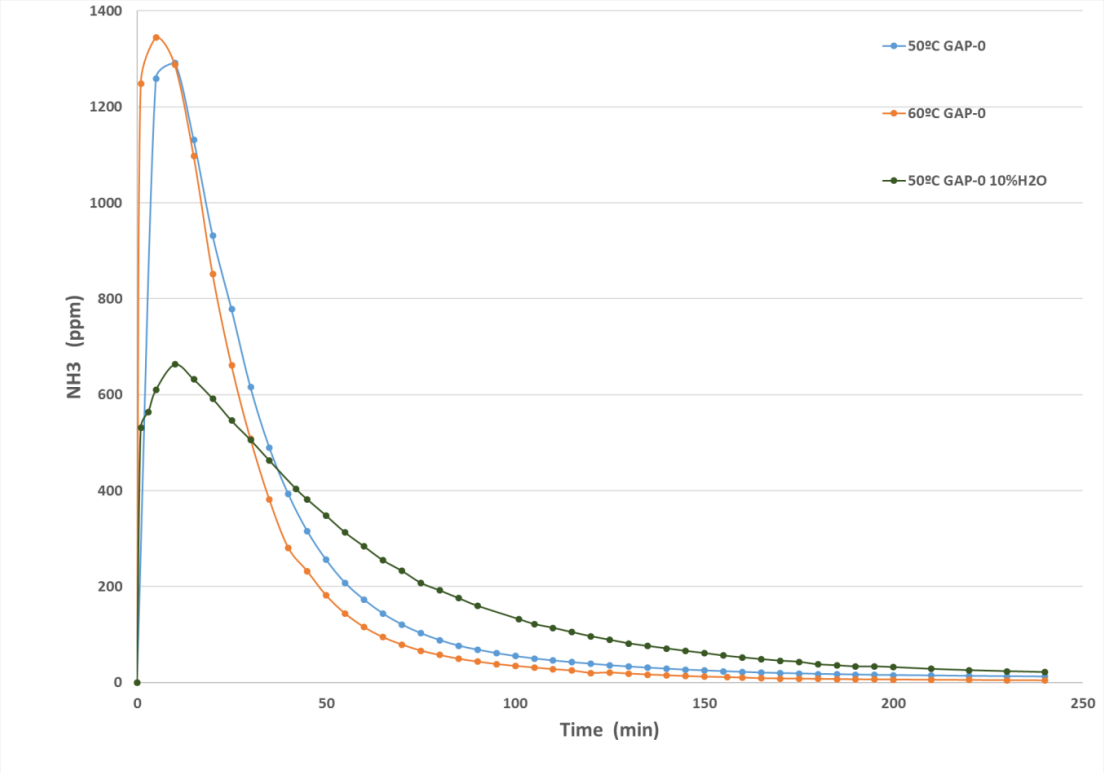

Figure 86. NH_3 evolution during initial purging of GAP-0 with N_2.

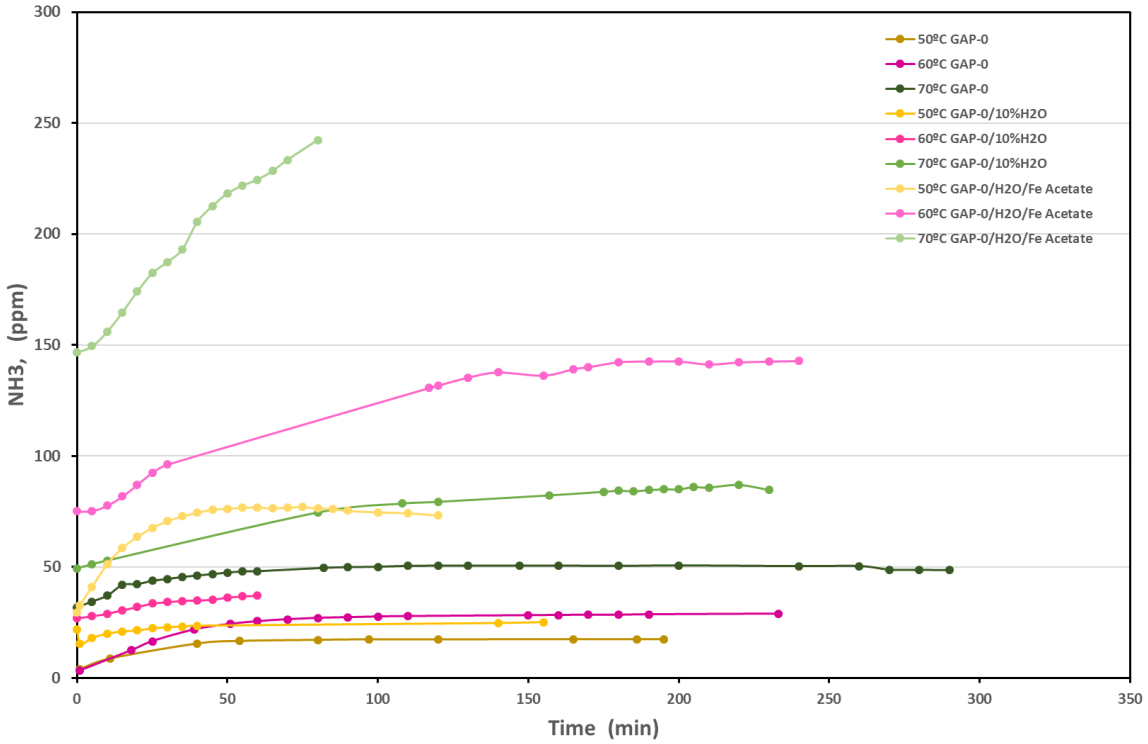

Figure 87. Ammonia Generation for GAP-0 oxidation in air: GAP-0 (dry), GAP-0 + 10 wt% H_2O, and GAP-0 + 10 wt% H_2O + $Fe(OAc)_2$ (2.5 mM).

Table 40. Ammonia Generation for GAP-0 vs. 60 wt. % GAP-1/ 40 wt% TEG (Sivance) vs. MEA (75 wt%)

	GAP-0		**GAP-1 / TEG**		**MEA (75 wt.%)**	
	NH3		NH3		NH3	
	ppmv	mmol/min 10^4	ppmv	mmol/min 10^4	ppmv	mmol/min 10^4
Baseline, FTIR	0					
N2, Initial	2	0.1	3	0.1	3	0.1
Air	50	2.2	130	5.8		
Air % & H2O (wt.%)	85	3.8			550	5.3
Air & Fe2+ (2.5 mM)	242	10.8	140	6.2	850	11*

Parr reactor, P = 2.5 Psig, T = 70°C, 1 SLM gas / 100 mL liquid.
* Normalized for amine content

GAP-0 oxidation was significantly accelerated when temperature was increased from 50°C to 70°C. This indicates that the temperature control in the absorber through inter-stage cooling may be an effective strategy to lower solvent oxidative degradation rate. Finally, it is expected that the oxidation rate will be also affected by the CO_2 content in the working solution. However, attempts to measure the rate of oxidation for the rich solvent (neat) were hampered by the solidification due to formation of the GAP-0 carbamate salt.

Table 41. Ammonia Generation for GAP-0 at 50 – 70°C

	Tenperature, oC		
	50	60	70
Air	18	29	50
Air % & H2O (wt.%)	25	60	85
Air & Fe2+ (2.5 mM)	73	142	242

Parr reactor, P = 2.5 Psig, T = 70°C, 1 SLM gas / 100 mL liquid.

Task 8.4 – Update economic analysis

The project was ended prior to completion of these deliverables.

Conclusions

A bench scale system was designed and built to test a phase-changing aminosilicone solvent. Process and economic models were developed based on experimental data and were used to develop cost and performance estimates for a commercial scale CO_2 capture system integrated with a 550MW_{net} coal-fired power plant. System and economic analysis for the carbon capture unit demonstrates that the phase-changing aminosilicone process has significant advantages relative to an aqueous amine (MEA) system. The first-year CO_2 removal cost for the phase-changing CO_2 capture process is $52.1/tonne, compared to $66.4/tonne for the aqueous amine process. The phase-changing CO_2 capture process is less costly than MEA because of advantageous solvent properties that include higher working capacity, lower corrosivity, lower vapor pressure, and lower heat capacity. The phase-changing aminosilicone process has approximately 32% lower equipment capital cost compared to that of the aqueous amine process. However, this solvent is susceptible to thermal degradation at CSTR desorber operating temperatures, which could add as much as $88/tonne to the CO_2 capture cost associated with solvent makeup. Future work should focus on mitigating this critical risk by developing an advanced low-temperature desorber that can deliver comparable desorption performance and significantly reduced thermal degradation rate.

Appendix A: Manufacturing Plan for Phase-Changing Aminosilicone CO_2 Absorption Material

Robert Perry

Acknowledgment
We wish to thank Kirk Vogt, Paul Kremer, Sasha Stankovich, and Sharon Koh-Fallet from SiVance, LLC, Milliken & Company for supplying much of the information contained in this report.

Abstract
The current process for producing GAP-0, the aminosilicone-based CO_2 capture solvent described in DE-FE0013687, uses the common route of hydrosilylation of tetramethyldisiloxane (TMDSO) with allyl amine, a costly and toxic reagent. An alternate, commercially cost effective manufacturing plan is proposed for GAP-0. The plan utilizes a commercially available hydride and a novel olefin intermediate in a hydrosilylation process to mitigate the cost and handling issues with allylamine. A number of silicone manufacturers have been contacted and several have supplied samples for evaluation. An estimate for the large scale manufacturing cost has been calculated and the raw material supply for reagents needed has been examined.

Introduction
GE Global Research has developed a novel technology that uses an aminosilicone based solvent to capture CO_2 from flue gas. As part of ARPA-e program DE-AR0000084, it was found that a low viscosity liquid denoted as GAP-0 (bis[3-aminopropyl]-1,1,3,3-tetramethyldisiloxane) readily reacted with CO_2 to form a solid, carbamate salt (eq. 1). This was unique as it was the first report of a phase-changing material being used as a CO_2 capture solvent.

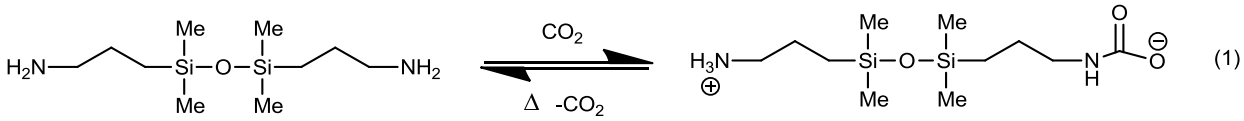

GAP-0 GAP-0 Carbamate (1)

Early work with this aminosilicone was performed on material obtained commercially from a specialty silicone manufacturer (Gelest). However, development of this potentially game-changing technology required substantially larger quantities of GAP-0 for bench-scale validation and ultimately commercial implementation at large scale.

This report describes possible synthetic routes to GAP-0, a route chosen for potential scale-up, the availability of raw materials, identification of silicone suppliers and an estimate of the cost for GAP-0.

I. Synthetic Routes

A. Hydrosilylation with Allylamine

One simple approach to the synthesis of GAP-0 is shown in equation 2 and consists of the hydrosilylation of 1,1,3,3-tetramethyldisiloxane (TMDSO) and allylamine with a Pt catalyst (Ashby's and Karstedt's are commonly employed).

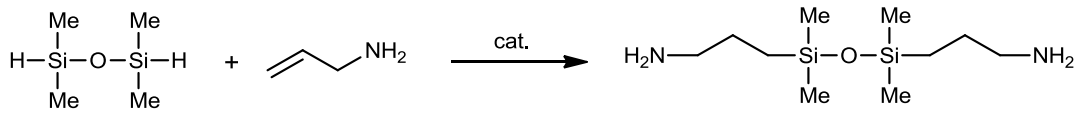

(2)

Ideally, a 2:1 stoichiometric ratio of olefin:siloxane is desired. However, because of the toxicity of allylamine, a slight deficit of that reagent is typically used. While all the allylamine is consumed in this hydrosilylation reaction, the yields are less than quantitative and some cyclic by-products are produced which must be removed. One manufacturer has found that a 1.5-fold excess of TMDSO is required to assure complete reaction of the allylamine. While greatly increasing raw material costs, it also complicates downstream processing by creating a wider distribution of molecular weights.

Additionally, hydrosilylation occurs with both anti-Markovnikov and Markovnikov regiochemistries. This reaction produces the desired γ,γ-isomer but also the β,γ- and β,β-isomers shown below. While these last two isomers are still reactive towards CO_2 capture, they act as impurities and negatively impact the solid properties of the carbamate.

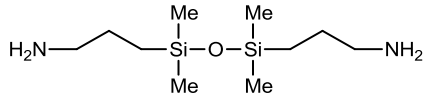

γ,γ-isomer

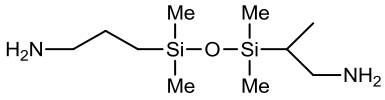

β,γ-isomer

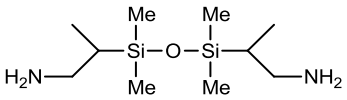

β,β-isomer

Another difficulty in the reaction is that primary amine-containing compounds poison platinum catalysts.[1] The reaction occurs in an irregular fashion that is difficult to control. To overcome this, large amounts of platinum catalyst are used to keep the reaction going to completion. Since platinum is an increasingly precious metal, the catalyst is a significant cost in the manufacture of the GAP material.

To prevent the amine from poisoning the catalyst, US3642854[2] and US4584393[3] describe changing the sequence of manufacture by reacting the dimethylchlorosilane with excess allylamine first to form N- allyl-dimethylsilazane (eq 3). After removal of the allylamine hydrochloride salt and remaining excess allylamine, platinum catalyst is added to affect intramolecular hydrosilylation. The resulting material can then be hydrolyzed to form the desired bis(3-aminopropyl)-tetramethyldisiloxane product.

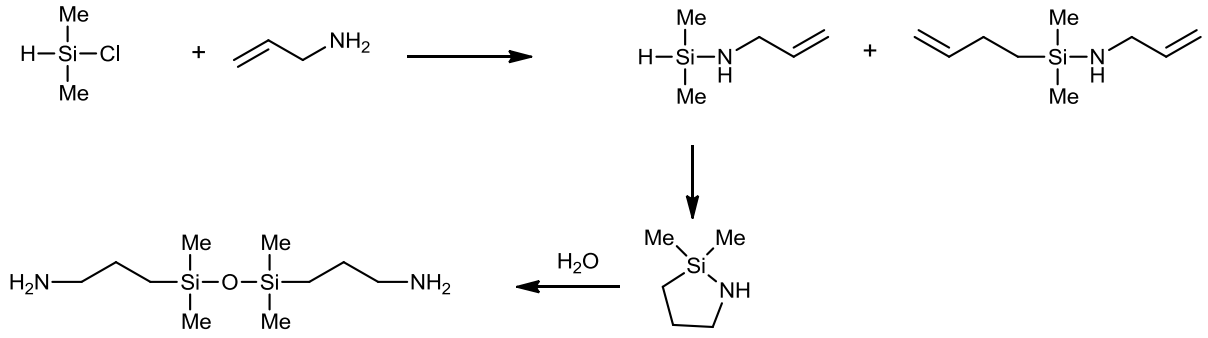

(3)

Unfortunately, this technique suffers from two issues. First, the process uses excess allylamine. Allylamine is a cardiovascular health hazard that must be handled carefully, and preferably used as the limiting reagent. Second, it is difficult to control the reaction to form only the preferred monosilazane product as opposed to a mixture of mono- and di-silazanes. The monosilazane is preferred because it hydrolyzes to pure bis(3-aminopropyl)tetramethyldisiloxane. With the mono- and disilazane blend, a mixture of oligomers is produced.

In other work, Webb[4] suggests that the yield of the desired GAP product can be improved by first reacting dimethylchlorosilane with ammonia to preferably form tetramethyldisilazane (eq 4). That product is then reacted with allylamine to form the N-allyl-dimethylsilazane. After hydrosilylation and hydrolysis, the product is primarily GAP-0. This has advantages that only stoichiometric amounts of allylamine are needed, and the final product has higher purity. Its disadvantages come from the need to manufacture tetramethyldisilazane which can be expensive. The chemistry necessary to limit the initial reaction to monosilylation on the allylamine nitrogen can also be difficult.

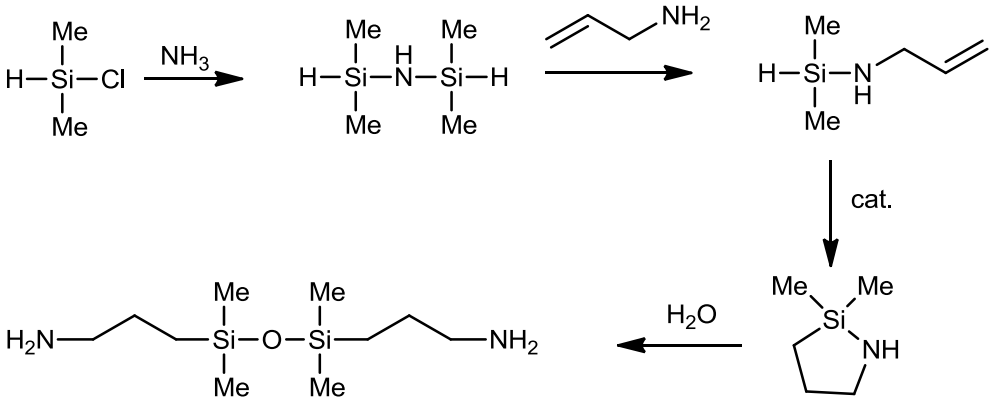

(4)

More interestingly, US4892918[5] suggests that secondary amines do not poison the platinum hydrosilylation catalyst as much as primary amines. They reported that they could hydrosilate N-methyl allyl amine with dimethylchlorosilane without any catalyst poisoning.

This suggested that protection[6] of the amine could aid the hydrosilylation reaction and lower catalyst usage. As shown in equation 5, the general reaction scheme changes the primary amine of allylamine with another reactant (PG) to form a secondary or tertiary amine. After hydrosilylation, the protecting group (PG) must be removed, restoring the primary amine functionality.

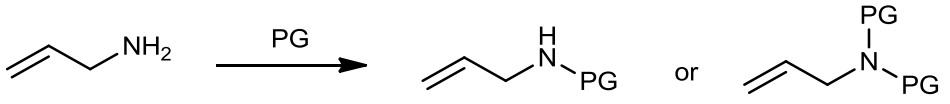

(5)

Several specific reaction schemes are published in literature, but a careful choice is important because many protection/deprotection processes are expensive and not likely suited for the projected volumes of aminosilicone solvent needed in large scale. Equations 6 and 7 show schemes where allylamine is reacted with phthalic anhydride or phthalic acid to form a phthalimide[7] or reacted with hexamethyldisilazane to create allyl hexamethyldisilazane[8]. In both cases, the protecting moiety is too expensive to be practical for this application.

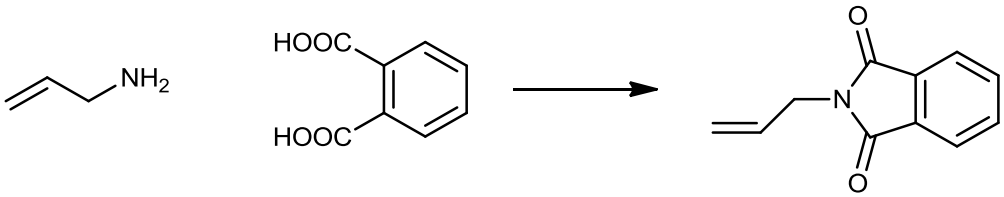

(6)

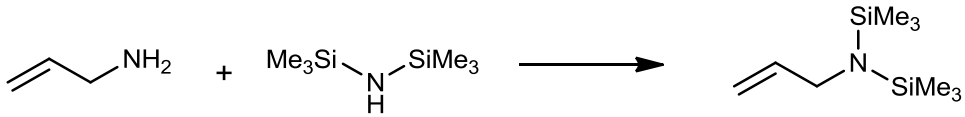

(7)

A more promising reaction scheme is the reaction of methyl chloroformate with allylamine to make methyl N-allylcarbamate[9],[10] as shown in equation 8. In this case, the resulting protecting group is methanol and carbon dioxide, less expensive materials that may make this process more feasible.

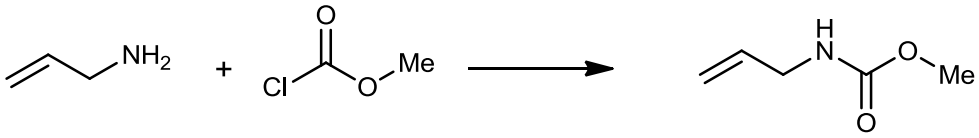

(8)

B. Hydrosilylation with Acrylonitrile

A second synthetic method entails reaction of a hydridosilane with acrylonitrile. As with allylamine, numerous routes can be contemplated, one of which is shown in equation 9.

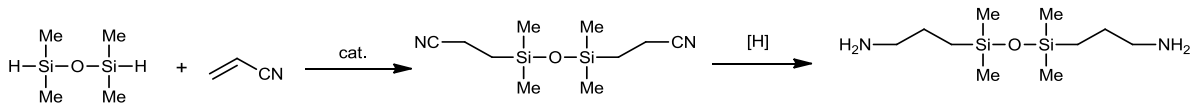

(9)

Selective reaction at the double bond terminus is rare although several reports have appeared that claim exclusive β-addition.[11-15] More commonly, several regioisomers are made as shown below, leading to a mixture of amine products after reduction.

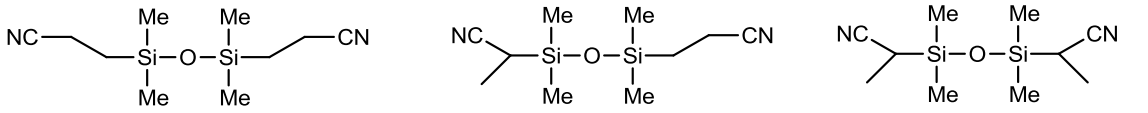

Reduction of the nitrile group can be accomplished with a variety of reagents including $LiAlH_4$, $BH_3.SMe_2$ or with catalytic hydrogenation, although secondary amines are a common side product.[16] Mitigating the chemical challenges still leaves a significant drawback to this route. Acrylonitrile is a toxic, low boiling liquid that the EPA has classified acrylonitrile as a Group B1, probable human carcinogen (cancer-causing agent).[17] Given these attributes, large scale synthetic routes to GAP-0 using this reagent were not considered further.

C. Hydrosilylation with Allylchloride

An alternate route to GAP-0 that does not involve the use of allylamine or acrylonitrile is shown in equation 10. This method relies on the amination of a chloropropyl group that is derived from allyl chloride. As seen in equation 10, the bis(3-chloropropyl)-1,1,3,3-tetramethyldisiloxane intermediate can be made directly from the TMDSO hydride. Treatment with ammonia yields the desired product.

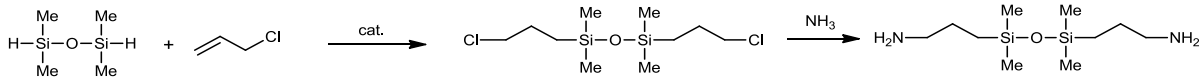

(10)

The most common methods of hydrosilylation use platinum as a catalyst. Unfortunately with allyl chloride, the hydrosilylation reaction competes with allyl chloride reduction and double bond migration.[18] Low yields of the desired bis-chloropropyl tetramethyldisiloxane result.

Two other catalysts have been found that do not catalyze the competitive reactions: copper[19] and iridium[20]. For copper, the reaction requires undesirably high temperatures (200°C) and pressurized conditions for long reaction times (45 hours). For iridium, the results are much better. The reaction can be run under reflux conditions at

atmospheric pressures for several hours to obtain a high yield (>90%) of bis-chloropropyl tetramethyldisiloxane material. While iridium is an expensive metal, Y. Tonomura[21] and others[22-25] suggest that co-catalysts can suppress deactivation, increasing lifetime.

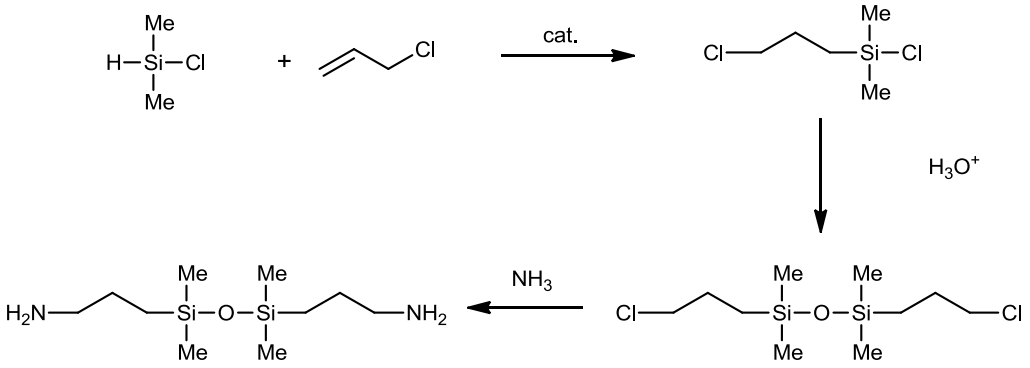

(11)

Hydrosilylation with TMDSO (eq. 3) did not work as well as hydrosilylation with chlorodimethyl-silane as shown in equation 11. The intermediate chloropropylchlorodimethylsilane can be readily hydrolyzed to the desired bis(3-chloropropyl)disiloxane followed substitution of chlorine by concentrated ammonia to form primary amine.[26]

For substitution by ammonia, two possible methods are disclosed in literature. First, the chloropropylchlorodimethylsilane can be hydrolyzed into bis(3-chloropropyl) tetramethyldisiloxane, which can be treated with excess ammonia to form GAP-0 (eq 11). The difficulty is that secondary and tertiary amines are usually formed even if the concentration (pressure) of ammonia is very high.

Alternatively, the chloropropylchlorodimethylsilane can be treated with excess ammonia before hydrolysis to form a cyclic silazane (eq 12) that converts to GAP-0 when hydrolyzed.[27] This process also requires a very high excess of ammonia to insure that a cyclic disilazane forms without any secondary or tertiary amines.

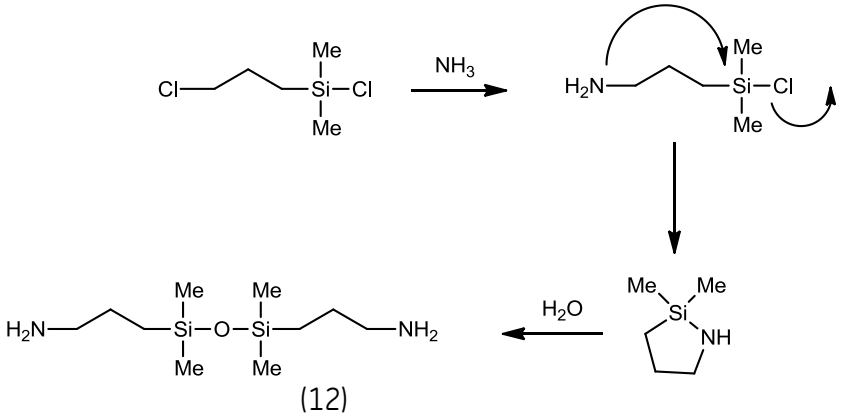

(12)

The high concentration and pressure of ammonia that is required in both of these processes decreases the possible yield per batch, making this process less desirable. While ammonia is safely handles on large scale, its volatile nature and potential purification difficulties removed this route from consideration.

An alternate method of introducing the amine group is conversion to a carbamate functionality and subsequent hydrolysis to primary amine. Fritz-Langhals[28] disclosed a process that uses potassium cyanate to convert the chloro- group on bis(3-chloropropyl)tetramethyldisiloxane to carbamate. These are then hydrolyzed to primary amines by refluxing in strong acid or base to release carbon dioxide, producing GAP-0. A possible disadvantage of the process is that the yields disclosed in the patent application ranged greatly, sometimes as low as 50%.

As discussed earlier, allyl chloride would be more preferred if the process to convert chloride to carbamate and then to primary amine was cheaper than the difference in raw material costs. In the late 1940's, Kaiser discovered that allyl chloride can be reacted with potassium cyanate[29] and methanol to produce methyl-N-allylcarbamate, as shown in equation 13.[30] As discussed above, carbamate can be converted to amine by hydrolysis with strong acid or base.[31] This is promising because the cost of these raw materials is quite low.

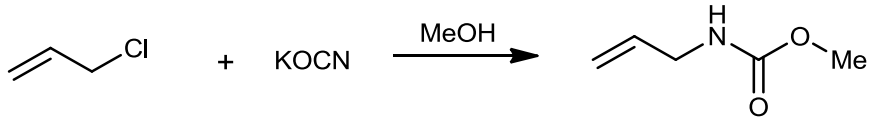

(13)

As shown in Scheme 1, process control of the process is important because many side reactions that that have the potential to occur. For example, the intermediate, allyl isocyanate, can dimerize or trimerize to form isocyanurate, a non-recoverable byproduct. Methanol must be controlled to a sufficient concentration to prevent the isocyanate side reactions. Unfortunately, excessive amounts of methanol will substitute onto the allyl chloride to create allyl methyl ether and hydrochloric acid. The acid reacts further with potassium cyanate to make isocyanic acid that reacts with methanol to make methyl carbamate. By carefully controlling the temperature and solubility of the potassium cyanate through solvent choice, one silicone manufacturer was able to minimize the formation of the undesired byproducts to an acceptable level.[32]

Scheme 1. Synthesis of Methyl-N-allylcarbamate.

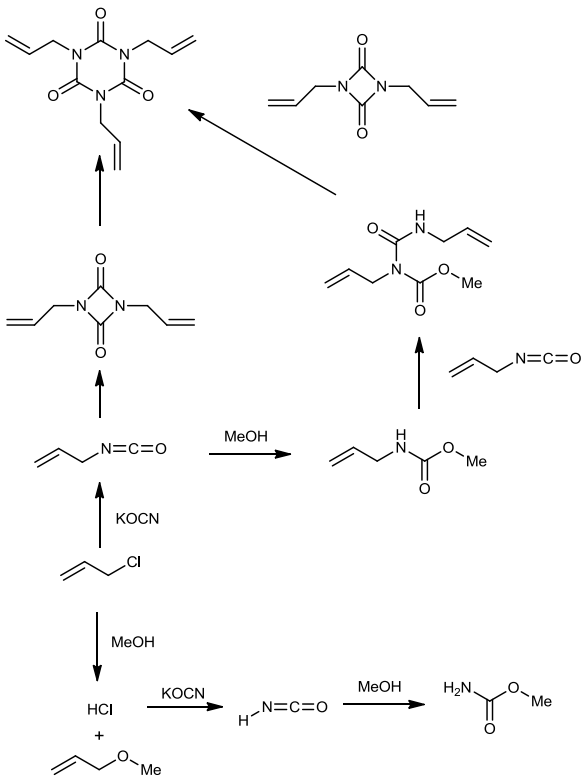

II. Scale-up Process

The most attractive route envisioned for the manufacture of GAP-0 is that derived from the reaction of KOCN with allyl chloride to generate methyl-N-allylcarbamate, as depicted in Scheme 1, followed by hydrosilylation with TMDSO (eq. 14). This route had the attributes of readily available starting materials, relatively uncomplicated reaction conditions and high yields.

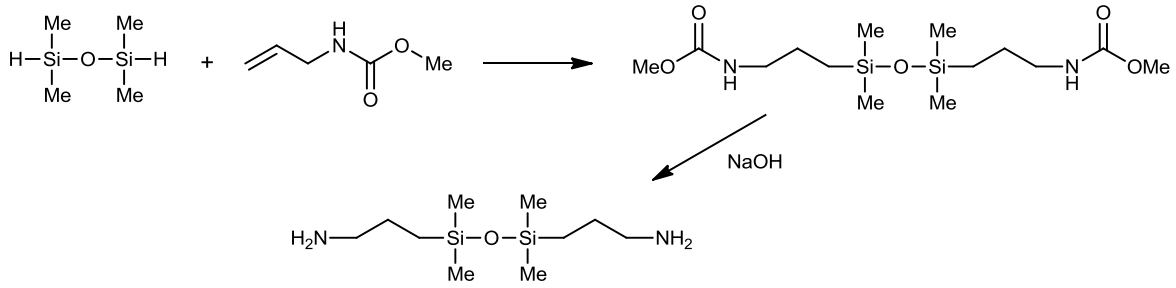

(14)

The block process diagram is shown in Figure 1 below with the input, recycle and waste streams identified.

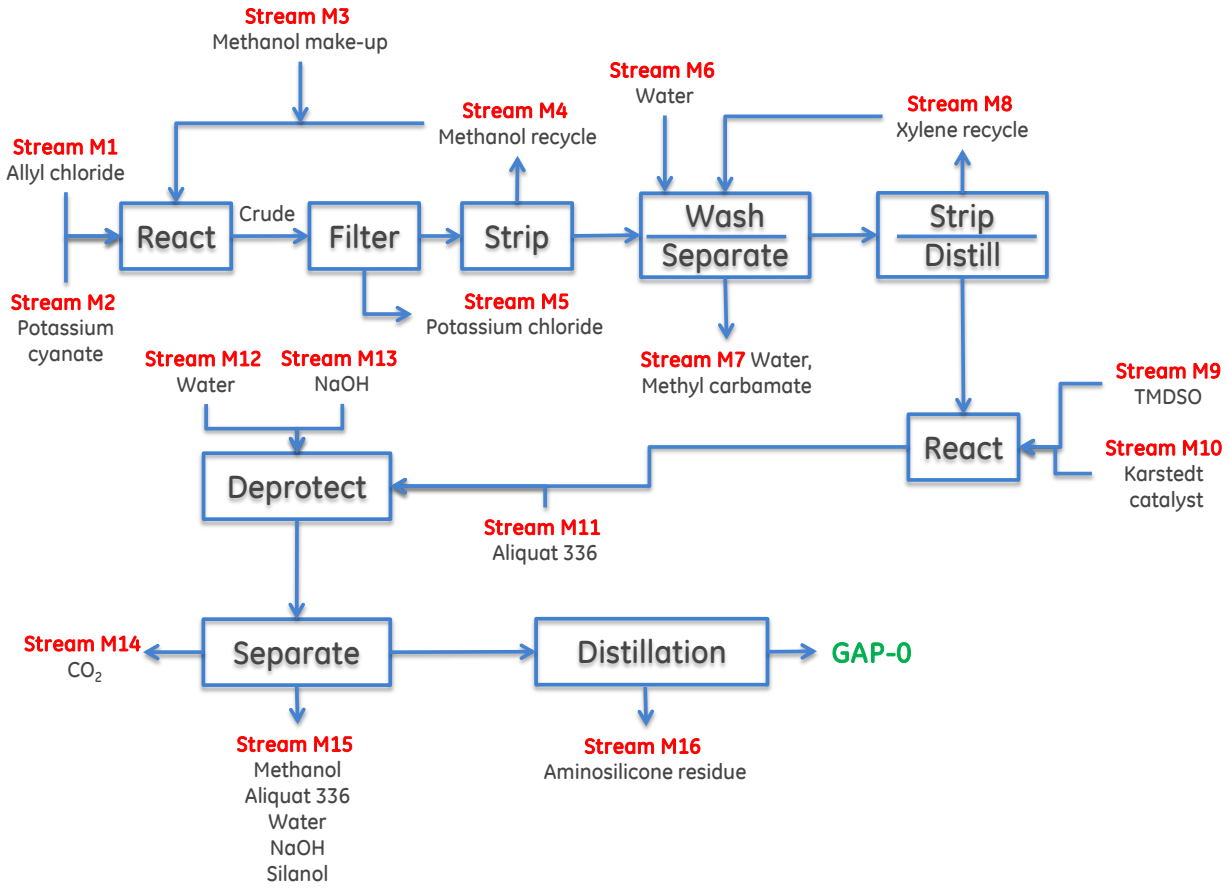

Figure A1. Proposed manufacturing process for GAP-0.

This procedure addresses deficiencies in the traditional GAP-0 manufacturing process. Catalyst poisoning has been minimized by using a protected amine during hydrosilylation, excess TSMDO has been eliminated as the hydrosilylation reaction can now be run stoichiometrically and allylamine has been replaced by allyl chloride.

III. Raw Material Availability

Methanol - No supply concerns. It is a global commodity with 75 million metric ton annual capacity. Six approved manufacturers and availability through multiple regional distributors; multiple suppliers have announced plans to build plants in the US to take advantage of US low global natural gas feedstock pricing due to shale gas.

Allyl Chloride - No supply concerns. It is produced domestically by Dow (794 MM pounds) and Solvay (400 MM pounds) and internationally by 11 others.

KOCN - No supply concerns. It is a global commodity with a supply that exceeds 20,000 tons.

Dimethylchlorosilane (DMCS) – There are numerous, large international suppliers that produce this material as a by-product of the direct process. If demand grows to outpace supply, technology is available for the industry to meet any extra demands that CO_2 capture will provide. (see appendix)

Xylene – No supply concerns. 3.7 million tons were produced in 2015 and is available globally.

Aliquat 336 - No supply concerns. It is a globally available phase-transfer catalyst used in catalyst quantities.

Sodium Hydroxide - No supply concerns. It is a global commodity.
Platinum Catalyst – No supply concerns are anticipated because the amount necessary for the CO_2 Capture application is tiny compared to the total amount necessary for the silicone industry.

IV. Silicone Manufacturers
There are five large, international silicone manufacturers, six intermediate size companies and numerous small, specialty producers of silicone products. The first five listed in Table 1 below are the large suppliers with sales of silicone products noted where available. All these companies were contacted to inquire about their capacity, capability and interest in producing the GAP-0 solvent. Not surprisingly, the smaller entities were not able to meet one or more of the requirements noted above.

However, very high levels of interest were demonstrated by two of the large manufacturers and three of the intermediate sized companies. Aminosilicone samples have been received from four of these five and have undergone extensive laboratory validation. Results have varied from nearly 100% all γ-isomer material to GAP-0 containing nearly 15% β-isomer. One manufacturer has already supplied over 400kg of excellent quality material for use in the current phase-change program. Conversations with the other interested parties are continuing and several NDA's are in place to facilitate more detailed communication.

Manufacturer/Supplier	Comments	Sales
Shin-Etsu	multiple functional fluids/large capacity	$11.3B
Momentive*	multiple functional fluids/large capacity	$7.8B
Wacker	multiple functional fluids/large capacity	$6.3B
Dow Corning	multiple functional fluids/large capacity	$6.2B
BlueStar (Rhone-Poulenc)	multiple functional fluids/large capacity	$0.65B
Emerald Performance Materials	aminosilicones + specialties/limited capacity	$0.40B
Evonik (Specialty materials)*	curable silicones/limited capacity	E4.6B
Silar	limited scope of materials	N/A
Gelest	multiple functional fluids/limited capacity	N/A
SiVance/Milliken	intermediate size/limited capacity	N/A
Bejing Entrepreneurial Co. Ltd	limited scope of materials/limited capacity	N/A
ICM Products	limited scale-up knowledge/ limited capacity	N/A

Qsi Quantum Silicones	coatings and resins - no fluids	N/A
CRI-SIL Silicone Technologies	RTV's and additives	N/A
Elkay Silicones (India)	multiple specialty silicones/emulsions	N/A
Clearco Silicones	aminosilicones for release agents	N/A
Silco Inc.	sealants and adhesives	N/A

* include non-silicone sales.

V. Appendix

In general, the organic chemistry of silicon is fed by two primary reactions, a) the thermal reduction of silicon dioxide with carbon to make silicon metal, and b) the Rochow Direct process to create organochlorosilanes. During the Rochow process, silicon metal is reacted with methyl chloride in the presence of copper catalyst to generate organochlorosilanes, $Me_aSi_bH_cCl_d$, where Me=methyl.[33-35] A complex mixture often results, dominated by Me_2SiCl_2. Among the minor components is our desired raw material, chlorodimethylsilane, Me_2SiHCl.[36] These components are typically collected, separated, and purified by distillation. The composition of the complex mixture is important to the commodity portion of the silicone business because it drives the economics. To be profitable, the producer must balance the cost of each material in proportion to the amount produced and the demand for each material. In the end, one must sell every pound of product produced to operate profitably. Since chlorodimethylsilane is not abundantly produced in the standard Rochow Process (<1%), it is expensive and sometimes has limited availability, especially for specialty silicone producers who make what they can sell and generally do not need to balance by-product and co-product streams. As a result, chlorodimethylsilane is currently several times more expensive than dichlorodimethylsilane, a workhorse raw material for the silicone industry.

Some literature suggests that the Direct Process can be modified by adding hydrogen or hydrogen chloride gas, changing the distribution of final products.[37-39] The resulting distribution contains higher concentrations of our desired product, chlorodimethylsilane, as shown in Figure 2. However, these changes are only justified economically if the demand is large and continuous.

A second method that is used to make more hydrogen-containing silanes is redistribution. As evidenced by the large distribution of products derived from the Direct Process, the chemistry of organochlorosilanes is a series of equilibrium reactions that can be influenced by temperature, concentration, and particular catalysts. Rhodia,[40] Wacker,[41] and Huels[42] disclose processes that largely recycle less valuable products and work to redistribute them into more valuable products, including chlorodimethylsilane.

Sundermeyer[43-44] was a leader in the use of metal hydrides to hydrodechlorinate and redistribute organochlorosilane products. His eutectic melt system is especially interesting as one of the few capable of reacting hydrogen directly with organochlorosilane to generate organochlorohydrosilanes. Handling of the high

temperature, acidic, metal-containing eutectic melts is likely a challenge, however.

More recently, Wacker disclosed the generation of organochlorohydrosilanes from the redistribution of trichlorosilane and various organochlorosilanes.[45] While this largely built on the previous redistribution work of others, it capitalized on the recent increase in supply of trichlorosilane. Trichlorosilane is used in the manufacture of high purity semiconductor grade silicon for semiconductors and photovoltaics. Since that manufacturing process is inefficient, a large amount of silicon tetrachloride waste is generated. The silane industry has thus developed large hydrogenation and redistribution processes to recycle silicon tetrachloride back into trichlorosilane.[46-47] Incorporation of a chlorodimethylsilane production process into large scale processes of this type benefits the economics of GAP production. This seems like an industry-leading innovation.

Lastly, on a smaller, specialty chemical scale, metal hydrides like lithium aluminum hydride and magnesium hydride continue to be used to hydrodechlorinate organochlorosilanes.[48]

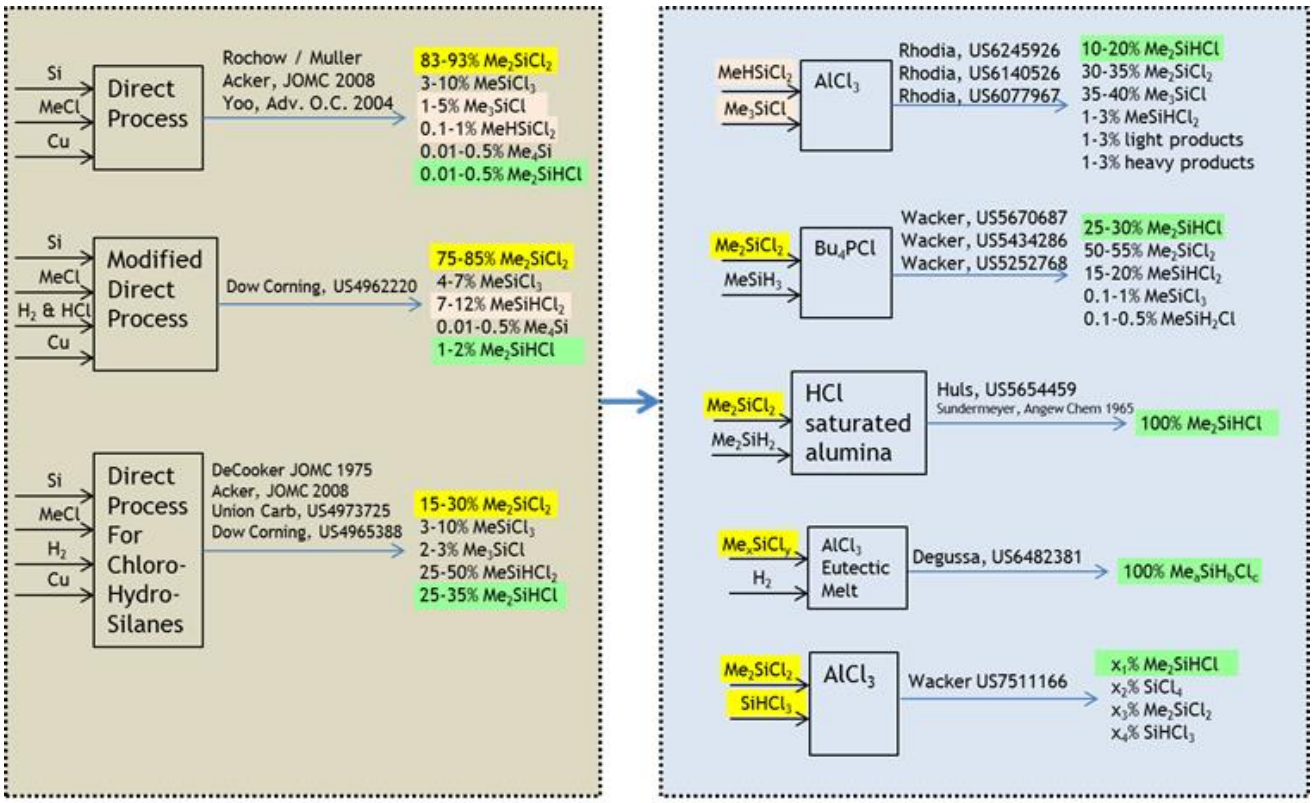

Figure A2: Illustration of possible methods to improve supply of chlorodimethylsilane.

Appendix A References

1. US 4892918, column 5, line 61.
2. V.P. Kozjukov, et al, US3642854, claim 12, Feb. 15, 1972.
3. J.L. Webb, et al, US4584393, April 22, 1986.
4. J.L. Webb, US4565885, Jan. 21, 1986.
5. H.S. Ryang, US4892918, Jan. 9, 1990.
6. http://www.organic-chemistry.org/synthesis/C1N/amines/protectedprimaryamines.shtm
7. Michael Palucki, et al., US6262268, 2001.
8. B.N. Ghose, Journal of Organometallic Chemistry, 1979, Vol. 164, p. 11-18.
9. T. W. Greene, Protective Groups in Organic Synthesis, 1981, p. 224.
10. P. J. Kocienski, Protecting Groups, 2000, p. 191-192.
11. Petrov, A. D.; Vdovin, V. M.; Izv. Akad. Nauk. SSSR, Ser. Khim. 1957, 1490.
12. Goodman, L.; Silverstein, R. M.; Benites, A., J. Amer. Chem. Soc., 1957, 79, 3073.
13. Petrov, A. D.; Mironov, V. F.; Sadykh-zade, S. I.; Izv. Akad. Nauk. SSSR, Ser. Khim. 1956, 256.
14. Saam, J. C.; Speier, J. L., J. Org. Chem., 1959, 24, 427.
15. (a) Rajkumar, A. B.; Boudjouk, P., Organomet., 1989, 8, 549. (b) Chauhan, M.; Chauhan, B. P. S.; Boudjouk, P.,Tetra. Lett., 1999, 40, 4127.
16. Smith, M.B.; March, J. "March's Advanced Organic Chemistry 6th Ed." Wiley Interscience, New Jersey, 2007, pgs 1813-1814.
17. http://www3.epa.gov/airtoxics/hlthef/acryloni.html
18. M. Jankowiak, et al, Journal of Organometallic Chemistry, 690 (2005) 4478-4487.
19. B.T. Nguyen, et al, US6713644, Oct. 3, 2002.
20. J.M. Quirk, et al, US4658050, March 31, 1986.
21. Y. Tonomura, et al, US6359161, May 11, 2001.
22. T. Kornek, et al, US7208618, June 12, 2003.
23. A. Bauer, et al, US7956210, Feb. 25, 2008.
24. K. Ramdani, et al, US7655813, April 7, 2008.
25. N. Guennouni, et al, US7884225, July 16, 2008.
26. http://www.docbrown.info/page06/OrgMechs2.htm#ammonia
27. L. Brader, et al, US6531620, Sept. 27, 2001.
28. E. Fritz-Langhals, US Pat. Appl. 2012/0004436, March 23, 2009.
29. Over 20,000 tons of potassium cyanate are used per year for manufacturing pesticides, drugs, and detergents; P.M. Schalke, et al.,"Cyanates, Inorganic Salts", Ullmann's Encyclopedia of Industrial Chemistry, 2006, Wiley-VCH, Weinheim.
30. D.W. Kaiser, US2647916, 1953.
31. E. Fritz-Langhals, US Pat. Appl. 2012/0004436, March 23, 2009.
32. SiVance ref.

33. R.J.H. Voorhoeve, Organohalosilanes, Precursors to Silicones, 1967, pp. 120-282.
34. Kalchauer, W. and Pachaly, B. 2008. Müller–Rochow Synthesis: The Direct Process to Methylchlorosilanes. Handbook of Heterogeneous Catalysis. 2635–2647
35. B.R, Yoo, et al, Advances in Organometallic Chemistry, Vol. 50, 2004. pp. 145-177.
36. Jörg Acker, Klaus Bohmhammel , Journal of Organometallic Chemistry, Volume 693, Issue 15, 15 July 2008 , Pages 2483-2493.
37. R.L. Halm, et al, US496220, US4965388, Jan. 2, 1990.
38. K.M. Lewis, et al, US4973725, June 13, 1989.
39. M.G.R.T. DeCooker, et al, Journal of Organometallic Chemistry, Volume 99, Issue 3, 1975, pp. 371-377.
40. Rhodia Chemie, US6077967, US6140526, and US6245926.
41. Wacker Chemie, US5252768, US5434286, US5670687.
42. F. Kropfgans, et al, US5654459, June 7, 1996.
43. W. **Sundermeyer, Angew. Chem**. 77, 241 (**1965**); **Angew. Chem**. internat. Edit. 4, 222 (**1965**).
44. W. Sundermeyer, US6482381, Sept. 25, 2000.
45. G. Geisberger, Wacker Chemie, US7511166, March 31, 2009.
46. http://gradworks.umi.com/14/95/1495987.html
47. http://www.modularprocess.com/polysilicon-tcs-stc.htm
48. A.R. Katritzky, et al, Comprehensive Organic Functional Group Transformations: Synthesis: carbon with one heteroatom attached by a single bond, 1995, p. 536

References

1 Murphy, J. T.; Jones, A. P. DOE/NETL's Carbon Capture R&D Program for Existing Coal-Fired Power Plants, DOE/NETL-2009/1356 February 2009.

2 Perry, R., et.al. "CO2 Capture Process Using Phase-Changing Absorbents – Final Technical Report." DOE Contract No. DE-AR0000084. December 2013.

3 Kuntz, J. and A. Aroonwilas. "Mass Transfer in a Spray Column for CO2 Removal." EIC Climate Change Technology, May 10-12, 2006. IEEE. http://ieeexplore.ieee.org/stamp/stamp.jsp?tp=&arnumber=4057341

4 Kohl, Arthur. "Absorption and Stripping." Handbook of Separation Process Technology. By Ronald W. Rousseau. New York: J. Wiley, 1987.

5 Seader, J. D., and Ernest J. Henley. Separation Process Principles. New York: Wiley, 1998.

6 McCabe, W.L., Smith, J.C., and Harriott, P. Unit Operations of Chemical Engineering. 5th ed. New York: McGraw-Hill, 2005.

7 Allen, J. "Concept Review: Unit Systems." Michigan Technological University. http://www.me.mtu.edu/~jstallen/courses/MEEM4200/lectures/energy_intro/Review_unit_systems.pdf Last accessed 14 October 2014.

8 Westendorf, T., et. al. "Bench-Scale Process for Low-Cost Carbon Dioxide (CO2) Capture Using a Phase-Changing Absorbent – Preliminary Process and Cost Modeling Report." DOE Contract No. DE-FE0013687. June 2015.

9 Westendorf, T., et. al. "Bench-Scale Process for Low-Cost Carbon Dioxide (CO2) Capture Using a Phase-Changing Absorbent – Quarterly Research Performance Progress Report." DOE Contract No. DE-FE0013687. July 2014.

10 Ashgriz, N. "Handbook of Atomization and Sprays." New York: Springer, 2011.

11 Kayano, A., and Kamiya, T., "Calculation of the Mean Drop Size of the Droplets Purged from the Rotating Disks", Proceedings of the 1st International Conference on Liquid Atomization and Sprays, Tokyo, 1978, pp. 133–143.

12 Perry, R., et.al. "CO2 Capture Process Using Phase-Changing Absorbents – Final Technical Report." DOE Contract No. DE-AR0000084. December 2013.

13 Wood, B., et.al. "Pilot-Scale Silicone Process for Low-Cost CO2 Capture – Quarterly Report 2nd 2015." DOE Contract No. DE-FE0013755. July 2015.

14 "ASTM G1-03 (2011): Standard Practice for Preparing, Cleaning, and Evaluating Corrosion Testing Specimens." ASTM International. http://www.astm.org/Standards/G1

15 Westendorf, T., et. al. "Bench-Scale Process for Low-Cost Carbon Dioxide (CO2) Capture Using a Phase-Changing Absorbent – 2Q2015 Quarterly Report." DOE Contract No. DE-FE0013687. October 2015.

16 Nainar, M., Veawab, A., "Corrosion in CO2 capture unit using MEA-piperazine blends.", Energy Procedia, 2009, 1, 231-235.

17 Tanthapanichakoon, W., Veawab, A., "Polarization Behavior and Performance of Inorganic Corrosion Inhibitors in Monoethanolamine Solution Containing Carbon Dioxide and Heat-Stable Salts." Corrosion, 2005, 61, 371-380.

18 Veawab, A., Tontiwachwuthikul, P., Bhole, S. D., "Studies of Corrosion and Corrosion Control in a CO2-2-Amino-2-methyl-1-propanol (AMP) Environment." Ind. Eng. Chem. Res., 1997, 36, 264-269.
19 Soosaiprakasam, I. R., Veawab, A., "Corrosion inhibition performance of copper carbonate in MEA-CO2 capture unit." Energy Procedia, 2009, 1, 225-229.
20 Soosaiprakasam, I. R., Veawab, A., "Inhibition Performance of Copper Carbonate in CO2 Absorption Process using Aqueous MEA." NACE Internation Corrosion Conference Series, 2007, 073961.
21 Tontiwachwuthikul, P., Idem, R., Kladkaew, N., Saiwan, C., (University of Regina). Corrosion Inhibitors. U.S. Patent Application US 2011/0300044 A1, 2011.
22 Srinivasan, S., Veawab, A., Aroonwilas, A., "Low Toxic Corrosion Inhibitors for Amine-based CO2 Capture Process." Energy Procedia, 2013, 37, 890-895.
23 Veawab, A., Tontiwachwuthikul, P., Chakma, A., "Investigation of Low-Toxic Organic Corrosion Inhibitors for CO2 Separation Process Using Aqueous MEA Solvent." Ind. Eng. Chem. Res., 2001, 40, 4771-4777.
24 Zheng, L., Landon, J., Koebcke, N. C., Chandan, P., Liu, K., "Suitability and Stability of 2-Mercaptobenzimidazole as a Corrosoin Inhibitor in a Post-Combustion CO2 Capture System." Corrosion, 2015, 71, 692-702.
25 "ASTM G1-03 (2011): Standard Practice for Preparing, Cleaning, and Evaluating Corrosion Testing Specimens." ASTM International. http://www.astm.org/Standards/G1
26 Westendorf, T., et. al. "Bench-Scale Process for Low-Cost Carbon Dioxide (CO2) Capture Using a Phase-Changing Absorbent – 2Q2015 Quarterly Report." DOE Contract No. DE-FE0013687. October 2015.
27 Hasib-ur-Rahman, M. and Larachi, F. "Prospects of Using Room-Temperature Ionic Liquids as Corrosion Inhibitors in Aqueous Ethanolamine-Based CO2 Capture Solvents." Ind. Eng. Chem. Res., 2013, 52, 17682-17685.
28 Kladkaew, N., Idem, R., Tontiwachwuthikul, P., and Saiwan, C. "Studies on corrosion and corrosion inhibitors for amine based solvents for CO2 absorption from power plant flue gases containing CO2, O2 and SO2." Energy Procedia. 2011, 4, 1761-1768.
29 Westendorf, T., et. al. "Bench-Scale Process for Low-Cost Carbon Dioxide (CO2) Capture Using a Phase-Changing Absorbent – 2Q2016 Quarterly Report." DOE Contract No. DE-FE0013687. July 2016.
30 ASPEN Plus Help: "Aspen Liquid Mixture Viscosity"
31 "Cost and Performance Baseline for Fossil Energy Plants, Volume 1: Bituminous Coal and Natural Gas to Electricity." Revision 2. DOE/NETL-2010/1397. November 2010. http://www.netl.doe.gov/File%20Library/Research/Energy%20Analysis/Coal/BitBase_FinRep_Rev2.pdf
32 "Updated Costs (June 2011 Basis) for Selected Bituminous Baseline Cases." DOE/NETL-341/082312. August 2012. http://www.netl.doe.gov/File%20Library/Research/Energy%20Analysis/Publications/BaselineCostUpdate.pdf
33 Wood, B., et.al. "Pilot-Scale Silicone Process for Low-Cost CO2 Capture – Quarterly Report 2nd 2016." DOE Contract No. DE-FE0013755. July 2016.

34 Rochelle, G.T. “Oxidative Degradation of Monoethanolamine.” Ind. Eng. Chem. Res. 2002, 41, 4178-4186; http://pubs.acs.org/doi/pdf/10.1021/ie010697c